④

AFGL-TR-89-0035   MCCI-TR-89-861002

AD-A211 265

STS-GPS Tracking Experiment for Gravitation Estimation: Feasibility Study

Triveni N. Upadhyay
George Priovolos
Wallace E. Vander Velde
Harley Rhodehamel

Mayflower Communications Company, Inc.
80 Main Street
Reading, MA 01867

6/:/942-366ᵇ

February 1989

Final Report
25 July 1986-25 October 1988

DTIC
S ELECTE
AUG 14 1989
E D

89   8   14   40

This technical report has been reviewed and is approved for publication.

CHRISTOPHER JEKELI
Contract Manager

THOMAS P. ROONEY, Chief
Geodesy & Gravity Branch

FOR THE COMMANDER

DONALD H. ECKHARDT, Director
Earth Sciences Division

REPORT DOCUMENTATION PAGE

1a. REPORT SECURITY CLASSIFICATION	1b. RESTRICTIVE MARKINGS
Unclassified	

2a. SECURITY CLASSIFICATION AUTHORITY	3. DISTRIBUTION / AVAILABILITY OF REPORT
2b. DECLASSIFICATION / DOWNGRADING SCHEDULE	Approved for public release; distribution unlimited

4. PERFORMING ORGANIZATION REPORT NUMBER(S)	5. MONITORING ORGANIZATION REPORT NUMBER(S)
MCCI-TR-89-861002	AFGL-TR-89-0035

6a. NAME OF PERFORMING ORGANIZATION	6b. OFFICE SYMBOL (If applicable)	7a. NAME OF MONITORING ORGANIZATION
Mayflower Communications Company, Inc.		Air Force Geophysics Laboratory

6c. ADDRESS (City, State, and ZIP Code)	7b. ADDRESS (City, State, and ZIP Code)
80 Main Street Reading, MA 01867	Hanscom AFB Massachusetts 01731-5000

8a. NAME OF FUNDING / SPONSORING ORGANIZATION	8b. OFFICE SYMBOL (If applicable)	9. PROCUREMENT INSTRUMENT IDENTIFICATION NUMBER
		F19628-86-C-0136

8c. ADDRESS (City, State, and ZIP Code)	10. SOURCE OF FUNDING NUMBERS			
	PROGRAM ELEMENT NO.	PROJECT NO.	TASK NO.	WORK UNIT ACCESSION NO.
	62101F	LCDP	6C	AA

11. TITLE (Include Security Classification)

STS-GPS Tracking Experiment for Gravitation Estimation Feasibility Study

12. PERSONAL AUTHOR(S) Triveni N. Upadhyay, George Priovolos, Wallace E. Vander Velde, Harley Rhodehamel

13a. TYPE OF REPORT	13b. TIME COVERED	14. DATE OF REPORT (Year, Month, Day)	15. PAGE COUNT
Final Report	FROM 7/25/86 TO 10/25/88	1989 February	160

16. SUPPLEMENTARY NOTATION

17.	COSATI CODES		18. SUBJECT TERMS (Continue on reverse if necessary and identify by block number)
FIELD	GROUP	SUB-GROUP	Space Transportation System (STS), Global Positioning
			System (GPS), Inertial Measurement Unit, (IMU), Gravitation,
			Space Shuttle, Estimation

19. ABSTRACT (Continue on reverse if necessary and identify by block number)

The report summarizes the results of a feasibility study to estimate the gravitation parameters using GPS and IMU measurements onboard the Space Shuttle. The primary objective of the study was to determine the feasibility of estimating perturbations in the gravity vector at the Shuttle altitude to an accuracy of 1 mgal or better (1-sigma) in each axis. A detailed error analysis of the effect of measurement errors on the Shuttle acceleration estimation accuracy was carried out which resulted in the identification of critical errors. Techniques to mitigate the effect of these critical errors were developed. A survey of available hardware to demonstrate the experiment on the Shuttle in 1990-1991 was undertaken and candidate instruments (e.g., GPS receiver, IMU, processor, tape recorder) to support the experiment objectives were identified. Integration of the experiment instrumentation system on the Shuttle as a mission kit was carried out. The results of the error analysis, hardware selection and Shuttle

(OVER)

20. DISTRIBUTION / AVAILABILITY OF ABSTRACT	21. ABSTRACT SECURITY CLASSIFICATION
☐ UNCLASSIFIED/UNLIMITED ☐ SAME AS RPT. ☐ DTIC USERS	

22a. NAME OF RESPONSIBLE INDIVIDUAL	22b. TELEPHONE (Include Area Code)	22c. OFFICE SYMBOL
Christopher Jekeli		AFGL/LWG

DD FORM 1473, 84 MAR 83 APR edition may be used until exhausted. SECURITY CLASSIFICATION OF THIS PAGE
All other editions are obsolete.

Unclassified

19. ABSTRACT (Continued)

integration analysis clearly established the feasibility of the proposed Air Force experiment to map the gravity field in regions where data availability is generally limited. The Air Force STS-GPS Tracking experiment is a low-cost alternative to obtain the gravitation data in restricted areas.

AFGL STS-GPS TRACKING EXPERIMENT

FOR GRAVITATION ESTIMATION

Table of Contents

4. MEASUREMENT ANALYSIS CONTINUED

5. PAYLOAD IMU TRANSFER ALIGNMENT

6. SHUTTLE PAYLOAD INTEGRATION

7. NASA SPACE SHUTTLE GPS EXPERIMENT

REFERENCES

FOREWARD

The work described in this report was sponsored by the Air
Force Geophysics Laboratory, AFGL/LWG, Hanscom Air Force Base,
MA. The study was carried out by Mayflower Communications
Company, Inc., Reading, MA under contract number F19628-86-C-
0136. The Air Force Project Scientist for this effort was Dr.
Christopher Jekeli, AFGL/LWG. The Principal Investigator at
Mayflower Communications Company, Inc. was Dr. Triveni N.
Upadhyay.

Several organizations and individuals contributed to the
research described in this report. The instrument error analysis
work was supported by Dr. Duncan B. Cox, Jr. and Mr. Harley
Rhodehamel, of Mayflower Communications and Dr. Chreston Martin
of EG&G WASC. The gravity anomaly simulation software described
in Section 2 was developed by Dr. George Priovolos of Mayflower
Communications. The investigation on Shuttle-IMU-to-experiment-
IMU transfer alignment problem was supported by Dr. Wallace E.
Vander Velde and Mr. Serge Karsenti of MIT. Data on GPS
satellite clock Allan variances were provided by Mr. Paul
Jorgensen and Mr. Philip Tally of Aerospace Corporation. A
survey of candidate inertial instruments and systems was carried
out by R.G. Brown Associates. The mathematical formulation to
investigate the benefits of 3 dimensional acceleration
measurements on gravitation parameter estimation was developed by
Dr. Richard Rapp of the Ohio State University. Finally, the
Shuttle payload integration and cost analysis was carried out by
Mr. Andy Van Leeuwen and Mr. Stan Sokol of Rockwell
International, Space Transportation Systems Division.

Excellent administrative support was provided by Ms. Jo Ann
Patti and Ms. Joan Beaulieu of Mayflower during the preparation
of this report.

Accession For	
NTIS GRA&I	X
DTIC TAB	☐
Unannounced	☐
Justification	
By	
Distribution/	
Availability Codes	
Dist	Avail and/or Special
A-1	

v

SECTION 1

INTRODUCTION

The report documents the results of a study to determine the
feasibility of estimating perturbations in the gravity vector at
the STS (Space Transportation System) Orbiter altitude to an
accuracy of 1 mgal (1 micro-g) or better using on-board GPS
(Global Positioning System) and IMU (Inertial Measurement Unit)
measurements. The study was carried out by Mayflower
Communications Company, Inc. for the Air Force Geophysics
Laboratory, under contract number F19628-86-C-0136. The
Mayflower effort was supported by its subcontractors: EG&G
Washington Analytical Services Company, Rockwell International
Space Transportation Systems Division. and R.G. Brown Associates,
Inc. The period of performance for the study effort was July 25,
1986 to October 25, 1988.

Throughout this report, the terms "Orbiter" and "Shuttle"
will be used interchangeably.

1.1 Background

In recent years there is an increased interest in the
accurate modeling of the Earth's gravity field. There are two
aspects in the precise determination of the Earth's gravitational
potential. The first one stems from the Newtonian nature of this
potential and dictates that it is preferable to study it by
measurements as close to the generating masses as possible.
However, surface measurements can not satisfy homogeneous
resolution and accuracy requirements over both land and ocean
areas for a variety of reasons. The alternative to surface
measurements is a space-based technique, where the gravity field
is sensed by a low-earth orbiting vehicle. At present, there are
two possible implementations of the space-based technique for

gravity field mapping. These are Satellite Gradiometry and Satellite-to-Satellite Tracking (SST). The former is an attractive concept since it has the potential to offer the best possible measurement accuracy, however it is still a few years away from being realized. Consequently, SST is presently considered the best feasible satellite method for gravity field improvement in the near future. It should be mentioned that the SST concept is rather old indeed - the first geodetic application of the SST concept was proposed in a paper by Wolff [1.1]* in 1969.

The basic concept of SST is that two satellites are placed in orbit (at least one of them is near-earth) and the range (or range-rate) between them is continuously monitored. The irregularities of the terrestrial field will result in variations of their range (or range-rate), the magnitude of which will primarily depend on the altitude of the low-flying satellite. There are two possible realizations of the SST concept that have been studied: (1) a high-low mode, and (2) a low-low mode. In the high-low mode the non-gravity sensing satellite is in a high orbit while in the low-low mode both satellites are in a low orbit.

Past examples of the high-low and low-low SST concepts are ATS-6/GEOS-3 [1.2] and Apollo-Soyuz, respectively. The most recent low-low SST mission was the GRM (Geopotential Research Mission) proposed by NASA. In the GRM two drag-free satellites at 160 km altitude (low-low) were proposed to measure the Earth's gravity field. The high cost estimate of the GRM experiment has precluded it from receiving funding support from NASA. The Air Force STS-GPS Tracking experiment analyzed in this report is a

---

* Numbers in the bracket refer to references at the end of the section

high-low mode SST concept. It offers a great opportunity to improve the Earth's gravity field at low cost.

1.2 AFGL STAGE Experiment

The present STS-GPS Tracking Experiment for gravitation estimation is one specific realization of the high-low SST concept. The experiment was conceptualized at the Air Force Geophysics Laboratory and has been designated by the Air Force as the STAGE (STS-GPS Tracking for Anomalous Gravitation Estimation) mission.

In the STAGE experiment the Space Transportation System (STS) Orbiter will be instrumented with a GPS receiver and an inertial measurement unit (IMU) and will use the existing GPS antennas (top and bottom) installed on the Orbiter. The GPS measurements of code and carrier phase, IMU measurements of translation and rotation acceleration, and the Orbiter IMU data and star tracker data will be recorded, and processed post-flight to estimate the gravity field parameters, e.g., mean gravity anomalies. Since the most accurate evaluation of the usual spherical harmonic coefficients requires global data, the STAGE measurements are not viewed as a way to estimate the coefficients. Only in the case of almost global coverage should such determination be made, otherwise any coefficients estimated will be subject to errors caused by lack of data as opposed to errors caused by measurement uncertainty.

The benefits and limitations of the STAGE mission over other SST concepts are documented in a recent paper by Jekeli and Upadhyay [1.3]. The primary benefit of the STAGE experiment will be to provide satellite tracking data at a very low cost to improve gravity field estimates in regions where data accessibility is generally limited. The reason for low-cost of

1-3

the STAGE experiment, as compared to other proposed SST experiments, is that the requisite hardware (GPS receiver, IMU, processor and tape recorder) is practically off-the-shelf and largely space qualified and the satellites (both the low (Orbiter) and the high (GPS)) are already operational and fully funded.

1.3 STAGE Study Objectives

The primary study objective was to determine the feasibility of GPS tracking of the STS Orbiter to estimate the perturbations in the gravity vector at the Orbiter altitude to an accuracy of 1 mgal or better. The feasibility study focused on the following three major areas.

1. instrumentation system error analysis: analyze the primary instrument errors, identify critical errors, and develop techniques to mitigate the effect of these errors on the Orbiter acceleration estimation.

2. instrumentation system hardware configuration: select candidate instrumentation systems (i.e., GPS receiver, IMU) for the STAGE experiment by carrying out a performance/cost trade-off of available hardware.

3. payload integration and cost analysis: develop a recommended location for the experiment hardware on the Orbiter and estimate integration hardware and support cost (ROM).

The secondary objective of the study was to identify the commonality (both hardware and data processing) between the Air Force STAGE experiment and a NASA-JSC flight experiment [1.4], and

1-4

anal⁻.e whether the NASA-JSC flight experiment objectives can be met if merged with the Air Force experiment objectives.

1.4 Study Conclusions

The feasibility study, the results of which are presented in this report, concluded that the Air Force STAGE mission objectives can be met. The study identified critical error sources, i.e., error sources that if untreated, will exceed the error budget, and techniques to mitigate their effect on the Shuttle acceleration estimation were identified and developed (Sections 4 and 5). EG&G supported the error analysis effort and contributed to Section 4 of this report.

A preliminary set of simulation software was developed and was used to recover 2° mean gravity anomalies from the simulated line-of-sight Shuttle/GPS acceleration measurements. The simulation software employed Least-Squares Collocation estimation technique for mean anomaly estimation. The preliminary simulation results indicated that recovery of the 2° mean anomalies was possible and verified that the 1 mgal measurement accuracy goal (at the Shuttle altitude) is reasonable, if not optimal. These results are presented in Section 2.

The study also identified candidate instrumentation systems (GPS receiver, IMU, Tape Recorder) to realize the STAGE experiment. Performance, size, power, weight and cost of the selected hardware is discussed in Section 6. The integration of the STAGE mission kit was analyzed with support from Rockwell International. A ROM cost estimate to implement the STAGE experiment into the Shuttle was developed. The total cost of the experiment including the instrumentation cost is estimated to be about $6-7 million for a mid-1990 Shuttle flight. The payload integration cost analysis results are summarized in Section 6.

A review of the NASA-JSC flight experiment requirements based on the ARL study report [1.4] was carried out and commonality between the Air Force STAGE experiment and the NASA-JSC flight experiment was identified. It was concluded on the basis of the results of the preliminary analysis that the NASA-JSC flight experiment objectives can be met by merging it with the Air Force STAGE experiment. Furthermore, it was shown that a combined Air Force/NASA Shuttle flight experiment will enhance the NASA-JSC flight experiment objectives and will provide critical technology support for the Space Station in the area of GPS-based rendezvous and docking of the Space Station with other spacecraft (e.g., OMV).

REFERENCES

1.1 Wolff, M., "Direct Measurement of the Earth's Gravitation Potential Using a Satellite Pair", J. Geophysics Res., Vol. 74, p.5295, 1969.

1.2 Lerch, F. J., S. M. Klosko, R. E. Laubscher, and C. A. Wagner, "Gravity Model Improvement Using GEOS-3 (GEM-9 and 10)", J. Geophysics Res., Vol. 84, No. B8, pp 3897-3916, July 1979.

1.3 Jekeli, Christopher and T. N. Upadhyay, "Gravity Estimation from Multiple-High-Single-Low Satellite-to-Satellite Tracking", J. Geophysics, Res., (submitted for publication).

1.4 Peters, J. G., "Feasibility of a GEOSTAR Experiment Onboard the Space Shuttle", Technical Report No. ARL-TR-83-18, Applied Research Laboratories, the University of Texas at Austin, June 1983; NSWC Contract No. N00024-79-C-6358.

SECTION 2
STS-GPS TRACKING CONCEPT FOR GRAVITATION ESTIMATION

In this section we discuss the general satellite-to-satellite (SST) tracking concept and contrast it with the Air Force STS-GPS Tracking Experiment for gravity field mapping. Preliminary simulation results using Least-Squares Collocation to estimate mean gravity anomalies are presented in this section.

2.1 Introduction

In recent years there is an increased interest in the accurate modelling of the Earth's gravity field. This interest is demonstrated by various disciplines, with a diversity of objectives. Orbital Dynamics require a precise potential field for the NASA TOPEX mission. Geophysics require gravity anomalies accurate to a few mgals at wavelengths shorter than 100 km and oceanography requires a 5-10 cm geoid for ocean circulation determinations. Consequently, efforts to model the geopotential have become very intense.

There are two aspects in the precise determination of the Earth's gravitational potential. The first one stems from the Newtonian nature of this potential and dictates that it is preferable to study it by measurements as close to the generating masses as possible. However, surface measurements cannot satisfy homogeneous resolution and accuracy requirements over both land and ocean areas, for a variety of geographical, historical and political reasons [Reigber et al., 1987]. The picture is further complicated when the cost as well as the time to complete the gravity survey become considerations. The alternative to surface measurements is a space-based technique, where the gravity field is sensed by a low orbiting vehicle.

The second aspect is better understood if one considers the terrestrial field as a series of spherical harmonics, i.e., as a superposition of its spectral components. The low frequencies describe global and regional features whereas the fine structure of the field is reflected on its high frequencies, whose effect is naturally pronounced in derivative (difference) quantities. Therefore, a detailed representation of the Earth's gravity field will be the outcome of a space-borne technique which will observe differential quantities. At present, the two methods which satisfy the above requirements are Satellite Gradiometry and Satellite-to-Satellite Tracking (SST). The former is an attractive concept since several second derivatives of the geopotential are observed simultaneously, however, the construction of a device to reliably sense the gravity gradients to within $10^{-2} - 10^{-4}$ Eötvös (1 Eötvös = 0.1 mgal/km) is a great challenge to present day technology [Reigber et al., 1987]. Consequently, SST is presently considered the best feasible satellite method for gravity field improvement in the near future [ibid, p. 49].

The basic concept of SST is that two satellites are placed in orbit (at least one of which is near-Earth) and the range (or range rate) between them is continuously monitored. The irregularities of the terrestrial field will result in variations of their range (or range rate), the magnitude of which will primarily depend on the altitude of the low flying satellite. There are two modes (variations) of SST. The first one is the high-low mode in which the non-gravity sensing satellite is in a high orbit, and the second one is the low-low mode in which both satellites are in a low orbit.

The SST concept is rather old indeed, originating probably in a paper by Baker in 1960 [Reigber et al., 1987]. In Baker's paper, however, the aim was orbit improvement. SST entered the

geodetic arena in a paper by [Wolff, 1969]. The first test of
SST in the low-low mode was performed with the Apollo-Soyuz
system, however unsuccessfully, due to background noise
[Weiffenbach et al., 1976]. The first successful data analysis
attempt was done by [Vonbun et al., 1975] in the high-low mode
with the ATS-6 as the high satellite and the Apollo-Soyuz system
as the low satellite. From then on, the data of two other SST
experiments in the high-low mode became available, namely for
ATS-6/Nimbus-6 and ATS-6/GEOS-3 and the analyses of these data,
as well as simulation SST studies flourished, e.g., [Schwarz,
1970], [Hajela, 1974], [Rummel et al., 1976], [Kahn et al.,
1977], [Hajela, 1978], [Kahn et al., 1982]. In the early
eighties NASA conceived the GRAVSAT idea, later renamed GRM, with
two drag-free satellites at 160 km altitude (low-low mode) which,
however, became secondary in NASA's priority list in the early
part of 1988.

Some of the research pertaining to the SST concept
verification includes the error analysis by Rummel, Hajela and
Rapp [1976], in which line-of-sight accelerations were used to
predict mean gravity anomalies using Least-Squares Collocation
(LSC). Hajela [1978] applied LSC to ATS-6/GEOS-3 data to
estimate $5°$ anomalies. Pisacane and Yionoulis [1980] addressed
the issues of orbit characteristics, data gathering system,
ground tracking requirements and performance error analysis to
the recovered mean anomaly signal. Kahn et al. [1982] used a
combination of the Apollo-Soyuz and GEOS-3 data to recover $10°$
and $5°$ mean anomalies. Other authors, such as [Kaula, 1983],
[Bose and Thobe, 1984] and [Colombo, 1984] suggested global
solutions.

Recently, Wichiencharoen [1985] described a simulation
analysis, where mean anomalies were computed with different
estimation techniques. His recovery was good except in areas

with large gravity gradients (e.g., the Tonga Trench). A very comprehensive analysis of SST including investigations regarding GRM as well as a possible POPSAT-GRM link is reported in [Reigber et al., 1987].

In Section 2.2 we describe the measurement system concept and discuss advantages of the STS-GPS tracking experiment over any other high-low configuration. Section 2.3 presents the estimation of mean gravity anomalies through the system. The Least- Squares Collocation Estimator is briefly discussed in subsection 2.3.1. Initial pre-processing of the data will yield line of sight accelerations to three GPS satellites. In order to predict the anomalies from the aforementioned observations, the relation of the line of sight accelerations to the gravity disturbance vector must be established. This relation is derived in subsection 2.3.2, and used for computation of the necessary covariances for the Collocation solution in subsection 2.3.3. A simulation study in the Southern U.S. to perform a preliminary evaluation of the STS-GPS concept is presented in Section 2.4. This section is concluded by summarizing the important results.

2.2 Measurement System

The Space Transportation System-Global Positioning System (STS-GPS) is a high-low SST configuration, with the Shuttle as the low (gravity sensing) vehicle and with the 18 GPS satellites at a much higher altitude. The measurement system for the STAGE experiment consists of a GPS receiver and an inertial measurement unit (IMU). The GPS receiver onboard the STS Orbiter (Space Shuttle) will measure the line-of-sight carrier doppler phase to three or more GPS satellites. This data will be used to estimate, post-flight, the line-of-sight accelerations (gravitation and non-gravitation) on the Shuttle. Simultaneously, an onboard IMU accelerometer will measure the

non-gravitation acceleration on the Shuttle. The measurements of acceleration will be in the Shuttle body coordinates while the GPS measurements of acceleration will be in the earth-centered, earth-fixed coordinates. After appropriate coordinate transformations, the GPS and IMU data will be processed to estimate Shuttle gravitation acceleration. The details of the measurement system hardware is presented in Section 3.

There are two distinct advantages of the STS-GPS system over any other high-low SST experiment such as the ATS-6/GEOS-3 and the ATS-6/Apollo-Soyuz. The first advantage is good visibility. The importance of this issue can be appreciated if one considers that for the same mission duration, a high-low system will supply only 20% of the data provided by a low-low system [Reigber, et al., 1987, p.309]. In the case of the STS-GPS system, the full constellation of 18 GPS satellites guarantees visibility to at least 4 GPS satellites at all times [Upadhyay, 1987]. Consequently, a serious drawback of the high-low mode is removed in this experiment.

The second advantage is that the STS-GPS system can track 3 or more GPS satellites simultaneously, resulting in line-of-sight accelerations to 3 (or more) vehicles, as opposed to one vehicle in the traditional SST case. This, in essence, enables the recovery of the gravity disturbance vector at the Shuttle altitude, as opposed to recovering the radial derivative of the anomalous potential, projected onto the line of sight connecting the two vehicles.

The Shuttle will be placed in an eccentric orbit at an altitude of about 300 km. The inclination of the Orbiter will be approximately 30°, which corresponds to coverage of about 1/3 of the globe. The complete GPS constellation will consist of 18 satellites, in 6 orbital planes at an altitude of 20,200 km. The

orbital periods will be approximately 90 minutes for the Shuttle and 12 hours for the GPS satellites.

The measurements from GPS and IMU will be recorded for post-flight processing, to estimate line of sight accelerations. We plan to use cubic splines to interpolate and filter the GPS carrier phase measurements and IMU accelerometer velocity measurements to arrive at the acceleration estimate. The cubic splines have been used by [Hajela, 1977] for a similar application.

From Velocities to Accelerations Via Cubic Splines

In order to obtain accelerations from the raw data, a cubic spline interpolation scheme will be used as proposed by Hajela [1977]. A description of the method follows.

Let a sequence of n points t_i, $i=1,2,\ldots,n$ be defined on a closed interval $I=[a,b]$ such that:

$$a \leq t_1 < t_2 < \ldots < t_n \leq b$$

and let $p(t)$ be a real valued continuous function such that

$$p_k = p(t_k) \text{ at } t_k, \text{ where } k=1,2,\ldots,n$$

Furthermore, let S_I be the vector space of the cubic spline functions on I. The members of S_I are cubic polynomials on I, which are twice continuously differentiable at each node t_k. The dimension of S_I is n+2 [ibid, p.17], thus any $S(t)$ within S_I can be represented as:

$$S(t) = \sum_{i=1}^{n+2} c_i \, q_i \, (t) \, , \, i = 1,2,\ldots,n+2$$

where c_i are real numbers and $q = [q_1(t), q_2(t), \ldots, q_{n+2}(t)]$ is a basis of S_1. Therefore, once a basis q is chosen, the determination of the cubic spline $S(t)$ reduces to solving the linear system

$$A \cdot \underline{x} = \underline{\ell}$$

where $\underline{x}$ is the vector of the unknown c_i coefficients, $\underline{\ell}$ is the vector of the observations and the elements a_{ij} of A are given by

$$a_{ij} = q_j(t_i)$$

An important property of S_1 is that if the data are ordered, then A is band limited with a bandwidth of 4 [Hajela, 1977, p.19], therefore, for each subinterval $I_k = (t_k, t_{k+1}]$, there are only four non-vanishing polynomials in q. Hajela [ibid, p.20] suggests the choice

$$p_1(u) = u^3/4, \quad p_2(u) = 1 - 3/4(1+u)(1-u)^2$$

such that

$$
\begin{aligned}
q_k(t) &= p_1(1-u) \\
q_{k+1}(t) &= p_2(1-u) \quad, \quad k = 1, 2, \ldots, n-1 \\
q_{k+2}t(t) &= p_2(u) \\
q_{k+3}(t) &= p_1(u)
\end{aligned}
$$

The transformation u(t) is defined as:

$$u = \frac{t-t_k}{t_{k+1}-t_k}, \text{ for } t \in I_k$$

Once the coefficients c_i are computed, the spline at each point x_i is given by

$$S(x_i) = \sum_{\ell=0}^{3} c_{k+\ell} \; q_{k+\ell}(x_i), \; x_i \in I_k \;, \; k = 1,2,\ldots,n-1.$$

At instances where the data vector $\underline{\ell}$ has some noise, $\underline{n}$, associated with it, the linear system becomes

$$A \; \underline{x} = \underline{\ell} + \underline{n}$$

and is solved by minimizing the L_2 norm of the error vector, i.e.:

$$\| \underline{n} \|_2 = \| \underline{\ell} - A\underline{x} \|_2 = \min$$

In our case, the raw data are velocities. The solution of the linear system will yield filtered data and the unknown vector $\underline{x}$. The required accelerations will be computed by differentiating $S(x)$.

2.3 Mean Gravity Anomaly Estimation

2.3.1 The Estimation Method

A widely used method for gravity field approximation is Least-Squares Collocation. The method is an analogue of the Kolmogorov-Wiener predictor [Moritz, 1980, p.80], and it is well established within the geodetic community.

2-8

` detailed account of the method can be found in
publications such as [Krarup, 1969] and [Moritz, 1980].
Consequently, only a brief description of it is given here.

Let $\underline{l}$ be a vector of observations, consisting of a signal
part $\underline{t}$ and a noise part $\underline{n}$, i.e.

$$\underline{l} = \underline{t} + \underline{n} \tag{1}$$

The minimum variance estimate $\underline{\hat{s}}$ of a signal $\underline{s}$, based on the
observation vector $\underline{l}$ is given by [Moritz, 1980]

$$\underline{\hat{s}} = C_{st} \; C^{-1} \underline{l} \tag{2}$$

where

$$C = C_{tt} + D \tag{3}$$

and C_{tt} is the signal auto-covariance matrix, C_{st} is the signal-
observation cross-variance matrix and D is the error variance
matrix of the observations. The error covariance matrix of the
predicted signals is given by

$$E_{ss} = C_{ss} - C_{st} \; C^{-1} \; C_{st}^{T} \tag{4}$$

In gravity field approximation, the signals t and s are
quantities related to the Earth's disturbing potential T.
Therefore, the signal covariances required in equations (2), (3)
and (4) will be computed based on the disturbing potential
covariance function $K(P,Q)$. Furthermore, under the usual
spherical approximation [Heiskanen and Moritz, 1967, p.87], the
signals are linear functionals of T, thus one can write

$$s = B \cdot T \tag{5}$$
$$t = L \cdot T$$

where B and L are linear operators. For example, if s is a

gravity anomaly, then

$$B = -\frac{\partial}{\partial r} - \frac{2}{r} \qquad (6)$$

The covariance matrices C_{ss}, C_{st} and C_{tt} will be determined through covariance propagation [Moritz, 1980, p.87, eq. (11-14)]. One has for the (i,j) element of C_{st} and C_{tt}

$$C_{st}^{ij} = B_i^P \ L_j^Q \ K(P,Q)$$

$$C_{tt}^{ij} = L_i^P \ L_j^Q \ K(P,Q) \qquad (7)$$

which enables the full implementation of (2) through (4), once $K(P,Q)$ is known.

2.3.2 Line of Sight Acceleration in Terms of Gravity Disturbance Vectors

At this point, the relation between the line of sight acceleration and the gravity disturbance vectors at Shuttle and at GPS-Satellite altitude will be derived. This relation will be used both for covariance propagation and for the generation of the observable in the simulation study.

Let us denote by x_s the position vector of the Shuttle and by x_k the position vector of the k-th GPS satellite. Their range (distance) ρ is given by ($\langle \cdot, \cdot \rangle$ denotes the inner product)

$$\rho = \langle \Delta \underline{x}, \Delta \underline{x} \rangle^{\frac{1}{2}} \qquad (8)$$

where

$$\Delta \underline{x} = \underline{x}_k - \underline{x}_s \qquad (9)$$

The range rate (velocity) between the two vehicles is

$$\dot{\rho} = 1/(2\rho) [\langle \Delta \dot{\underline{x}}, \Delta \underline{x} \rangle + \langle \Delta \underline{x}, \Delta \dot{\underline{x}} \rangle]$$

or

$$\dot{\rho} = 1/\rho \langle \Delta \underline{x}, \Delta \dot{\underline{x}} \rangle \tag{10}$$

The unit vector $\underline{e}$ in the k-S direction is given by

$$\underline{e} = \frac{\Delta \underline{x}}{\rho} \tag{11}$$

thus (10) becomes

$$\dot{\rho} = \langle \Delta \dot{\underline{x}}, \underline{e} \rangle \tag{12}$$

The range rate change (acceleration) is obtained by differentiating (12) with respect to time. One gets

$$\ddot{\rho} = \langle \Delta \ddot{\underline{x}}, \underline{e} \rangle + \langle \Delta \dot{\underline{x}}, \dot{\underline{e}} \rangle \tag{13}$$

The second term in equation (13) deserves special attention because it is a low frequency phenomenon, and it can be neglected if the line-of-sight acceleration is referred to a low degree field.

Differentiating the unit vector e in equation (11) with respect to time yields

$$\dot{\underline{e}} = \frac{\rho \Delta \dot{\underline{x}} - \dot{\rho} \Delta \underline{x}}{\rho^2}$$

or

$$\dot{\underline{e}} = \frac{\Delta \dot{\underline{x}}}{\rho} - \frac{\dot{\rho} \Delta \underline{x}}{\rho^2} \tag{14}$$

Forming the dot product to obtain the second term in (13) yields

$$\langle \Delta \dot{\underline{x}}, \dot{\underline{e}} \rangle = \langle \Delta \dot{\underline{x}}, \Delta \dot{\underline{x}}/\rho - \dot{\rho}/\rho^2 \Delta \underline{x} \rangle$$
$$= 1/\rho \langle \Delta \dot{\underline{x}}, \Delta \dot{\underline{x}} \rangle - \dot{\rho}/\rho^2 \langle \Delta \dot{\underline{x}}, \Delta \underline{x} \rangle \tag{15}$$

Upon substitution of $\dot{\rho}$ from (10) into (15) one obtains

$$\langle \Delta \dot{\underline{x}}, \dot{\underline{e}} \rangle = 1/\rho \langle \Delta \dot{\underline{x}}, \Delta \dot{\underline{x}} \rangle - 1/\rho^3 \langle \Delta \dot{\underline{x}}, \Delta \underline{x} \rangle \langle \Delta \dot{\underline{x}}, \Delta \dot{\underline{x}} \rangle \tag{16}$$

or, upon simplification

$$\langle \Delta \dot{\underline{x}}, \dot{\underline{e}} \rangle = 1/\rho [\langle \Delta \dot{\underline{x}}, \Delta \dot{\underline{x}} \rangle - 1/\rho^2 \langle \Delta \dot{\underline{x}}, \Delta \underline{x} \rangle^2] \tag{17}$$

In order to compute $\langle \Delta \dot{\underline{x}}, \dot{\underline{e}} \rangle$, the following procedure was followed. Orbits for both the Shuttle and 3 GPS satellites were generated assuming that the perturbations to a central force field were those induced by the OSU86F field to degree and order 180 [Rapp and Cruz, 1987]. This resulted in the term $\langle \Delta \dot{\underline{x}}, \dot{\underline{e}} \rangle_{TRUE}$. Consequently, the same orbits were generated using GEM-T1 to degree and order 36 [Marsh et. al., 1987], which resulted in the term $\langle \Delta \dot{\underline{x}}, \dot{\underline{e}} \rangle_{REF}$. The term $d\langle \Delta \dot{\underline{x}}, \dot{\underline{e}} \rangle = \langle \Delta \dot{\underline{x}}, \dot{\underline{e}} \rangle_{TRUE} - \langle \Delta \dot{\underline{x}}, \dot{\underline{e}} \rangle_{REF}$ is shown in Table 2.1.

From Table 2.1, one can see that the term $d\langle \Delta \dot{\underline{x}}, \dot{\underline{e}} \rangle$ is negligible at all instances. This confirms similar tests carried out by other authors, such as [Rummel, 1980] and [Hajela, 1978].

Now that the negligibility of the second term in equation (13) is established, one may proceed with the first term. Differentiating (9) twice with respect to time one obtains

$$\Delta \ddot{\underline{x}} = \ddot{\underline{x}}_k - \ddot{\underline{x}}_s \tag{18}$$

Furthermore, the accelerations of the vehicles in the Earth's

disturbing potential field are given by

$$\ddot{\underline{x}}_k = grad\ T_k$$

$$\ddot{\underline{x}}_s = grad\ T_s \qquad\qquad (19)$$

TABLE 2.1

Term $d\langle \Delta \dot{\underline{x}},\ \underline{e}\rangle$ in mgals for three GPS satellites and for different orbit generating time intervals.

TIME sec.	(mgals)	GPS SV No. 1	GPS SV No. 2	GPS SV No. 3
	AVE	1.1×10^{-9}	1.1×10^{-9}	1.2×10^{-9}
	RMS	1.5×10^{-9}	1.6×10^{-9}	1.7×10^{-9}
1	MIN	0	0	0
	MAX	2.5×10^{-9}	2.7×10^{-9}	2.9×10^{-9}
	AVE	3.5×10^{-6}	3.7×10^{-6}	3.8×10^{-6}
	RMS	4.8×10^{-6}	5.0×10^{-6}	5.2×10^{-6}
50	MIN	0	0	0
	MAX	7.8×10^{-6}	8.2×10^{-6}	8.5×10^{-6}
	AVE	4.4×10^{-6}	4.6×10^{-6}	4.7×10^{-6}
	RMS	5.4×10^{-6}	5.7×10^{-6}	5.8×10^{-6}
75	MIN	0	0	0
	MAX	7.2×10^{-6}	7.6×10^{-6}	7.7×10^{-6}

Hence (13) becomes

$$\ddot{\rho} = \langle grad\ T_k\ -\ grad\ T_s\ ,\ \underline{e}\rangle \qquad\qquad (20)$$

The gravity disturbance vector $\underline{\delta}$ in spherical geocentric coordinates $r,\ \Phi, \lambda$ is defined as [Heiskanen and Moritz, 1967, p.233]

$$\underline{\delta} = \text{grad } T = \begin{bmatrix} \delta_r \\ \delta_\phi \\ \delta\lambda \end{bmatrix} \begin{bmatrix} \partial T/\partial r \\ 1/r * \partial T/\partial \phi \\ 1/r\text{Cos}\phi * \partial T/\partial\lambda \end{bmatrix} \tag{21}$$

or equivalently

$$\underline{\delta} = \delta_r \underline{e}_r + \delta_\phi \underline{e}_\phi + \delta\lambda \underline{e}\lambda \tag{22}$$

where $\underline{e}_r$, $\underline{e}_\phi$, $\underline{e}\lambda$ are the unit vectors in the spherical coordinate system. Their relation to the unit vectors $\underline{i}$, $\underline{j}$, $\underline{k}$ of a Cartesian Rectangular Coordinate System is given by [ibid, p.230]

$$\underline{e}_r = \cos\Phi \cos X \underline{i} \cos\Phi \cos X \underline{j} + \sin\Phi \underline{k}$$
$$\underline{e}_\phi = -\sin\Phi \cos X \underline{i} - \sin\Phi \sin X \underline{j} + \cos\Phi \underline{k} \tag{23}$$
$$\underline{e}\lambda = -\sin X \underline{i} + \cos X \underline{j}$$

On the other hand

$$\underline{e} = e_x \underline{i} + e_y \underline{j} + e_z \underline{k} \tag{24}$$

where

$$e_x = (x_k - x_s)/\varrho; \quad e_y = (y_k - y_s)/\varrho; \quad e_z = (z_k - z_s)/\varrho \tag{25}$$

where ϱ is given by (8) and $\underline{x}_k = [x_k \ y_k \ z_k]^T$, $\underline{x}_s = [x_s \ y_s \ z_s]^T$.

Now the inner product $\langle \underline{\delta}, \underline{e} \rangle$, using (22) and (24) can be written as

$$\langle \underline{\delta}, \underline{e} \rangle = \langle \delta_r \underline{e}_r + \delta_\phi \underline{e}_\phi + \delta\lambda\underline{e}\lambda, e_x \underline{i} + e_y \underline{j} + e_z \underline{k} \rangle =$$
$$= \delta_r e_x \langle \underline{e}_r, \underline{i} \rangle + \delta_r e_y \langle \underline{e}_r, \underline{j} \rangle + \delta_r e_z \langle \underline{e}_r, \underline{k} \rangle +$$
$$+ \delta_\phi e_x \langle \underline{e}\Phi, \underline{i} \rangle + \delta\Phi e_y \langle \underline{e}\Phi, \underline{j} \rangle + \delta\Phi e_z \langle \underline{e}\Phi, \underline{k} \rangle +$$
$$+ \delta\lambda e_x \langle \underline{e}\lambda, \underline{i} \rangle + \delta\lambda e_y \langle \underline{e}\lambda, \underline{j} \rangle + \delta\lambda e_z \langle \underline{e}\lambda, \underline{k} \rangle$$

or, in matrix form

$$\langle \underline{\delta}, \underline{e} \rangle = \underline{e}^T A \underline{\delta} \tag{26}$$

where

$$A = \begin{bmatrix} \langle \underline{e}_r, \underline{i} \rangle & \langle \underline{e}_\ast, \underline{i} \rangle & \langle \underline{e}\lambda, & \underline{i} \rangle \\ \langle \underline{e}_r, \underline{j} \rangle & \langle \underline{e}_\ast, \underline{j} \rangle & \langle \underline{e}\lambda, & \underline{j} \rangle \\ \langle \underline{e}_r, \underline{k} \rangle & \langle \underline{e}_\ast, \underline{k} \rangle & \langle \underline{e}\backslash, & \underline{k} \rangle \end{bmatrix} \tag{27}$$

But from (23), the coordinates of e_r, $e_\ast$, $e\backslash$ with base (unit) vectors $\underline{i}$, $\underline{j}$, $\underline{k}$ can be read off, therefore

$$A = \begin{bmatrix} \cos\Phi\cos\lambda & -\sin\Phi\cos\lambda & -\sin\backslash \\ \cos\Phi\sin\lambda & -\sin\Phi\sin\backslash & \cos\lambda \\ \sin\Phi & \cos\Phi & 0 \end{bmatrix} \tag{28}$$

Now equation (20) can be written as

$$\ddot{\rho} = \langle \underline{\delta}_k - \underline{\delta}_s, \underline{e} \rangle = \langle \underline{\delta}_k, \underline{e} \rangle - \langle \underline{\delta}_s, \underline{e} \rangle$$

or using (26)

$$\ddot{\rho} = \underline{e}^T (A_k \underline{\delta}_k - A_s \underline{\delta}_s) \tag{29}$$

With equation (29) at one's disposal, one may proceed with computing covariances relating $\ddot{\rho}$ and any gravity related quantity.

2.3.3   Determination of Covariances

In the STS-GPS experiment, the observables will be line-of-sight accelerations $\ddot{\rho}$ to at least three GPS satellites. From these observations, the aim is to estimate mean gravity anomalies via equation (2). The successful application of (2) requires the computation of the covariance matrices $C_{\Delta\Delta}$, $C_{\Delta\Delta}$, which in this

case become

$$C_{a\,i} = C_{\Delta \bar{g}, \ddot{\rho}} \quad \text{and} \quad C_{t\,i} = C_{\ddot{\rho}, \ddot{\rho}} \tag{30}$$

Using equation (29), the (i,j) element of $C_{\ddot{\rho}, \ddot{\rho}}$ can be written as

$$C^{i,j}_{\ddot{\rho}, \ddot{\rho}} = Cov(\ddot{\rho}_i, \ddot{\rho}_j) = Cov[\underline{e}^T_i (A_{k\,i} \underline{\delta}_{k\,i} - A_{s\,i} \underline{\delta}_{s\,i}), \underline{e}_j (A_{k\,j} \underline{\delta}_{k\,j} - A_{s\,j} \underline{\delta}_{sj})]$$

$$= \underline{e}^T_i \, Cov(A_{k\,i} \underline{\delta}_{k\,i} - A_{s\,i} \underline{\delta}_{s\,i}, A_{k\,j} \underline{\delta}_{k\,j} - A_{s\,j} \underline{\delta}_{s\,j}) \, \underline{e}_j$$

$$= \underline{e}^T_i \, [Cov(A_{k\,i} \underline{\delta}_{k\,i}, A_{k\,j} \underline{\delta}_{k\,j}) - Cov(A_{s\,i} \underline{\delta}_{s\,i}, A_{k\,j} \underline{\delta}_{k\,j})$$

$$- Cov(A_{k\,i} \underline{\delta}_{k\,i}, A_{s\,j} \underline{\delta}_{s\,j}) + Cov(A_{s\,i} \underline{\delta}_{s\,i}, A_{A\,s\,j} \underline{\delta}_{s\,j})] \, \underline{e}_j$$

or

$$C^{i,j}_{\ddot{\rho}, \ddot{\rho}} = \underline{e}^T_i [(A_{k\,i} Cov(\underline{\delta}_{k\,i}, \underline{\delta}_{kj}) - A_{s\,i} Cov(\underline{\delta}_{s\,i}, \underline{\delta}_{k\,j})) A^T_{k\,j}$$

$$- (A_{k\,i} Cov(\underline{\delta}_{k\,i}, \underline{\delta}_{s\,j}) - A_{s\,i} Cov(\underline{\delta}_{s\,i}, \underline{\delta}_{s\,j})) A^T_{s\,i}] \, \underline{e}_j \tag{31}$$

Similarly, the (i,j) element of $C_{\Delta \bar{g}, \ddot{\rho}}$ can be written as

$$C^{i,j}_{\Delta \bar{g}, \ddot{\rho}} = Cov(\Delta \bar{g}_i, \ddot{\rho}_j) = Cov(\Delta \bar{g}_i, \underline{e}^T_j (A_{k\,j} \underline{\delta}_{k\,j} - A_{s\,j} \underline{\delta}_{s\,j})) =$$

$$= Cov(\Delta \bar{g}_i, A_{k\,j} \underline{\delta}_{k\,j} - A_{s\,j} \underline{\delta}_{s\,j}) \, \underline{e}_j,$$

or

$$C^{i,j}_{\Delta \bar{g}, \ddot{\rho}} = [Cov(\Delta \bar{g}_i, \underline{\delta}_{k\,j}) A^T_{k\,j} - Cov(\Delta \bar{g}_i, \underline{\delta}_{s\,j}) A^T_{s\,j}] \underline{e}_j \tag{32}$$

2.4   A Simulation Study

In order to perform a preliminary evaluation of the STS-GPS concept, a simulation study was employed in the Southern United States. The area of interest was bound by parallels 26° North and 20° South and by meridians 262° East and 252° West. One week
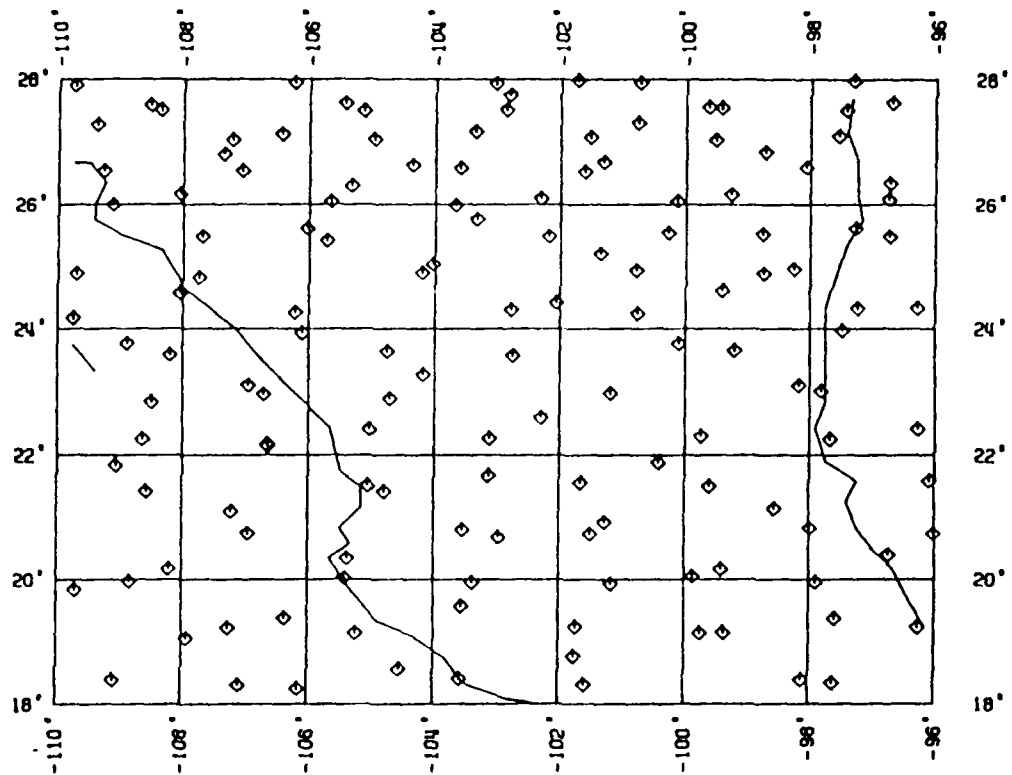
Figure 2.1: Distribution of the 143 points of the Shuttle Orbit in the Southern U.S.

long orbits for the Shuttle and the 18 GPS satellites were simulated in intervals of 30 seconds. The arcs with sub-satellite points within the area of interest plus a 2° border surrounding it were selected. This resulted in 143 points whose distribution is shown in Figure 2.1.

From Figure 2.1, one can observe an average density of about 1 point per (1°x1°) block, varying from about 0.5 to about 1.75.

For each point of the Shuttle orbit, the three GPS satellites with the minimum PDOP were selected and the line of sight accelerations residual to GEM-T1 were computed. Figures 2.2, 2.3 and 2.4 show these residual quantities for the three satellites. From these figures one can see that the residual accelerations are in the order of a few mgals and rather smooth. The small magnitude of the residual accelerations indicates that at an altitude of 300 km, the features of the gravity field beyond degree 36 are attenuated. Therefore, only slight improvement of the higher frequencies is expected. However, low degree fields (such as the GEM-T1) can benefit from the experiment, especially in areas with poor coverage of satellite tracking stations.

In the aforementioned area of interest, 2° mean anomalies were computed assuming that the OSU86F field to degree and order 180 represents the true gravity field. The computed mean anomalies were subsequently referred to the GEM-T1 field, which resulted in residual means $V^c_{\overline{\Delta g}}$. Contours from these residual anomalies are shown in Figure 2.5.

The residual line of sight accelerations shown in Figures 2.2-2.4 were utilized as observations and 2° residual mean anomalies $V^P_{\overline{\Delta g}}$ were recovered using Least-Squares Collocation. The covariance matrices were computed using the Tscherning /Rapp model [Tscherning and Rapp, 1974]. The mean anomaly covariances

Figure 2.2: Contours of the line of sight acceleration to the first GPS satellite.

LINE OF SIGHT ACCELERATION TO THE SECOND GPS SAT.

RESIDUAL VALUES | CI = 1 MGAL
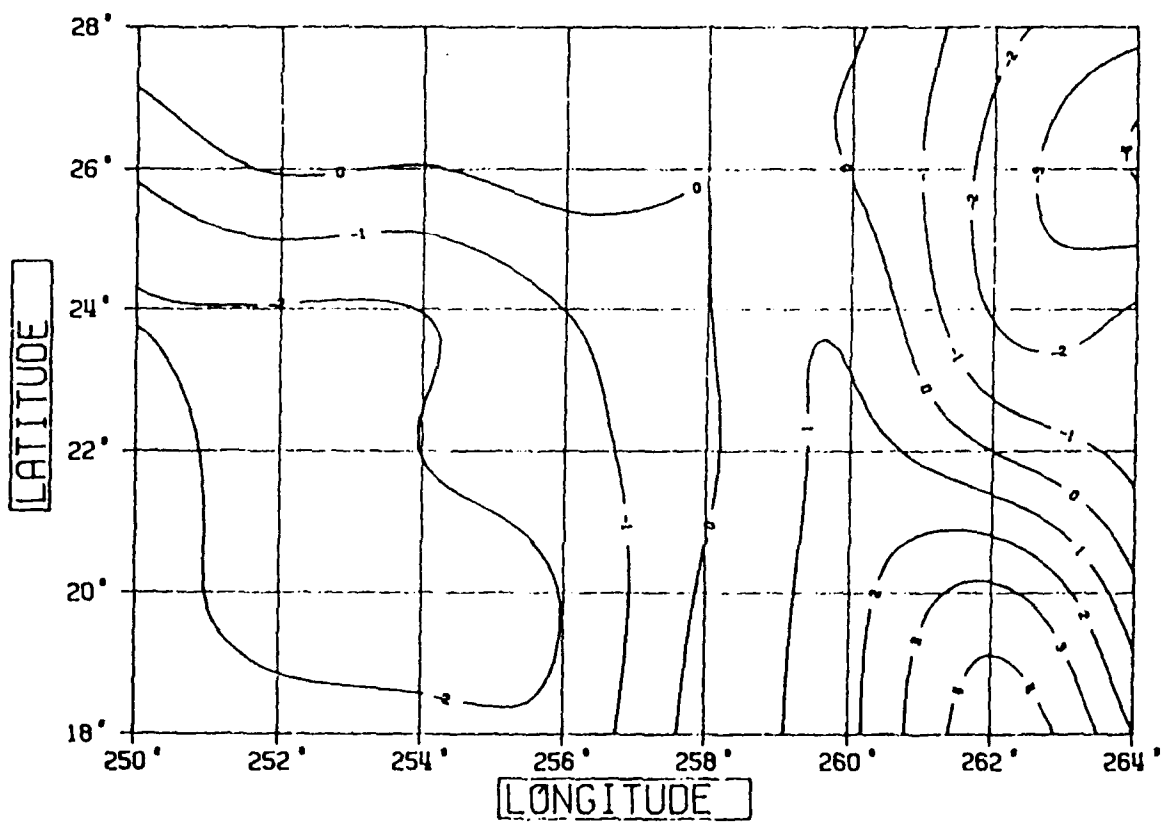
Figure 2.3: Contours of the line of sight acceleration to the second GPS satellite.
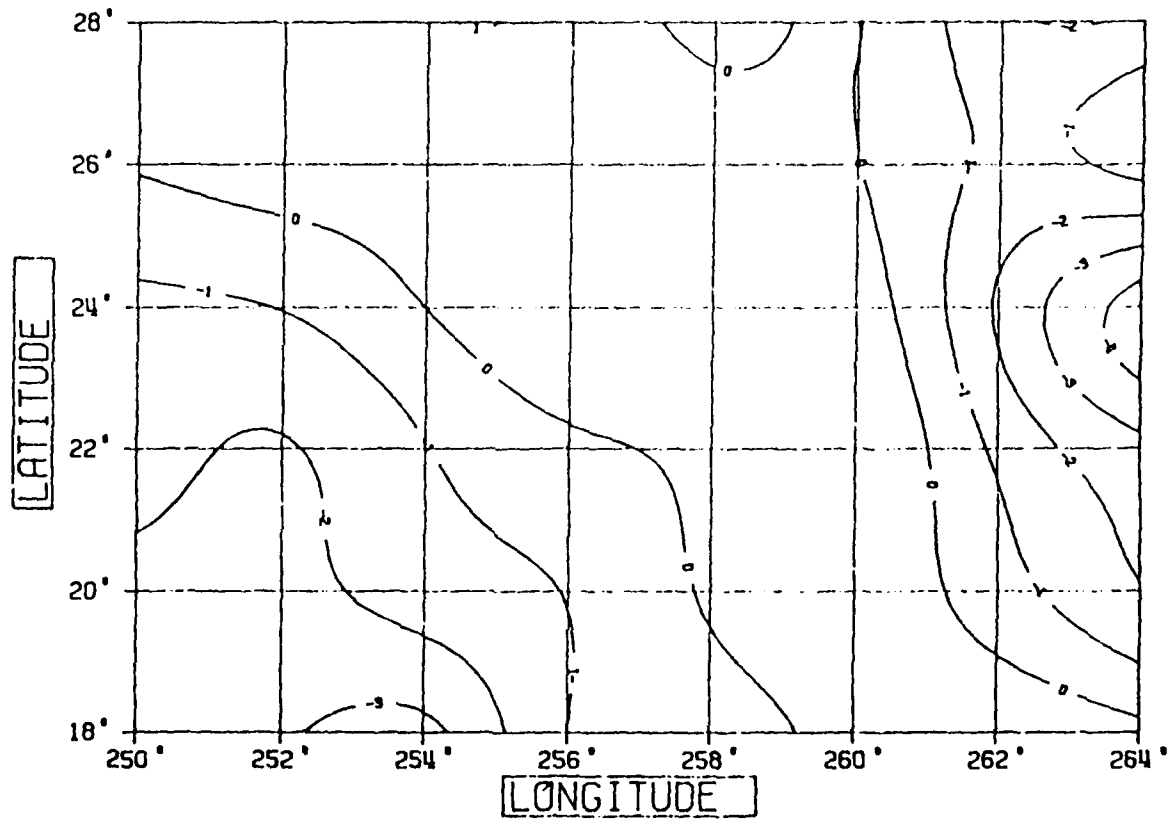
Figure 2.4: Contours of the line of sight acceleration to the third GPS satellite.

MEAN ANOMALIES (2 DEG X 2 DEG) / SOUTHERN U. S.

RESIDUAL (O-C) FIELD	CI = 10 MGALS
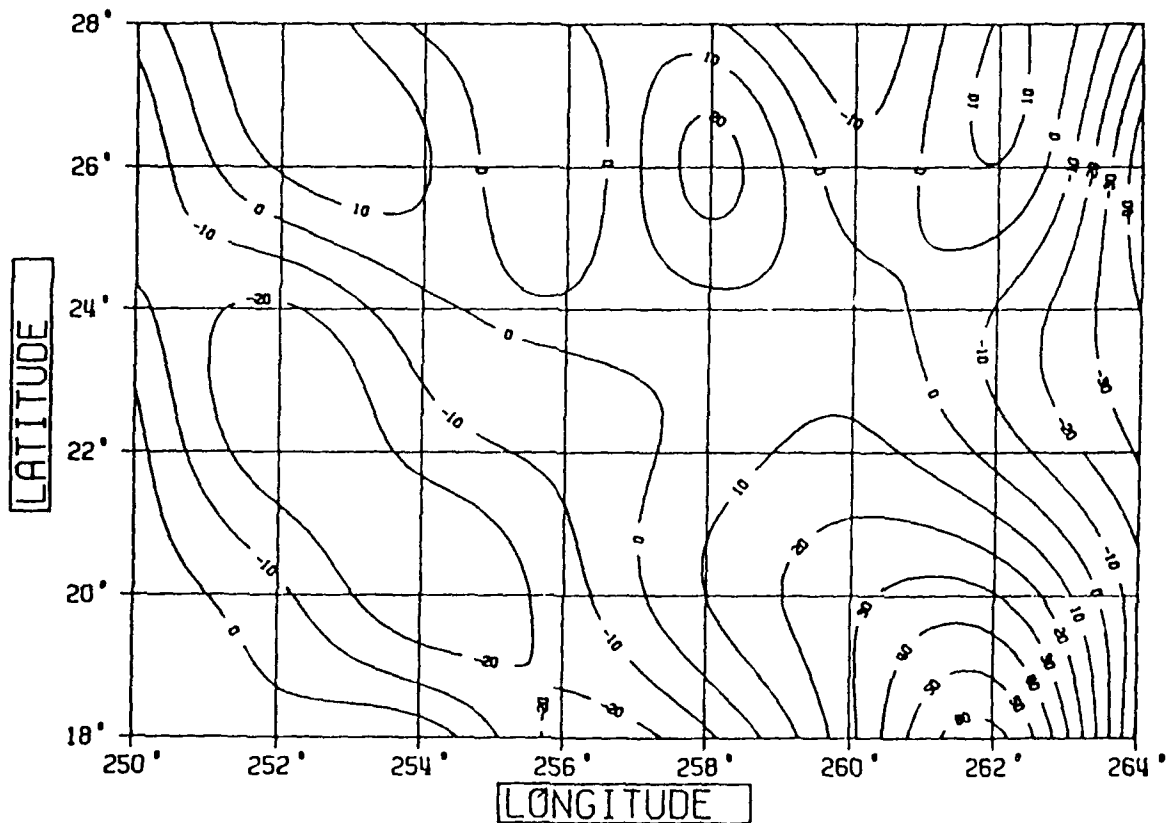
Figure 2.5:   Contours of 2° mean anomalies residual to GEM-T1
CI=10 mgals.

were computed by numerical integration of point values on a (6x6) grid of mesh-size 20'. Each mean anomaly was estimated using data inside a circular cap. Three different cap radii were used, namely 1°, 2° and 3°. The case of the 1° was poor in data coverage, rendering the prediction meaningless. For a cap radius of 2°, the average block contained approximately 23 data points. Figure 2.6 shows the RMS difference of control $(V^P_{\overline{\Delta g}})$ minus predicted $(V^C_{\overline{\Delta g}})$ residual mean anomalies as a function of the observational accuracy.

In Figure 2.6, the line parallel to the observational accuracy indicates the RMS magnitude of the residual 2° control mean anomaly $V^C_{\overline{\Delta g}}$. From Figure 2.6 one can conclude the following. At first, the smallest RMS difference (control minus predicted) was about 10 mgals, whereas the RMS $V^C_{\overline{\Delta} g}$ was about 13 mgals. Therefore, the 2° anomalies were meaningfully predicted in the RMS sense. Secondly, the best prediction results were attained with a standard deviation of the observations of 1 mgal. This fact confirms the accuracy goal of 1 mgal for the measurement system, set in Phase I of this feasibility study, as indeed reasonable.

Another issue which is apparent in Figure 2.6 is that there is a narrow range of standard deviations (0.5 to 2 mgals) in which the observations are contributing to the predicted 2° anomalies. Last but not least, Figure 2.6 demonstrates the instability of the downward continuation in the form of deterioration of the predictions as the observational accuracy increases beyond the 1 mgal level.

In the case of 3° cap radius, the average block contained 30 observations. The predictions were meaningful in this case also, however, the results were inferior to the 2° radius case. This is an indication to the effect that more distant data points do

2 deg. Mean Anomaly Recovery

SOUTHERN U.S.
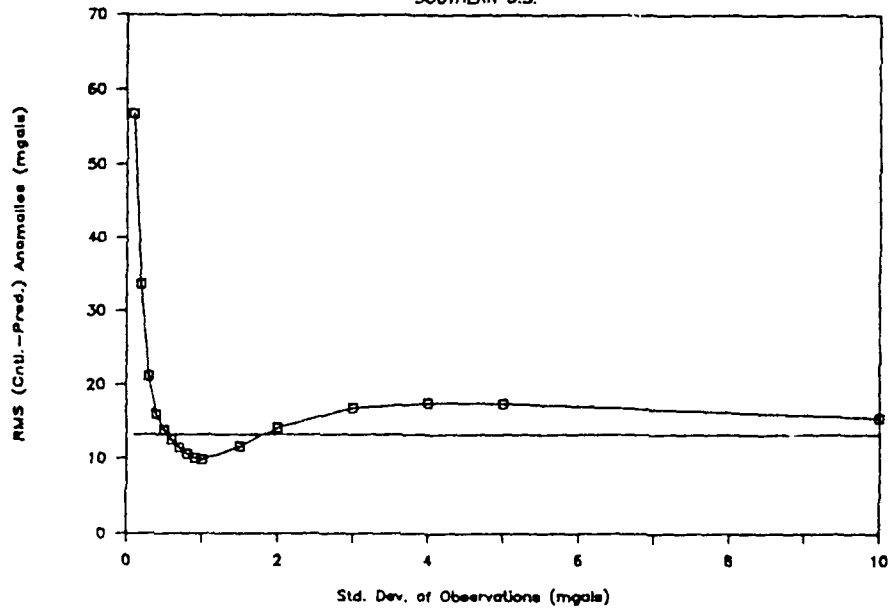
Figure 2.6: RMS differences of control minus predicted 2°
residual mean anomalies as a function of the
observational accuracy.

not necessarily contribute to the estimated mean anomalies.

A recovery attempt in the Southern U.S.. using the OSU86F
implied anomaly degree variances from degree 37 to 180 yielded
very similar results to the ones using the Tscherning/Rapp model.
This came as no surprise due to the following. At first, since
the computed covariances always related quantities at least one
of which was at altitude, only the first 200 anomaly degree
variances of the Tscherning/Rapp model were used. Secondly, the
two degree variance sets do not differ tremendously beyond degree
36.

An effort to perform a prediction at an altitude of 300 km
was not conclusive since the $2°$ mean anomaly signal residual to
GEM-T1 at that altitude was very weak (with average and RMS
values of -0.56 mgals and 1.78 mgals, respectively).

In order to examine the influence of the local gravity
gradient on the quality of the predictions, a similar study was
carried out in the Tonga Trench, in the South Pacific Ocean. The
results of this experiment were very similar to the Southern U.S.
case. Hence, the local gravity gradient appears not to be an
observable feature at the 300 km altitude.

2.5 Conclusions - Recommendations

In this investigation, $2°$ mean anomalies have been predicted
from line of sight accelerations, both residual to GEM-T1. Some
of the significant results of these preliminary simulations are
as follows.

First and foremost, the best possible predictions were
attained at an observational accuracy of 1 mgal. This confirms
the 1 mgal accuracy goal set earlier in the feasibility study.

Secondly, the magnitude of the residual line of sight accelerations seems to indicate that at an altitude of 300 km, the features of the Earth's gravity field beyond degree 36 are attenuated. This implies small improvement in the high frequencies. However, it suggests the usefulness of the STS-GPS system for low degree fields at areas poor in accessibility and/or tracking station coverage. Observations from additional GPS satellites (in addition to the three considered in the simulations here) improved measurement accuracy (say 0.5 mgal) and more data (i.e., about 1 month) will further improve the estimation accuracy.

The data density generated by a mission duration of one week appears to be insufficient. A data cap radius of 1° yielded meaningless predictions. A 2° radius rendered successful estimates and so did a 3° radius. However, the results of the 3° radius were inferior to the ones of the 2° radius, indicating that more distant data points do not necessarily contribute to the predictions.

A similar study at an area with large gravity gradient indicated no difference in the quality of the results.

This investigation answered some questions, but it opened up some new ones. One such issue is the influence of the data density on the quality of the predictions. Is it beneficial to decrease the observational accuracy in favor of the data coverage; i.e., get more data points (shorter integration intervals) but less accurate as compared to 1 mgal. More general areas of insight include examination of the covariance function and application of regularization to the estimator. Furthermore, alternate satellite selection schemes should be tested. Also, similar investigations should be performed for the recovery of 1° anomalies.

REFERENCES

2.1.   Bose, S., G. Thobe, Gravity Field Recovery by Fourier Analysis of Satellite to Satellite Range Rate, Report No. ASA-TR-84-4 Applied Science Analytics, Inc., Canoga Park, CA 91303, 1984; NASA Contract No. NAS5-27743.

2.2.   Colombo, O. L., The Global Mapping of Gravity with Two Satellites, Report of the Geodetic Commission of the Netherlands, Vol. 7, No. 3, Delft, 1984.

2.3.   Hajela, D. P., Direct Recovery of Mean Gravity Anomalies from Satellite to Satellite Tracking, Report No. 218, Dept. of Geodetic Science, The Ohio State University, Columbus, 1974; NASA Grant No. NGR 36-008-161.

2.4.   Hajela, D. P., Recovery of 5° Mean Gravity Anomalies in Local Areas from ATS-6/GEOS-3 Satellite to Satellite Range-Rage Observations, Report No. 259, Dept.of Geodetic Science, The Ohio State University, Columbus, OH, 1977; AFGL-TR-77-0272; ADA 053233.

2.5.   Hajela, D. P., Improved Procedures for the Recovery of 5° Mean Gravity Anomalies from ATS-6/GEOS-3 Satellite to Satellite Range-Rate Observations Using Least Squares Collocation, Report No. 276, Dept. of Geodetic Science, The Ohio State University, 1978; AFGL-TR-78-0260; ADA 063990.

2.6.   Heiskanen, W. A., and H. Moritz, Physical Geodesy, W. H. Freeman, San Francisco, 1967.

2.7.   Kahn, W. D., S. M. Klosko, W. T. Wells, Mean Gravity
        Anomalies from a Combination of Apollo/ATS-6 and GEOS-
        3/ATS-6 SST Tracking Campaigns, J. Geophysical Res., 87,
        2904-2918, 1982.

2.8.   Kahn, W. D., J. W. Sirg, W. T. Wells, Gravity Model
        Improvement, NASA-GSFC, 1977.

2.9.   Kaula, W. M., Inference of Variations in the Gravity
        Field from Satellite-to-Satellite Range Rate, J.
        Geophysical Res., 10, 8345-8349, 1983.

2.10.   Krarup, T., A Contribution to the Mathematical
        Foundation of Physical Geodesy, Publ. 44, Danish
        Geodetic Institute, Copenhagen, 1969.

2.11.   Marsh, J. G., et al., An Improved Model of the Earth's
        Gravitational Field: GEM-T1, NASA Technical Memorandum
        4019, 1987.

2.12.   Moritz, H., Advanced Physical Geodesy, Abacus Press,
        Tunbridge Wells, Kent, U. K. 1980.

2.13.   Pisacane, V. L., S. M. Yionoulis, Recovery of Gravity
        Variations from Satellite-to-Satellite Tracking, Report
        No. SDO 5583 Applied Physics Laboratory, The Johns
        Hopkins University, Laurel, MD, 1980; Contract No.
        N00024-78-C-5384.

2.14.   Rapp, R. H., and J. Y. Cruz, Spherical Harmonic
        Expansions of the Earth's Gravitational Potential to
        Degree 360 Using 30' Mean Anomalies, Report No. 376,
        1986; NASA Grant No. NGR36-008-101.

2.15.   Reigber, C., et al., Study of a Satellite-to-Satellite
         Tracking Mission, ESA Contract Report, Munich, 1987.

2.16.   Rummel, R., Geoid Heights, Geoid Height Differences, and
         Mean Anomalies from "Low-Low" Satellite-to-Satellite
         Tracking - An Error Analysis, Report No. 306, Dept. of
         Geodetic Science, The Ohio State University, Columbus,
         OH 1980;   AFGL-TR-80-0294;   ADA 092707.

2.17.   Rummel, R., D. P. Hajela, R. H. Rapp, Recovery of Mean
         Gravity Anomalies from Satellite-to-Satellite Range Rate
         Data Using Least Squares Collocation, Report No. 248,
         Dept. of Geodetic Science, The Ohio State University,
         Columbus, OH, 1976;   AFGL-TR-76-0291;   ADA 038630.

2.18.   Schwarz, C. R., Gravitational Field Refinement by
         Satellite to Satellite Doppler Tracking, Report No. 147,
         Dept. of Geodetic Science, The Ohio State University,
         Columbus, 1970.

2.19.   Tscherning, C. C., and R. H. Rapp, Closed Covariance
         Expressions for Gravity Anomalies, Geoid Undulations,
         and Deflections of the Vertical Implied by Anomaly
         Degree Variance Models, Report No. 208, Dept. of
         Geodetic Science, The Ohio State University, Columbus,
         OH, 1974;   AFGL-TR-74-0231;   ADA 786417.

2.20.   Upadhyay, T. N., SBIR Program, Phase 1 - FY 1988,
         Project Summary, Mayflower Communications Co., Inc.,
         Wakefield, MA   01880, 1987.

2.21.   Vonbun, F. O., W. D. Kahn, J. W. Bryan, P. E. Schmid, W.
         T. Wells, T. D. Conrad, Gravity Anomaly Detection from
         ATS-6/Apollo-Soyuz, 1975.

2.22.   Weiffenbach, G. C., M. D. Grossi, P. W. Shores, Apollo-
         Soyuz Doppler Tracking Experiment MA - 089, SAO, 1976.

2.23.   Wichiencharoen, C., Recovery of 1° Mean Anomalies in a
         Local Region from a Low-Low Satellite-to-Satellite
         Tracking Mission, Report No. 363, Dept. of Geodetic
         Science, The Ohio State University, Columbus, OH, 1985;
         NASA Grant No. NGR-36-008-161.

2.24.   Wolff, M., Direct Measurements of the Earth's Gravity
         Potential Using a Satellite Pair, J. Geophysical Res.,
         14, 5295-5300, 1969.

SECTION 3

EXPERIMENT SYSTEM HARDWARE

This section presents the results of a cost/performance trade-off analysis to select candidate hardware subsystems for the STAGE experiment. Preliminary specifications on each of the subsystems were developed and size, power, weight and cost data from the equipment manufacturers was obtained. These size, power and weight estimates were used in the experiment payload integration analysis, the results of which are described in Section 6.

The experiment instrumentation system consists of a GPS receiver, an inertial measurement unit (IMU), a microprocessor control system, and a tape recorder. The GPS receiver will measure the Shuttle line-of-sight acceleration (acceleration is estimated from line-of-sight pseudo-range and delta range measurements) to the selected set of 3 or more GPS satellites. The inertial measurement unit will measure the translational and rotational dynamics of the Shuttle and compute the (non-gravitation) Shuttle acceleration. The microprocessor control system will control the operations of the GPS receiver (i.e., select the appropriate top or bottom antenna), the IMU (i.e., set the full scale on the accelerometer to correspond to the on-orbit dynamics), and the tape recorder (i.e., set the recording speed), and will be used to interface with a control and display system. The microprocessor system will also be used, if required, for data compression prior to storing the data on the recorder. In what follows, preliminary specifications on each of these subsystems are discused and the results of the industry survey, in terms of available hardware, are summarized.

It should be emphasized here that the STAGE experiment data will be collected only during the on-orbit phase of the Shuttle

flight. The power to the experiment will be turned-off during the lift-off and landing phases of the flight, therefore the specification does not call for operation of the equipment (except for survivability) during these phases.

3.1 GPS Receiver Unit

This section presents a preliminary specification and results of the industry survey for a GPS receiver for the STAGE experiment.

3.1.1 Preliminary Specification

The preliminary specification on the STAGE experiment GPS receiver requires a 5-channel P-code receiver with L_1/L_2 tracking to correct for the ionospheric errors. The multi-channel capability (in contrast to a single channel multiplex receiver) allows the receiver to simultaneously track GPS signals from several satellites. This capability is crucial for the present application since the cancellation of satellite clock errors in the double-difference processing technique (see also Section 4) relies on this fact. The number of parallel receiver channels required should b: at least three for the Shuttle acceleration estimation, a fourth channel measurement is required to solve for receiver clock time bias and drift. The fifth channel is required to sequentially track the same satellite on L_2. Ideally, one would like to have simultaneous continuous tracking of L_2 signals in order to minimize the effect of ionospheric errors, but sequential tracking of L_2 signals is considered acceptable since ionosphere effects are not expected to change significantly over few seconds.

The receiver measurements of code phase (pseudo-range) and

integrated carrier doppler phase (delta-range) from all
satellites being tracked should be available once per second.
The 1-sigma rms code phase and carrier phase errors over 1 second
should be less than 0.5 meter and 2 mm, respectively. The
uncalibrated interchannel bias error due to all effects should be
less than 0.5 m. Even though the STAGE experiment is a post-
mission data processing application, the GPS receiver processor
should implement the real-time navigation function for display
purposes and for consistency check. The navigation solution
should be output at least once per minute. Since the receiver
measurements will be recorded for the entire flight, no interface
to the Shuttle telemetry is required.

Finally, the candidate GPS receiver should have the
capability to track GPS signals on either (and preferably both)
of the two GPS antennas on the Shuttle. This last requirement
will provide continuous tracking capability regardless of the
Shuttle orientation. The above specifications are summarized in
Table 3.1.

3.1.2 GPS Receiver Availability

This section summarizes the results of an industry survey
carried out in early 1987 to select a candidate GPS receiver for
the experiment. We contacted four receiver manufacturers: Texas
Instruments, Rockwell International, Magnavox, and Motorola. The
result of this survey is summarized in Table 3.2. A comparison
of the data, using the cost as a criterion, excludes Rockwell
International's spaceborne GPS from the list because of its high
cost. [Since this survey, however, Rockwell Autonetics Division
has been selected by TRW to develop a GPS receiver for the NASA
OMV spacecraft and we estimate the cost now to be in the ballpark
of other manufacturers].

Table 3.1: STAGE Experiment GPS Receiver Specification (Preliminary)

Receiver Mode/ Function	Performance/Capability
Space Qualification	Desirable but not required
Number of Channels	5 parallel channels
Signal Tracking	P-code, L_1 and L_2
Data/Measurements	Code phase (pseudo-range), carrier doppler phase (delta-range), receiver status, mode, ephemerides, signal-to-noise power ratio, navigation solution

Data Rate
  raw measurements
  receiver status/C/No
  navigation solution
  ephemerides
	
	1 per second from all SVs
	1 per minute
	1 per minute
	as needed

Measurement Accuracy
  code phase
  carrier phase
  uncalibrated bias
	
	0.5 m (1-sigma)
	2 mm (1-sigma)
	0.5 m

Track Multiple Antennas	Yes
Size, Power and Weight	size $\approx$ 500 cu in power $\approx$ 50 watts weight < 50 lbs

**Table 3.2: Candidate GPS Receiver Hardware
for STAGE Experiment**

Manufacturer	# Ch	RAM	Space Qual.	Size WxLxH (in)	Power Watts	Weight lbs	Cost $ M
MOTOROLA TOPEX GPSDR[1]	5-ch simult	yes	yes	6x16x6	40 w	20 lbs	$ 1 M
MAGNAVOX GPSPAC[2] Mod. GPSPAC[2]	2-ch (seq)	yes yes	yes yes	8x16x12 8x8x12	45 w 20 w	43 lbs 20 lbs	$ 0.75 M $ <1 M
TEXAS INSTRUMENTS TI 4100 TI 440	1-ch 1-ch (mux)	yes yes	no no (MilSP)	17x11x8 4.8x7.6x12	50 w 85 w (I²L)	50 lbs 19 lbs	$ <1M $ 1-2 M
ROCKWELL Spaceborne GPS	1-ch (seq)	yes	yes	7.5x11x7.6	27 w	24 lbs	$ 5 M (first) $0.6 - 0.7 M

Cost estimates are informal ROM,

(1)   Development contract awarded by JPL, cost for second unit,
(2)   Cost for second unit only, otherwise GPSPAC is $1.4-1.7M.

Except for the Motorola's TOPEX GPS receiver, all other receivers have limited capability (1 or 2 sequential/multiplex) and do not meet our specification. Magnavox has offered to modify their GPSPAC receiver which has successfully flown on the LANDSAT satellites. Texas Instruments proposed their 1-channel multiplex design (TI 4100 or a militarized version TI 440). From a performance and cost viewpoint Motorola's TOPEX GPSDR receiver offered the best solution for the present application. Furthermore, the TOPEX GPSDR receiver is space qualified, which is an added plus. For the above reasons, the Motorola's receiver was selected as a candidate for the experiment feasibility study.

A preliminary packaging diagram of this receiver is shown in Figure 3.1.

3.2 Inertial Measurement Unit

This section presents a preliminary specification and results of industry survey for an IMU for the STAGE experiment. The industry data was collected by R.G. Brown Associates, Inc. under a subcontract from Mayflower Communications.

3.2.1 Preliminary Specification

The on-orbit Shuttle dynamics environment and general requirements on the accelerometer and gyro for the experiment IMU is presented in Table 3.3.

For the above Shuttle environment and based on the error budget a preliminary set of specifications for the experiment IMU was developed. These specifications are contrasted with the Shuttle IMU specifications in Table 3.4 below.
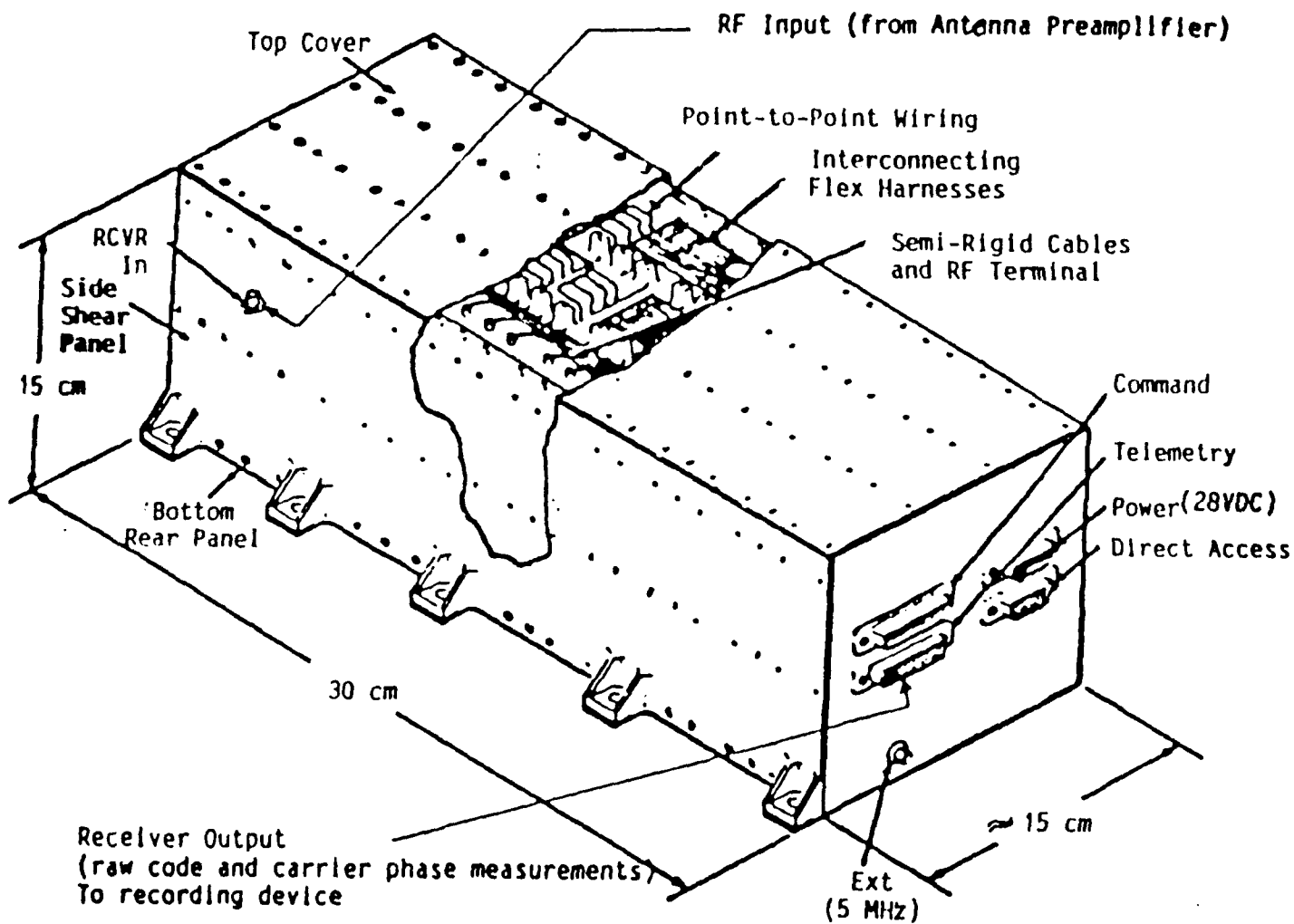
Figure 3.1   Preliminary Packaging Diagram of Motorola's
TOPEX GPS Receiver (courtesy of Motorola)

TABLE 3.3: **Nongravitation Shuttle Environment and Inertial Requirements**

Dynamics Environment	
Primary and Vernier Thrusters Outgassing Crew Activities Drag: 0.6 to 1 micro g	
Primary Thrusters ≥	≈ 8 - 10 mg angular acceleration ≈ 2 mg[1] translational acceleration
Vernier Thruster ≥	0.4 mg (for short time 80 msec) to 4 mg (0 . 02°/sec² over 40 ft lever arm) due to lever arm and angular acceleration 0.2 mg/axis translational acceleration

IMU ACCELEROMETER	
Measure	≈ 1 mg (typical), 10 mg (max) ~ 1 mg with an accuracy of 0.1 micro g alignment stability 20 arc sec; scale factor 100 ppm

IMU GYRO	
Angular Rate	= 4°/min = 4 arc min/sec
Drift Rate	= 0.0036°/hour = > 20 arc sec in one STS orbit (≈ 1.5 hr)
Random Noise	= 0.005°/√hr
Scale Factor	= 15 ppm => 20 arc sec in one STS orbit

[1] mg = mili-g

Table 3.4   STAGE Experiment IMU Instrument
Specification (Preliminary)

Instrument	Experiment IMU (Strapped-down)	Shuttle IMU (Gimballed)
Application	on-orbit phase only	entire shuttle flight
Space Qualificatn.	not required	not required
Gyro bias drift	0.004°/hr	0.05°/hr
Gyro scale factor	5 ppm	1700 ppm
Gyro random walk	0.001°/hr	–
ACCELEROMETER		
Accelerometer bias	10 micro-g with 0.1 micro-g stability	
Temperature sensitivity	0.25 micro-g/°F	
Scale Factor	500 ppm	
Misalignment	< 200 arcsec (with transfer alignment)	70 arcsec (star tracker update)

From the above table we observe that the experiment IMU gyro has about an order of magnitude lower bias drift and significantly lower scale factor error as compared to the Shuttle IMU. The reason for this requirement is that the experiment IMU has to keep the alignment error to within 1 mrad (in between the transfer alignment from the Shuttle IMU) without a direct star tracker update. The accelerometer specifications are also tight, specifically the bias stability and the bias temperature sensitivity, because of the overall requirement to contain the IMU acceleration measurement error to substantially below 1 micro-g (see also Section 4: Measurement Error Analysis).

3.2.2 Experiment IMU Availability

A survey of qualified inertial instrument manufacturers was conducted by R.G. Brown Associates under Mayflower supervision. Two inertial systems, a Northrop NAS-21A Stellar Inertial System and Litton LN-20, with self-contained star trackers, were analyzed to keep the alignment error within the specifications. Both of these systems use a gimbal platform and meet our alignment specification but were eliminated early-on because they would require major modification to the Shuttle to integrate their star trackers. The payload integration analysis (see Section 6) eliminated this configuration because of its higher hardware cost and integration cost. The selected IMU configuration is a strapped down IMU, which will keep the alignment error low by employing a Shuttle-IMU-to-experiment-IMU transfer alignment technique (see Section 5 for details on the transfer alignment technique).

The IMU instruments for the selected strapped down configuration consists of ring laser gyros and precision accelerometers. Based on the results of the industry survey, the Honeywell advanced ring laser gyro RLG 1342 was selected as the candidate gyro for this application. The RLG 1342 gyro's performance meets the current specification with substantial margin: gyro bias drift = $0.002°/hr$ (3 sigma) and gyro scale factor = 2 ppm (3 sigma). For the experiment accelerometer, two candidates were evaluated: a Bell Aerospace Miniature Electrostatic Accelerometer (MESA) and a modified version of an earlier space configured triad from Sundstrand. Characteristics of these two accelerometers are summarized below in Table 3.5

3-10

**Table 3.5 Candidate Accelerometer Instruments for
the Stage Experiment IMU**

| Manufacturer	Full Scale	Resolution	Space Qual.	Size Inch	Power Watt	Weight lbs.	Cost $
Sunstand* Q-flex, single-axis unit	3 g	10^7	yes	2.5x2.5	0.3	0.2	100K
Bell MESA 3-axis unit	1 10 milig** 2 1 milig 3 100 micro-g	10^8	yes	5x9x4	9	5	500K

* Sundstand unit will be developed under R&D, not yet available; Bell MESA is available as a product

** range (1,2 or 3) selectable by the user

The data in Table 3.5 clearly demonstrates the superior performance of the Bell MESA unit. The advantages of Bell MESA over Sundstrand Q-flex unit are its higher level of performance and low-risk (product availability) proven technology. Even though the estimated cost is higher than the Sundstrand Q-flex accelerometer, it is still recommended for the experiment because of its proven technology. The Sundstrand accelerometer will represent a higher risk to the experiment.

The Bell MESA accelerometer and the Honeywell RLG-3142 will be used to develop the strapped-down experiment IMU. The accelerometer will be mounted on a Motor Table System (MTS), similar to the NASA OARE (Orbiter Acceleration Research Experiment), for on-orbit calibration of the accelerometer bias and scale factor errors. A preliminary packaging diagram of the experiment IMU is shown in Figure 3.2. An alternate concept which will eliminate the MTS is under investigation.

IMU With Precision Accelerometer*
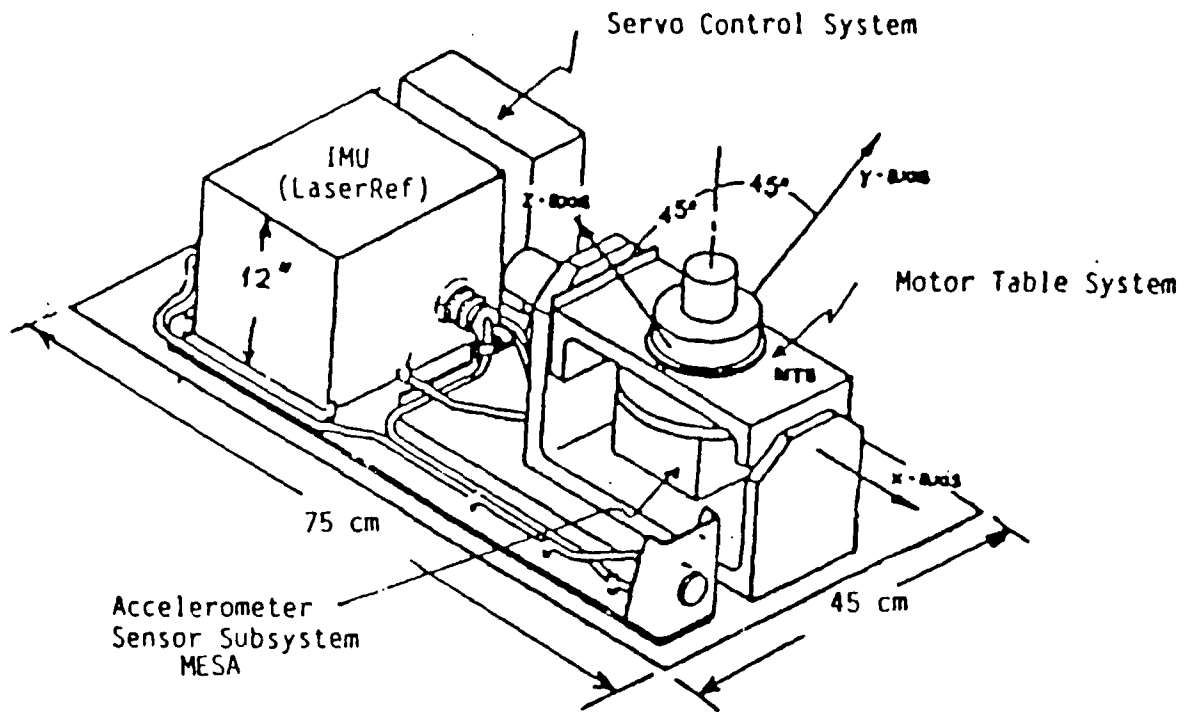
Figure 3.2   Preliminary Packaging Concept
for the STAGE Experiment IMU

3.3 Data Receiver

Preliminary calculation of the amount of experiment data
that will be stored indicate a requirement of about 1 to 2K
bytes/sec. The experiment data will include GPS receiver
measurements from three or more satellites per second, receiver
status including signal-to-noise power ratio, ephemerides data,
navigation solution including filter gain and covariances every
minute, gyro delta-Θ and accelerometer delta-v measurements once
per second, direction cosine matrices (or quaternions) once per
second, timing data and other data of interest for simplifying
the post-mission processing. The above data will be recorded for

a period of up to five days. An important requirement on the selection of the data recorder is driven by the concern to minimize the Shuttle crew interface. This requirement led us to the selection of Data Tape's MARS Tape Recorder Model 1428. The MARS tape recorder has successfully flown on previous Shuttle missions and is an off-the-shelf product.

At a tape speed of 1 7/8 inch/second (selectable), the MARS tape recorder can record up to 30K bits/sec ≈ 4K bytes/sec, which meets the experiment data rate requirement of 1-2K bytes/second. At this speed one 14" tape (9200 feet) on MARS 1428 with sequential recording will last for 0.3 to 0.5 day per track - a total of 28 tracks will support a mission of up to 15 days. This analysis suggested that one 14" tape on MARS 1428 will support the data recording requirements of the experiment for the entire Shuttle flight without the need for changing the tape.

3.4 Summary

This section has presented the results of industry survey to select candidate GPS, IMU and data recorder subsystems for the experiment. A preliminary set of performance specifications for these subsystems was presented. The candidate hardware subsystems are:

1. GPS Receiver   - modified Motorola TOPEX GPSDR

2. IMU   - Honeywell LaserRef (strapdown) system
                     with RLG1342 gyros and Bell MESA
                     Accelerometer

3. Recorder   - Data Tape MARS 1428 Tape Recorder

A size, power and weight estimate for the selected hardware system configuration is given below in Table 3.6.

TABLE 3.6 EXPERIMENT HARDWARE SIZE, POWER, WEIGHT BREAKDOWN

Hardware Module	Size Cu inch	Power Watts	Weight lbs	Cooling
GPS Receiver	6"x6"x12"	35 W	14 lbs	Air Cooled
Inertial Measurement Unit (IMU)	17"x30"x12"	180 W	120 lbs	Heat Sink
Tape Recorder	23"x16"x7 1/2	115 W	57 lbs	Air Cooled
Processor	18"x12"x8"	50 W	30 lbs	Air Cooled

SECTION 4

MEASUREMENT ERROR ANALYSIS

The results of an error analysis for the experiment GPS and IMU subsystems are described in this Section. The purpose of the error analysis was to estimate the effect of primary GPS and IMU measurement errors on the Shuttle acceleration estimation accuracy and identify those errors which, if not removed, will prevent the Air Force STAGE experiment from meeting its accuracy goal of 1 mgal (per axis). In particular, the effects of Shuttle-GPS geometry, the GPS orbit error, the GPS satellite clock and receiver measurement noise, and IMU instrument errors on the Shuttle acceleration error are analyzed here. The latter part of this Section (Section 4.2) identifies the critical measurement errors and discusses the processing techniques that can be employed to mitigate the effect of these errors.

4.1   Error Analysis

4.1.1   Shuttle-GPS Geometry

For low earth orbit space vehicles, like the Shuttle, the line-of-sight between the spacecraft and GPS satellites changes rapidly. The Shuttle visibility to a GPS satellite depends, amongst other things, on the antenna look angle, i.e., angle coverage from zenith into which the antenna would attempt to acquire and/or track GPS satellite signals. It has been shown, [Klein and Parkinson, 1984 [4.6]] that the error in the estimate of Shuttle position using GPS is directly proportional to a quantity, called GDOP (Geometric Dilution of Precision), which is defined as a function of the line-of-sight vectors from the user

to the selected set of four GPS satellites. The GDOP is defined as:

$$GDOP = tr \ [A^TA]^{-1} \qquad (1)$$

The matrix A is 4 x 4 matrix consisting of

$$A = \begin{bmatrix} \underline{p_1} & 1 \\ \underline{p_2} & 1 \\ \underline{p_3} & 1 \\ \underline{p_4} & 1 \end{bmatrix} \ 4 \times 4$$

where p_i is a unit line-of-sight vector from the Shuttle to the ith GPS satellite. The GDOP factor takes into account the geometric observability of the measurement errors on to the errors in the Shuttle position and GPS/receiver clock timing estimate. If the user clock timing estimation error was not to be included then we define a quantity, called PDOP (Position Dilution of Precision), which is similar to equation -1 expect that the trace operation is for the top 3 x 3 subset of $[A^TA]^{-1}$.

The navigation position estimate is given by

$$\delta \underline{r} = (A^TRA)^{-1} \ A^TR\varrho \qquad (2)$$

where R is the variance of the measurement noise and ϱ is the range measurement vector.

Since PDOP directly affects the position estimation error, we would be interested in observing the variations in PDOP for the Shuttle orbit. This quantity was computed by simulating the GPS satellite constellation and the Shuttle orbit. For this study, an 18-satellite GPS constellation was utilized to study the dependence of geometry on the propagation of measurement

errors into acceleration estimate. The orbit parameters of the 18-satellite constellation are given in Table 4-1.

Table 4-1 - Symmetric 18 Satellite Constellation (18/6/3)

Satellite Number	Longitude of Ascending Node*	Argument of Latitude*
1	0 deg	0 deg
2	0	120
3	0	240
4	60	40
5	60	160
6	60	280
7	120	80
8	120	200
9	120	320
10	180	120
11	180	240
12	180	360
13	240	160
14	240	280
15	240	40
16	300	200
17	300	320
18	300	80
Spare #1	0	30
Spare #2	120	170
Spare #3	240	310

* At Epoch

Period = 11 hr. 58 min. = 43,080 sec.

Inclination = 55 deg.

Eccentricity = 0

With the above 18-satellite constellation [Klein and Parkinson, 1984 [4.6]] and a circular Shuttle orbit of 296 km (160 nmi) altitude and 28.5 degree inclination [Profumo, 1987 [4.7]], the PDOP for different antenna look angles was computed. The antenna look angle was varied between 90° to 110° with 10° increments. It should be noted that increasing the angle increases 'geometric' visibility (lower PDOP) but decreases received signal-to-noise power ratio at the receiver input because of the lower antenna gain at low elevations. Therefore, an optimum value is selected which offers the best trade-off between these two effects on GPS receiver performance. From the data we observe that a 100° look angle eliminates large PDOP values (i.e., PDOP larger than 6) and offers 25% improvement in PDOP over 90° look angle. Plots of PDOP for the 90° case and 100° case are shown in Figure 4.1 and 4.2 respectively. The data is plotted for about 100 minutes (slightly longer than one Shuttle revolution).

The value of PDOP and its three components along the three principal axes, i.e., radial, along-track and cross-track were computed for the selected visibility criterion of 100° look angle. The PDOP components for this case are plotted in Figures 4.3 through 4.5. The largest component of PDOP is along the radial direction. The effect of these geometric quantities on the Shuttle position estimation and, therefore, Shuttle acceleration estimation is discussed next.

4.1.2 GPS Orbit Errors

In this analysis the error sources affecting the GPS ephemerides are propagated through the ephemerides into the estimated Shuttle (STS) positions. It is postulated that GPS
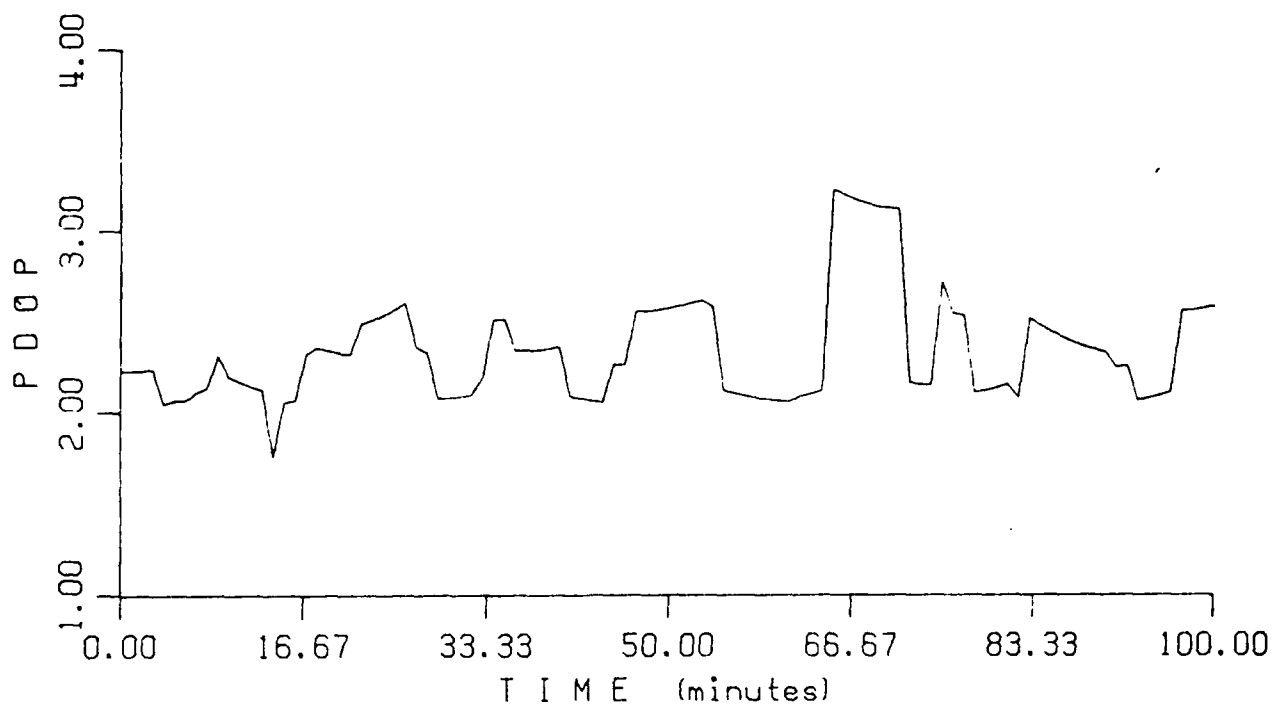
Figure 4.1 Plot of PDOP for the STAGE Experiment
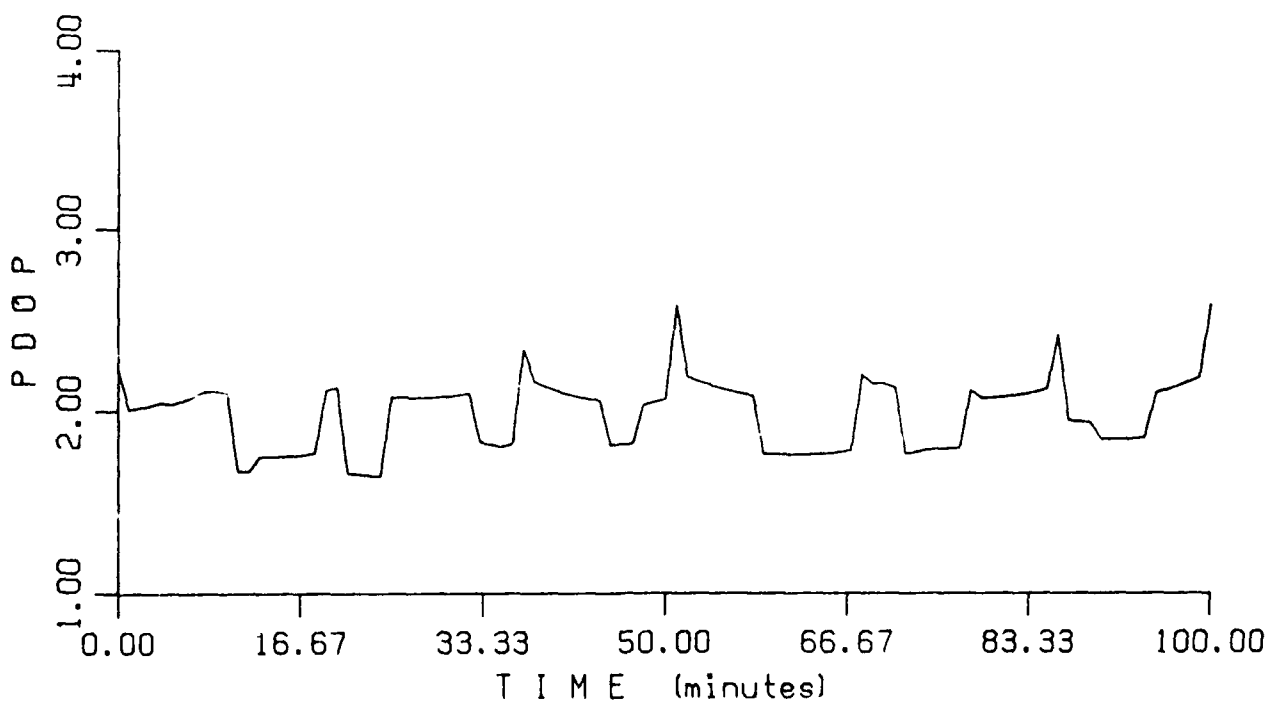for antenna look angle of 90 degrees

Figure 4.2 Plot of PDOP for the STAGE Experiment
for antenna look angle of 100 degrees

ephemerides will be determined using phase tracking data. The
effect of major systematic error sources on GPS orbit accuracy
was analyzed by EG&G using the ORAN simulations [Martin and
McCarthy, 1987 [4.8]]. These error sources and their effect on
the Shuttle position and acceleration estimation error in each
axis, i.e., radial, along-track, and cross-track was analyzed.
The largest component of the acceleration errors due to GPS orbit
errors is summarized in Table 4-2.

Table 4-2: Effect of GPS Orbit Errors on the
Shuttle Acceleration Estimation
(Largest Component)

Error Term	Magnitude	Shuttle Acceleration Estimation Error (mgal)
Geopotential Field	0.4 (GEM5-GEM7)	0.01-0.04
Solar Radiation Pressure	1% error	0.1 -0.28
Geocentric Gravitational Constant (GMe)	0.005 km³/sec²	0.1 -0.35
Tracking Station Location Errors	10 cm in each station coordinate	0.05-0.15
RSS		$\approx$ 0.15-0.47 mgal

The range of values in Table 4-2 reflects the variations in
these quantities over one Shuttle revolution. The effects of GPS
receiver measurement noise (white noise) and the GPS satellite
clock error (white noise in frequency) on the Shuttle
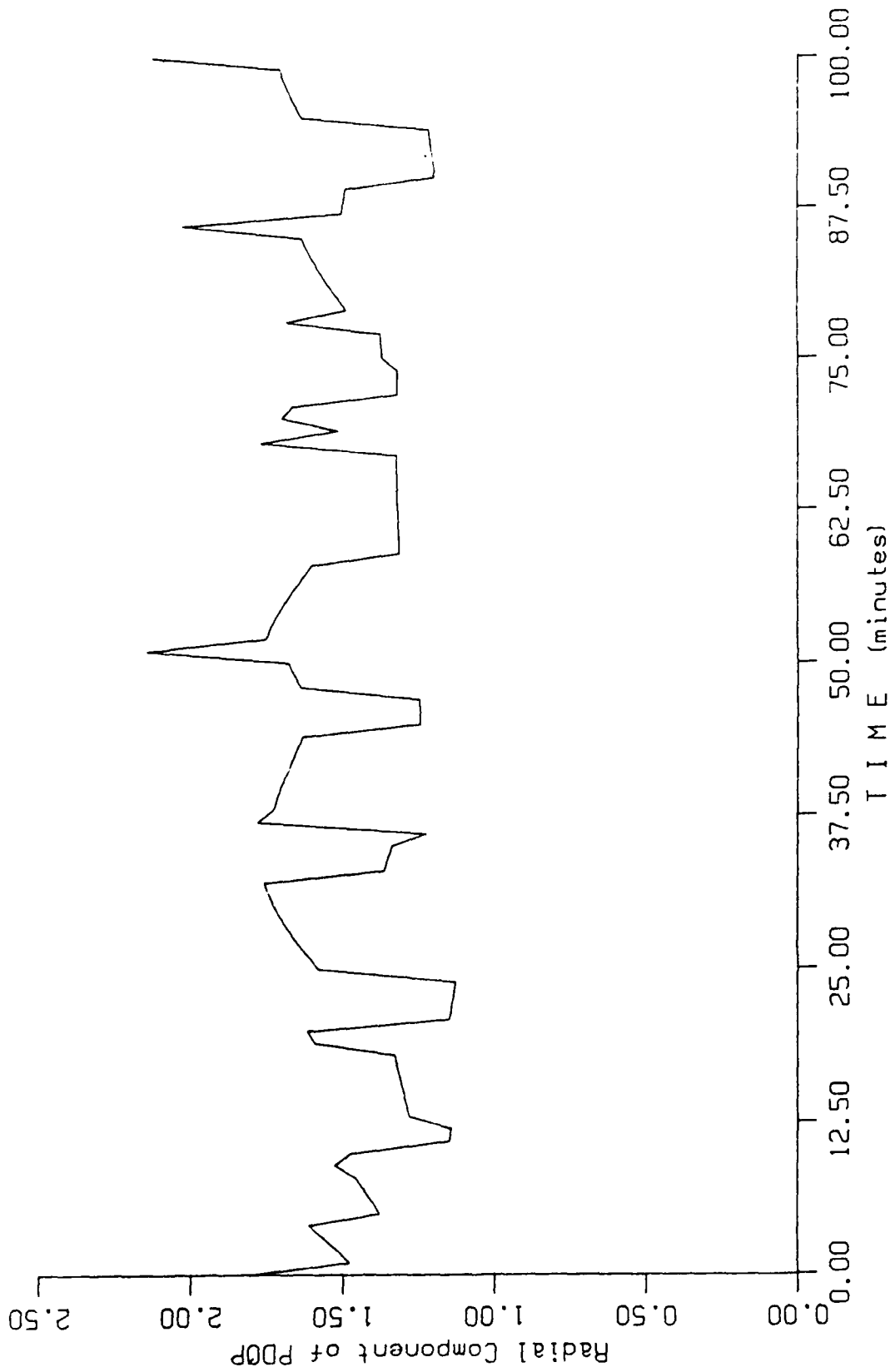acceleration estimation are discussed in the next section.

Figure 4.3 Radial component of PDOP for the STAGE Experiment
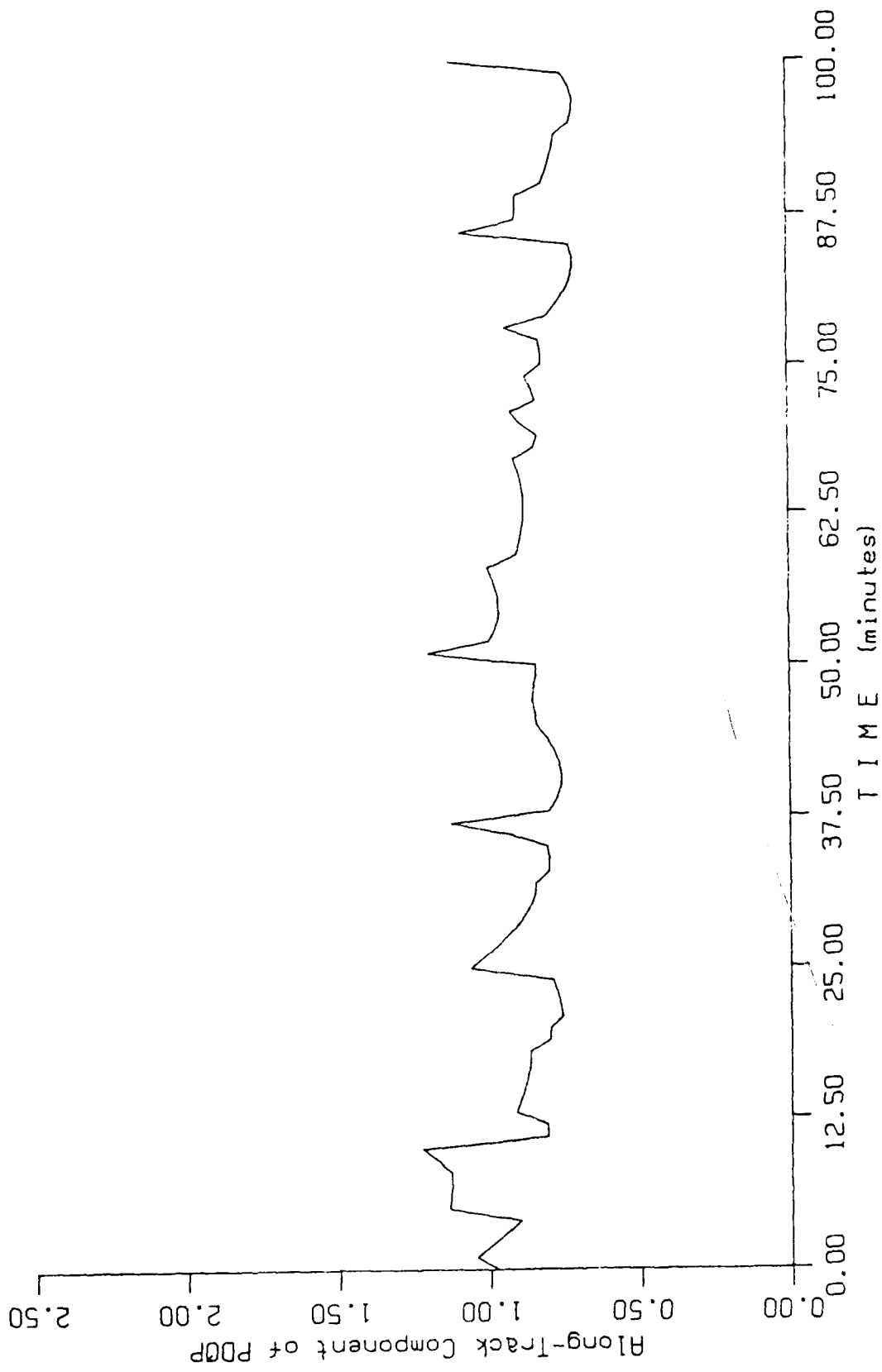for antenna look angle of 100 degrees

Figure 4.4 Along-track component of PDOP for the STAGE Experiment
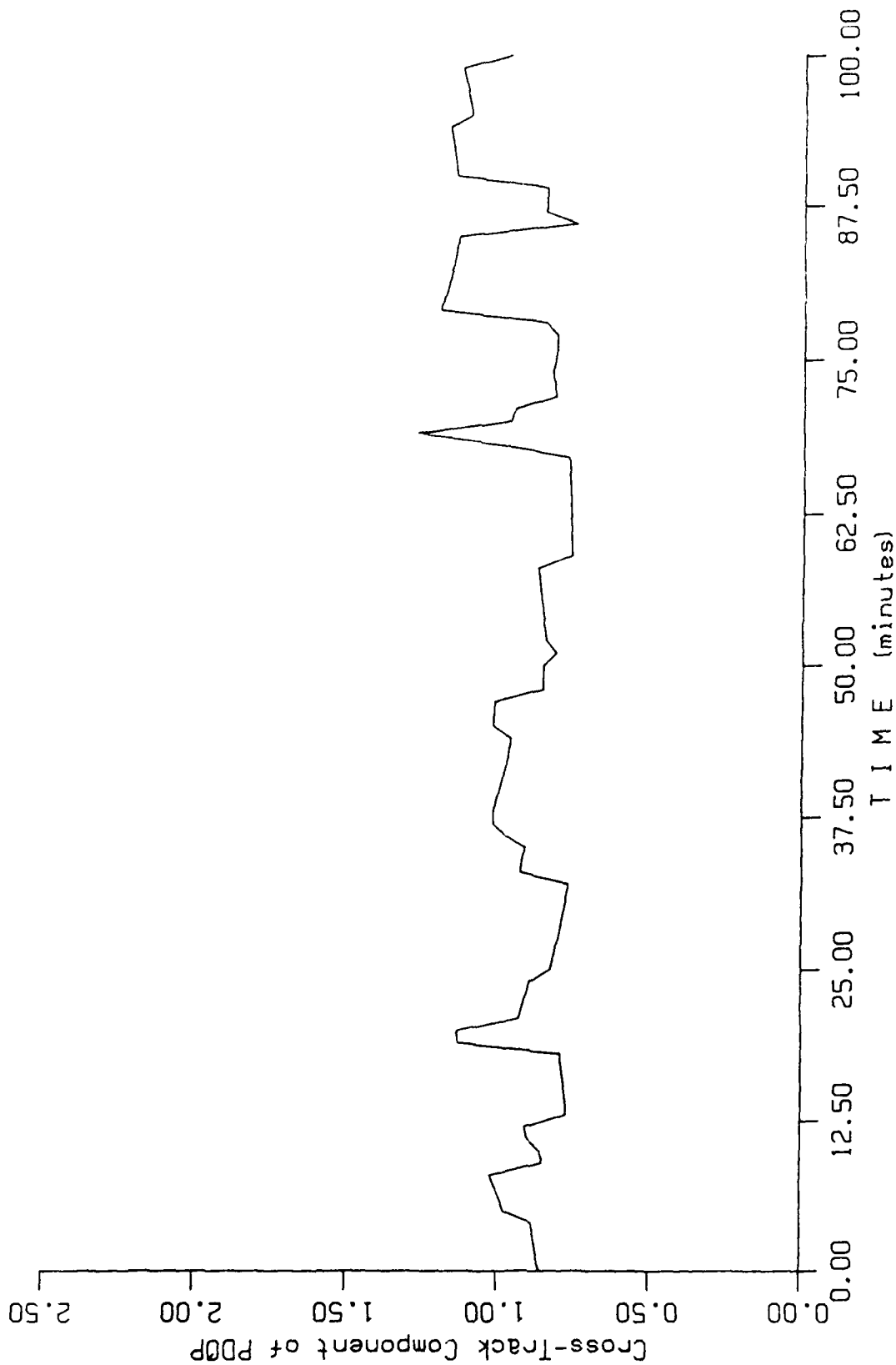for antenna look angle of 100 degrees

Figure 4.5 Cross-track component of PDOP for the STAGE Experiment
for antenna look angle of 100 degrees

4.1.3 GPS Measurement Errors

The GPS measurement errors discussed in this section are :
(1) carrier phase measurement noise and bias error (due to e.g.,
incomplete carrier phase ambiguity resolution), and (2) GPS
satellite clock frequency error. The effects of these errors are
analyzed in terms of their contribution to the Shuttle position
estimation error. The Shuttle position estimation accuracy
relates to these errors through the PDOP, which was discussed in
Section 4.1.1. The larger the PDOP, the larger the effect of
these errors on the position estimation error. The acceleration
estimation error was obtained by a quadratic fit in time to the
position errors over some interval, i.e.,

$$\delta r (t) = a_0 + a_1 t + a_2 t^2 \tag{3}$$

The coefficients a_0, a_1 and a_2 are computed through a least-
squares fit to the smoothed position errors. We note here that
the acceleration error is twice the error estimate in a_2.

The derivations for the acceleration error estimates are detailed
in [Martin and McCarthy, 1987 [4.8]]. If the interval between
measurements is 1 second then the variance of the acceleration
error due to receiver measurement noise is:

$$var(\delta \hat{a}_2)_{noise} = \frac{30}{n(n+1)(2n+1)(3n^2+3n-1)} \sigma_{noise}^2 \cdot PDOP \tag{4}$$

for σ_{noise} = 6 mm (3 times the raw measurement noise of 2mm, the
factor 3 accounts for increased noise due to L_1/L_2 ionospheric
correction), we obtain the receiver measurement noise induced
acceleration error to be:

$$var (\delta \hat{a}_2)_{noise} = (0.27 \times 10^{-6} \text{ m/sec}^2)^2 \cdot PDOP, \quad n = 75 \text{ sec}$$

$$\sigma \text{ (estimation error) }_{noise} = 0.055 \cdot \text{PDOP mgal}$$

We note here that the above computation reflects the worst-case (when L_1 and L_2 measurements are used simultaneously for ionospheric correction) since the ionospheric corrections will be done less frequently than 1 per second. Hence, most of the time the acceleration errors will be 1/3 of the above quantity. These results indicate that measurement noise is not a major error source in the 1 mgal error budget.

An analysis of the satellite clock effects on the acceleration estimation error leads to the following result:

$$\text{var}(\delta \hat{a}_z)_{clock} = \frac{15}{7} \frac{(15n^4 + 30n^3 + 21n^2 + 6n - 2)}{n(n+1)(2n+1)(3n^2 + 3n - 1)} (c^2 N_o) \text{ PDOP} \qquad (5)$$

where c is the speed of light (approximately 3×10^8 m/s) and Noise the satellite clock noise spectral density which is related to the clock Allan variance by

$$\text{(Allan Variance)}_{clock} = \frac{N_o}{\tau} \qquad (6)$$

where τ is the averaging interval. Taking the value of 1.2×10^{-23} /τ for the clock Allan variance, which is lower than the specification value by a factor of 100, we obtain via (6) that N_o = 1.2×10^{-23}. Substituting N_o and c in equation (5) we get

$$\text{var}(\delta \hat{a}_z)_{clock} = (2.117 \times 10^{-6} \text{ m/sec}^2)^2 \cdot \text{PDOP}, \qquad n = 75 \text{ sec}$$

or

$$\sigma \text{ (acceleration)}_{clock} = 0.432 \cdot \text{PDOP mgal}, \qquad n = 75 \text{ sec}$$

$$= 0.153 \cdot \text{PDOP mgal}, \qquad n = 150 \text{ sec}$$

The above result indicates that the acceleration error induced by the satellite clock is a significant contributor to the total experiment error budget of 1 mgal. This result was obtained by using the value for the clock Allan variance which assumes that a significant part of the clock errors (a factor of 100 reduction) can be compensated by post-processing of the GPS ground tracking data with the Shuttle GPS tracking data.

The short-term variations in the satellite clock error were analyzed and were determined to be observable in the ground tracking GPS data. To this end, we analyzed the clock Allan variance computed from the ground tracking data and compared it with the clock Allan variance computed from the in-plant test data for several cesium and rubidium clocks. This comparison clearly demonstrated the observability of the short-term clock behavior in the ground tracking data. From this analysis, it was determined that a factor of 100 reduction in Allan variance can be realized. This reduction was factored in the above clock error induced acceleration error. The details of the analysis and evaluation are described in Section 4.2.

The Shuttle acceleration estimation error induced by the satellite clock (the largest component) is plotted in Figure 4.6 for 5° averaging (n=75 sec) and 10° (n=150 sec), averaging intervals, respectively. The effect of receiver measurement noise on the acceleration error is plotted in Figure 4.7 for a 5° and for a 10° averaging intervals. The effect of receiver measurement bias error of 0.5m on acceleration estimation error was determined to be between 0.05 to 0.15 mgal.
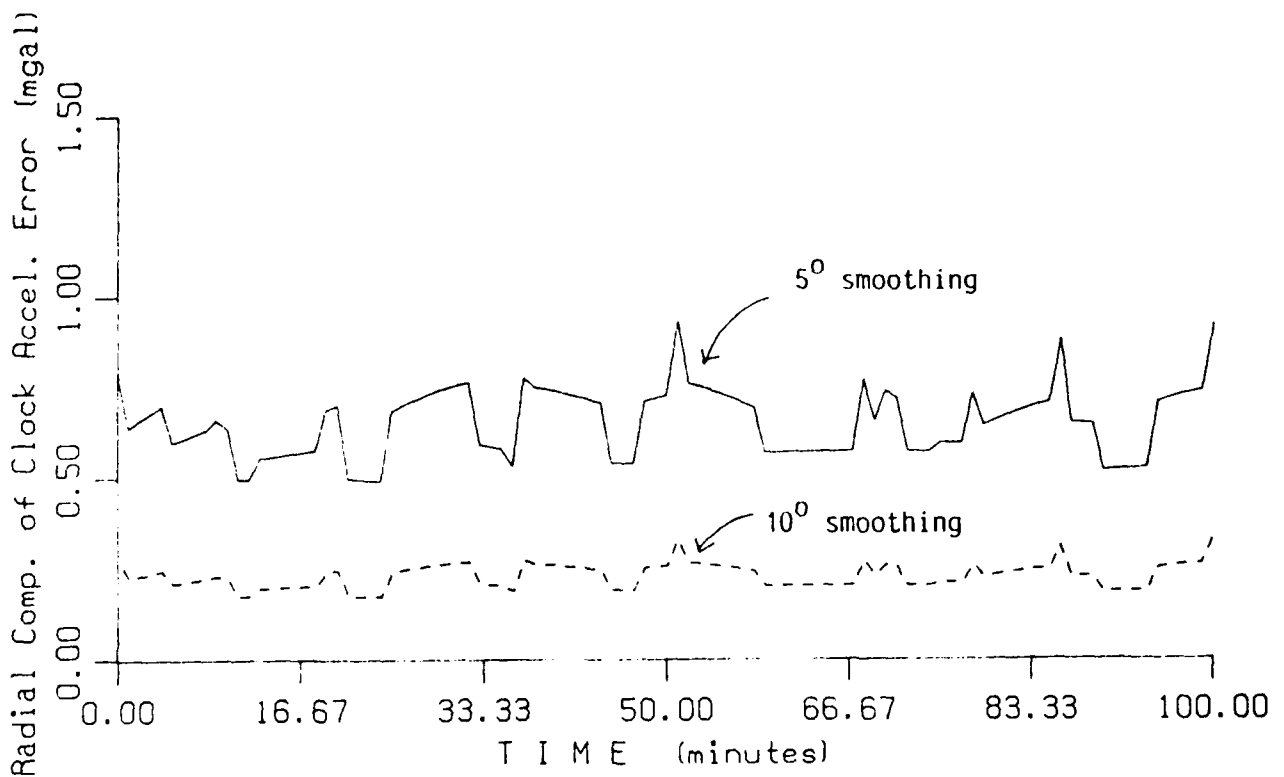
Figure 4.6 Radial component (largest) of the shuttle acceleration error due to the GPS satellite clock for a 5^0 and 10^0 averaging interval (75 and 150 seconds)
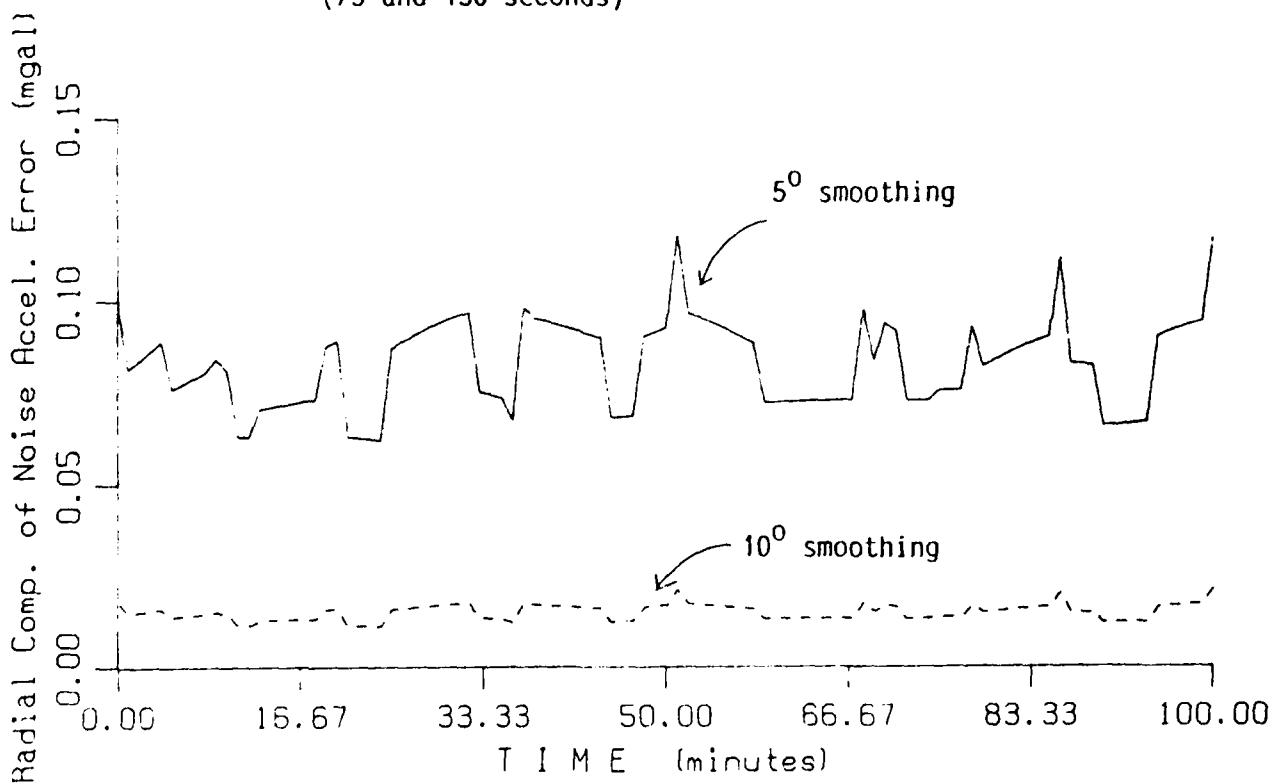

Figure 4.7 Radial component (largest) of the shuttle acceleration error due to the receiver measurement noise for a 5^0 and 10^0 averaging interval

4-13

These results indicate that the GPS satellite clock errors
even after the assumed two order of magnitude compensation are a
significant contributor to the overall acceleration estimation
error budget of 1 mgal. Recent results indicate that post-
interferometric processing (double difference) of the Shuttle GPS
measurements and ground station GPS measurements would further
reduce the effect of this error significantly and therefore,
improve the total measurement accuracy of the STAGE experiment.
These results are documented in [Upadhyay et al, 1989 [4.3]].

4.1.4 IMU Instrument Errors

As discussed earlier in Section 2 an inertial measurement
unit (IMU) onboard the Shuttle will measure the nongravitational
accelerations. The IMU consists of a 3-axis high precision
accelerometer assembly and a set of 3 gyros to measure the
translational and rotational dynamics, respectively. An
evaluation of the Shuttle on orbit dynamics environment has
resulted in an assessment that the acceleration level to be
measured by the STAGE experiment IMU is less than 200 micro-g
(about 170 micro-g). Assuming that the experiment IMU can be
aligned (with respect to inertial space) to an accuracy of about
1.4 mrad (recent simulation results indicate than an accuracy of
better than 1 mrad can be achieved by processing the quaternion
data from the Shuttle IMU and the STAGE experiment IMU during a
Shuttle rotation maneuver), the acceleration measurement error
due to alignment error will be significantly less than 0.28 mgal
(0.17-0.28 mgal).

The accelerometer bias and scale factor errors for the
candidate accelerometer assembly are:

Accelerometer bias: 10 micro-g at full scale, assumed
calibratable in orbit to better than 0.1
micro-g using LOGACS experiment
technique.

Bias temperature
coefficient: 0.25 micro-g/°F

Accelerometer scale
factor: 500 ppm

The above data indicates that accelerometer bias in the
onboard inertial measurement unit, if uncalibrated, will be a
dominant error source. Like gravity, these biases cannot be
measured directly, but must be inferred from other observations
of the vehicle position and velocity time histories. The
accelerometer scale factor will produce an acceleration error of
0.1 mgal (max). The bias errors can be calibrated on orbit using
a technique proven on an earlier Air Force experiment [Pearson,
1973 [4.4]]. In this technique, the accelerometer is mounted on
a rotating table, and the table acts as a centrifuge with a known
angular velocity. It is estimated that using this technique or a
similar technique, the accelerometer bias can be calibrated to
about 0.1 micro-g, resulting in an acceleration error of 0.1
mgal. An alternate technique using Shuttle rotation maneuvers is
also being investigated. It is based on a similar principle but
it does not require the use of a rotating table to calibrate the
accelerometer bias. In this technique the 3 axis accelerometer
assembly is mounted in such a way that its input axes (sensitive
axes) are skewed with respect to the Shuttle principal axes. The
Shuttle rotation maneuver creates a centrifugal force which is
sensed by the accelerometers.

The gyro bias drift and scale factor errors of 0.004 deg/hr and 5 ppm, respectively for the candidate ring laser gyros are not a significant error source as long as the STAGE IMU misalignment error can be maintained at 1 mrad. Over a 12-hour period (to coincide with the manned star tracker updates at every 12 hours) the gyro bias drift would add about 0.87 mrad to the misalignment, thereby causing an acceleration error of about 0.1 mgal. Table 4-3 summarizes all the error sources and their effect on the Shuttle acceleration estimation.

Since the IMU measurement errors are independent of the GPS measurement errors, the total acceleration error is taken as the RSS of the two errors. The total acceleration estimation error (magnitude) and its largest satellite clock component for one revolution of the Shuttle orbit is plotted in Figure 8. Further work is underway to develop a post processing technique to mitigate the effect of satellite clock errors and thereby improve on the total acceleration measurement error budget to about 0.5 mgal.

4.2 Critical Measurement Errors

The error analysis results for the STAGE experiment were described in the previous section and an error budget for the significant errors was developed. The critical errors, i.e., error sources that may contribute an error in the shuttle acceleration estimation accuracy of 0.5 mgal or larger, if untreated, were identified and rationale for their error budgets were described. These critical error sources are: (1) GPS satellite clock frequency error; (2) accelerometer bias error; (3) gyro bias drift error; (4) experiment IMU alignment error. Other error sources, which may be critical but were not fully investigated are: multipath error and the shuttle body flexure between the GPS antenna location and the experiment IMU location

Table 4-3: Shuttle Acceleration Estimation Error

(One Component)

Error Source	Error Per Axis	Effect on Shuttle Acceleration (1-sigma)
GPS Orbit Error - geopotential field - solar radiation pressure - GMe - tracking station location	0.4 (GEM5-GEM7) 1% $0.005 km^3/sec^2$ 10 cm	0.13 mgal
Receiver phase measurement noise[1]	6 mm	0.06 mgal
Receiver phase bias error	0.5 m	0.1 mgal
Satellite clock frequency error[2]	$1.2 \times 10^{-23}/\tau$	0.43 mgal
Accelerometer bias error	10 micro-g[3]	0.1 mgal
Accelerometer scale factor error	500 ppm	0.1 mgal
Gyro bias and scale factor error	0.004 deg/h, 5 ppm	0.05 mgal 0.17 mgal
Alignment error	1 mrad[4]	0.2 mgal
Other (multipath, Shuttle flexure)		0.1 mgal
RSS		$\approx$ 0.56 mgal

Notes:

1   an averaging interval of 75 seconds is taken
2   an averaging interval of 75 seconds and a factor of 100 reduction in clock Allan variance is taken
3   an on-orbit calibration scheme similar to LOGACS is assumed
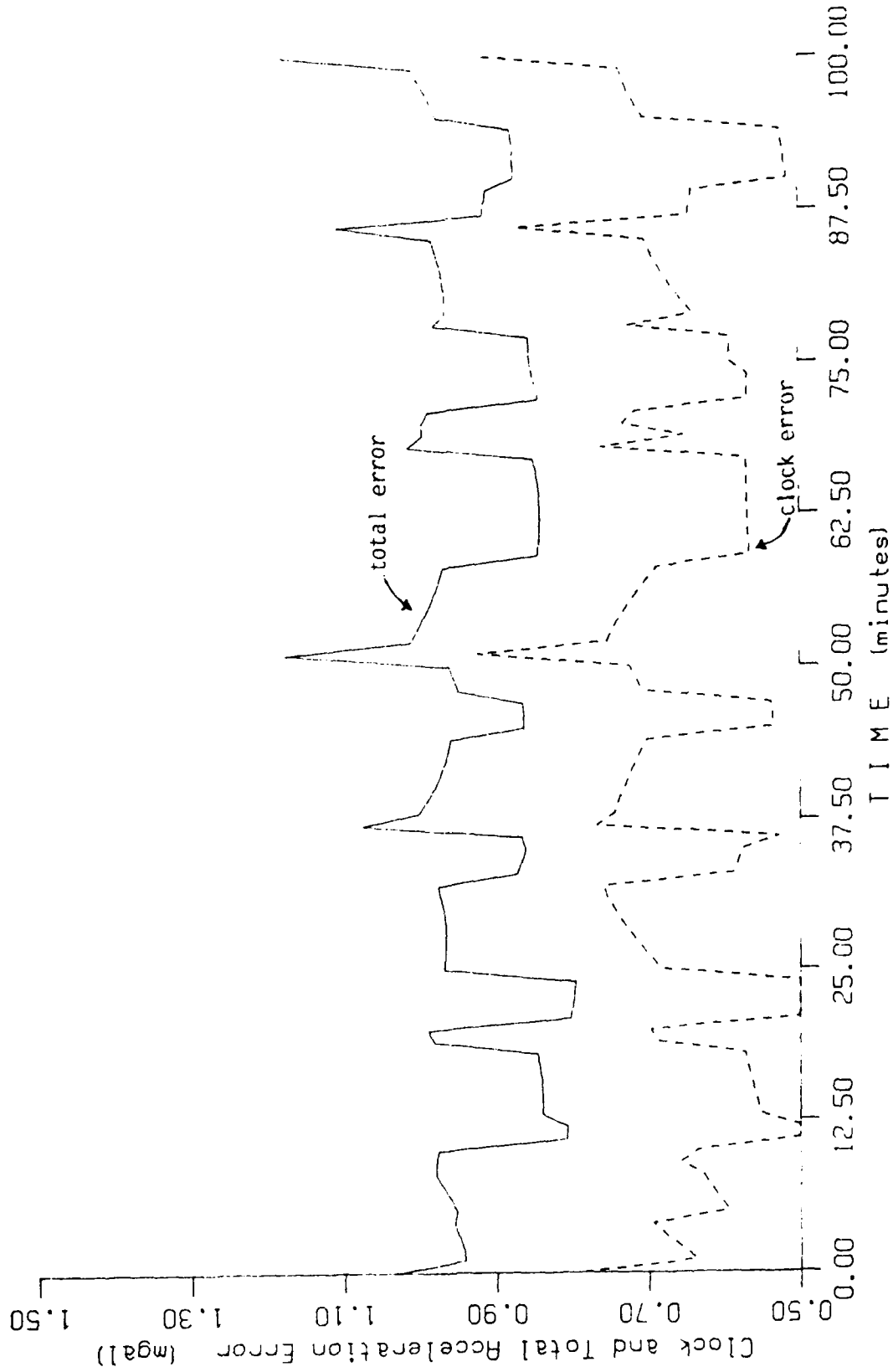4   a transfer alignment between Shuttle IMU to the STAGE IMU is assumed

Figure 4.8 Total acceleration estimation error (all 3 components)
and the effect of GPS clock error (radial component)
for the STAGE Experiment for 5° averaging (75 seconds)

(also refer to Section 6 for the experiment location on the Shuttle). A preliminary analysis of the multipath error assumed that if the multipath signal is attenuated by about 70 dB (due to both the absorbtion of the signal energy by the ground plane material and by the reduced antenna gain at low elevation angles for the multipath signals), then its effect on the Shuttle acceleration estimation accuracy will be less than 0.1 mgal. The effect of the Shuttle structure flexure was not investigated in this analysis explicitly, however, the IMU transfer alignment problem discussed in the next section (Section 5) models the shuttle body flexure (angle error) between the shuttle IMU and the experiment IMU in estimating the transfer alignment accuracy. Additional work is required to properly account for the Shuttle body flexure effect.

In the remainder of this section the above identified critical errors are dealt with in some detail, and justifications for assigning the error budget for each of these error sources are presented.

4.2.1   GPS Satellite Clock Errors

The performance of the GPS satellite clocks (cesium standard) is generally specified in terms of their Allan variance parameters. The Allan variance of the clock time error, for M successive samples, is defined as:

$$\sigma_y{}^2 = 1/2(M-1) \sum_{K=1}^{M-1} (Y_{k+1} - Y_k)^2 \tag{7}$$

where

$$Y_k = \frac{t_k+1 - t_k}{\tau}$$

t_k is the satellite clock phase at time k, τ is the averaging internal i.e.,

$$\tau = (k+1)\Delta t - k\Delta t = \Delta t \qquad (8)$$

The Allan Variance can be modeled as a function of the clock noise spectral density N_0 and the averaging time τ as

$$\sigma_y{}^2 = N_0/\tau$$

where

$$N_0 = 1.2 \times 10^{-21} \text{ and } \tau \text{ is in seconds}$$

Typical short-term specifications on the stability of the GPS cesium frequency standard, in terms of its Allan variance, and the model values are given in (Table 4.4).

Table 4.4: Satellite Clock
Allan Variance Specification Values

Averaging Time	Allan Variance 1-Sigma	
	Specification	Model Values
$\tau = $ 1 sec	$\leq 1 \times 10^{-11}$	3.5×10^{-11}
$\tau = $ 10 sec	$\leq 1 \times 10^{-11}$	1.1×10^{-11}
$\tau = $ 100 sec	$\leq 3.7 \times 10^{-12}$	3.5×10^{-12}
$\tau = $ 1000 sec	$\leq 1.4 \times 10^{-12}$	$1.1. \times 10^{-12}$

From the above table one easily concludes that the clock model, i.e.,

$$\sigma_y{}^2 = \frac{1.2 \times 10^{-21}}{\tau} \qquad (9)$$

reasonably approximates the specification values for averaging intervals of interest, i.e., $10 \leq \tau \leq 100$. Substituting the above

value for N_0 in the equation for acceleration estimation error we obtain, for $\tau = 75$ seconds, the 1-sigma acceleration error uncertainty as:

$$\sigma(\text{acceleration})_{\text{clock}} = 4.32 \cdot \text{PDOP mgal}$$

where the typical PDOP values for the Shuttle are around 2. This result clearly demonstrates that if the satellite clock frequency error is not treated properly in the analysis then this error source alone will exceed the total 1 mgal error budget for the experiment. Fortunately, the satellite clock error effect can be reduced significantly by post-processing of the GPS shuttle tracking data along with the GPS ground tracking data. The feasibility of this technique, of course, depends on whether the short-term fluctuations in GPS satellite clock can be observed from ground tracking GPS data at the GPS tracking stations. It should be noted that previous studies have focused on long-term behavior ($\tau > 1000$ sec) of the GPS satellite clock.

In this study we undertook to investigate the short-term behavior of the clock. The approach employed here is based on an observation that if the effect of all other known systematic errors in the ground tracking data is removed (i.e., the effect of GPS orbit errors, ionospheric errors, tropospheric errors) then the remaining error must be a composite of the errors in GPS satellite clock and ground monitor station clock. Therefore, if the remaining errors in the satellite tracking data, for short intervals, compare favorably (within the accuracy of the ground clock) with the measurement data on the same satellite clock (collected prior to the satellite deployment) then one can successfully argue that the ground tracking data does not destroy the short-term behavior of the satellite clock. We should emphasize here that this approach for observing satellite clock behavior works very well for long averaging intervals and so the

open question addressed here applies only for short-term
averaging intervals, i.e., $10 \leq \tau \leq 100$ seconds.

To this end, we collaborated with and received substantial
cooperation and support from Mr. Paul Jorgensen and Mr. Philip
Tally of Aerospace Corporation. Mr. Jorgensen [4.1], [4.2]
provided us for the study the Allan variance plots of processed
ground tracking data (after taking out the effect of known
errors) for several satellite cesium and rubidium clocks. Mr.
Tally provided us the in-plant Allan variance test data for the
same clocks. This test data was collected earlier as part of the
in-plant acceptance test at FTS. In what follows, we present a
comparison of the Allan variance statistics on the clock data
collected at two different times (and in two different
conditions) for several of the GPS clocks to establish the main
point, i.e., the behavior of GPS satellite clocks over short time
periods is observable in the ground tracking data.

Figure 4.9 shows a plot of the Allan variance 1-sigma value
as a function of averaging interval τ for NAVSTAR 3 rubidium
clock. This plot was generated by Jorgensen [4.1] by processing
the GPS tracking data collected at the Hawaii tracking station.
Superimposed on this plot are the Allan variance 1-sigma values
computed from the in-plant acceptance test data collected at FTS
in March 1978. The exceptional match between the two Allan
variance values is remarkable and confirms the hypothesis. The
post-processing technique of ground tracking data to take out the
effect of all other known errors is described in Jorgensen [4.1].
Similar comparison of Allan variance sigma was carried out for
several other GPS clocks. Figure 4.10 shows a plot of Allan
variance sigma for NAVSTAR 10 cesium clock (serial number 005)
tracking data collected at Diego Garcia on April 26, 1985. This
data is compared with the in-plant acceptance test data collected
at FTS in May 1982. Once again the close match between the two

Figure 4.9 Comparison of Allan Variance Sigma Values for NAVSTAR 3 Rubidium Clock (ground tracking data versus in-plant test data)

1 - sigma Allan variance

4.9 x 10^-12
6/30/82

3.99 x 10^-12
τ = 10 s
FTS 5/82

4.6 x 10^-12
τ = 30 s

3.09 x 10^-12
τ = 100 s
FTS 5/82

1.8 x 10^-12
τ = 300 s

94 x 10^-12
τ = 1000 s

τ

Legend:
— Ground Tracking Data, Diego Garcia, April 26, 1985

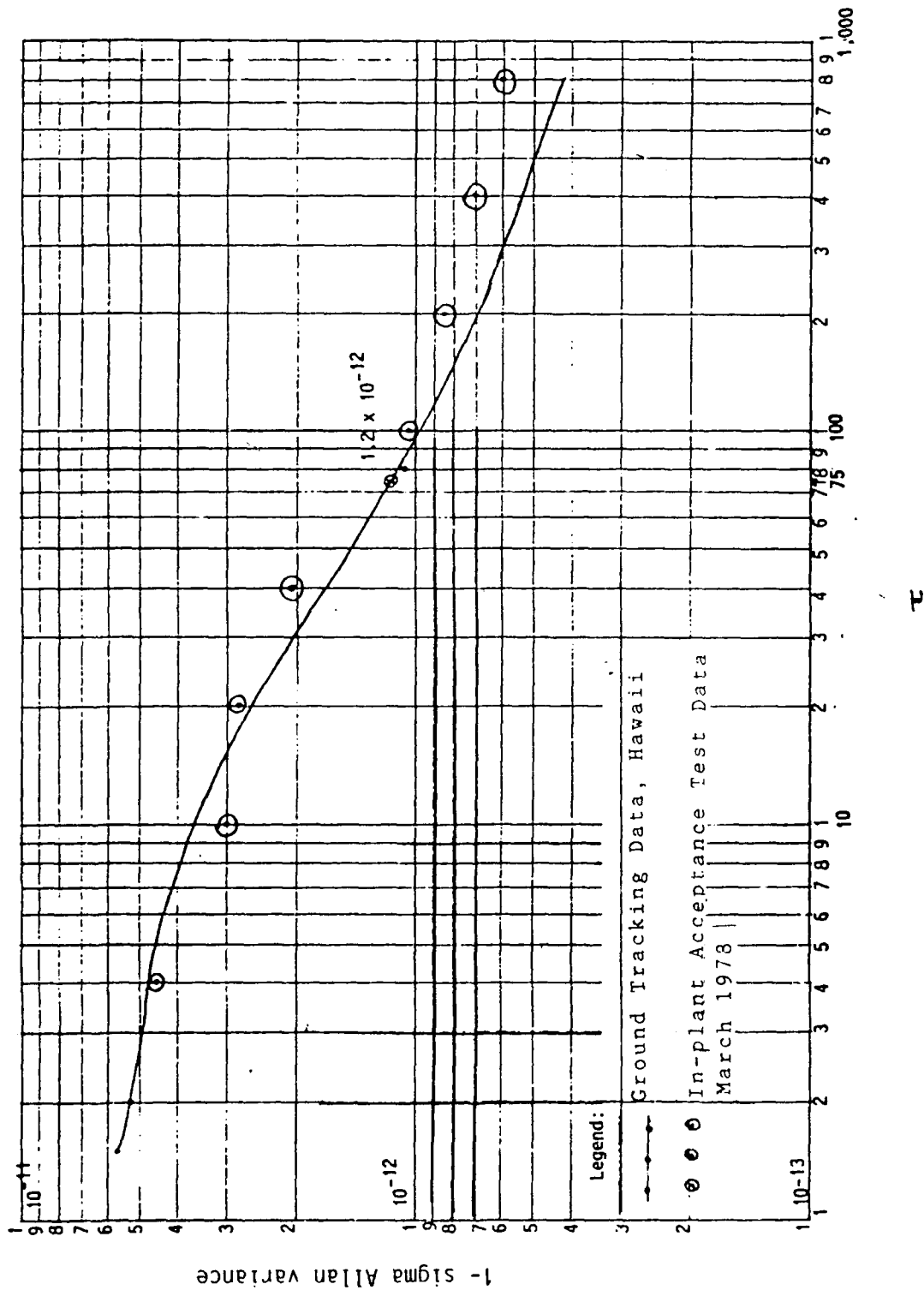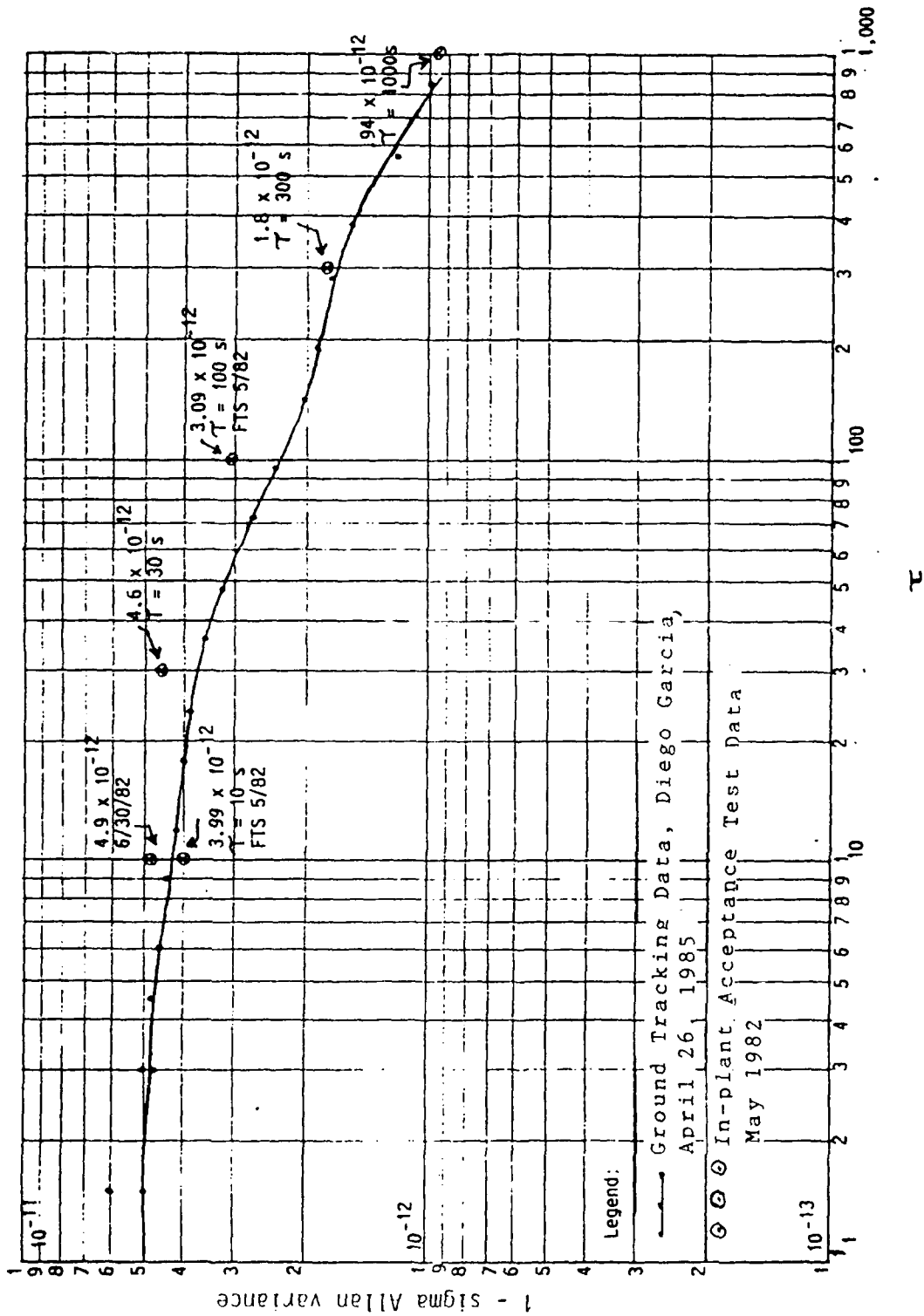⊖ ⊘ ⊙ In-plant Acceptance Test Data May 1982

Figure 4.10 Comparison of Allan Variance Sigma Values for NAVSTAR 10 Cesium Clock (ground tracking data versus in-plant test data)

Figure 4.11 Comparison of Allan Variance Sigma Values for NAVSTAR 9 Cesium Clock (ground tracking data versus in-plant test data)
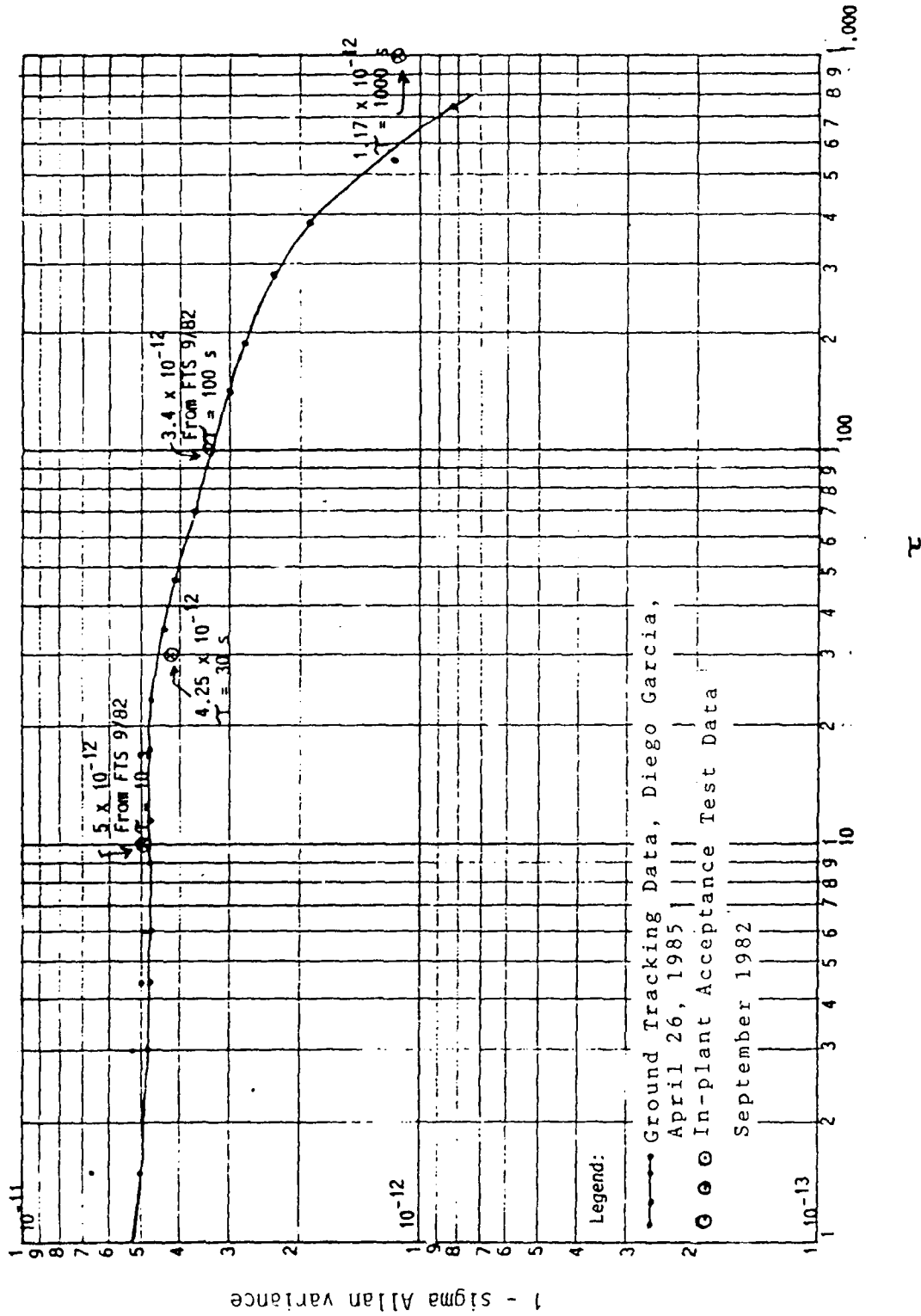
4-25

data is striking and proves the hypothesis. The last comparison
presented here, Figure 4.11, is for NAVSTAR 9 cesium clock
(serial number 004). The ground tracking data was collected at
Diego Garcia on April 26, 1985 while the in-plant test data was
collected in September 1982. The close match between the Allan
variance sigma values computed from two different data sets is
obvious. These evaluations of the performance of different
clocks using GPS tracking data demonstrate that post-processing
techniques can be used to take out or significantly reduce the
effect of satellite clock fluctuations on the acceleration
estimate. Specifically, we present below (Table 4.5) the Allan
variance sigma values for the NAVSTAR 10 cesium clock for
different values of τ for the in-plant test data and for the
ground tracking data.

Table 4.5   NAVSTAR 10 Allan Variance Sigma Values

Averaging Time τ	Allan Variance 1-sigma Ground Tracking data (4/85)	Allan Variance 1 sigma In-plant data (5/82)	Difference 1-sigma	Specification 1-sigma
10 sec	4.2×10^{-12}	3.99×10^{-12}	0.2×10^{-12}	$\leq 1 \times 10^{-11}$
100 sec	2.4×10^{-12}	3.09×10^{-12}	0.69×10^{-12}	$\leq 3.7 \times 10^{-12}$

From the above table we observe the significant reduction in clock error by processing the ground tracking data. The residual error is bounded by the error in the monitor station clock which will be removed by the double differencing technique proposed for reducing the effect of clock errors.

This preliminary analysis indicated that the short-term fluctuations in the GPS clock frequency is observable in the ground tracking data and that this fact can be used to reduce, by a factor of about 100 (goal), the clock Allan variance for $10 \leq \tau \leq 100$. An exact analysis using the double differencing technique for the GPS carrier phase measurements at the Shuttle and at the tracking stations is being developed to assess the improvement in reducing the GPS satellite clock effect on the shuttle acceleration estimation error [4.3].

4.2.2   Experiment IMU Alignment and Calibration

In this section, the approach to ameliorate the effect of the remaining three errors namely, accelerometer bias, gyro bias and misalignment error is discussed.

The experiment IMU consists of a 3-axis high precision accelerometer assembly and a set of 3 gyros to measure the translational and rotational dynamics of the Space Shuttle. The candidate accelerometer assembly is the Bell MESA (Miniature Electrostatic Accelerometer) with accelerometer bias specification of 10 micro-g and a scale factor of 500 ppm. In order to measure non-gravitational Shuttle acceleration to an accuracy of less than 1 micro-g (1 milligal) the accelerometer bias error need to be calibrated on-orbit. Previous work by others [4.4] using the Bell MESA have shown that ground calibration of accelerometer bias error does not hold accurately during the on-orbit phase of the flight where the experiment data

will be collected. One can argue that the accelerometer bias (if it is truly a bias error) can be taken out during post-processing and therefore does not need calibration. However, the bias error stability will remain an issue especially if there are other effects, such as temperature effect, that influence the bias error. For these and other reasons, it is felt that it is advisable to estimate these errors in their environment so that their effect can be accounted for. This establishes the need for an on-orbit technique to calibrate the accelerometer bias and scale factor errors. Similarly, the experiment IMU ring laser gyros have a bias drift rate specification of 0.004 deg/hour (1-sigma) and a scale factor error of 5 ppm (e.g., Honeywell RLG 1342 has bias drift of 0.002 deg/hour [3-sigma] and a scale factor of 2 ppm and is better than the specification for our experiment IMU gyro) which will cause an alignment error over the expected 5 days mission duration to exceed the budget of 1 mrad. Therefore, there is a requirement to align (i.e., estimate the misalignment) the experiment IMU on-orbit to an accuracy of about 1 mrad so that its effect on acceleration estimation is less than 1 micro-g. Techniques for on-orbit calibration and alignment for the experiment IMU is described below.

4.2.2.1 On Orbit Accelerometer Bias and Scale Factor Calibration

The experiment IMU accelerometer bias and scale factor errors will require on-orbit calibration so that their effect on the Shuttle acceleration estimation can be contained to within our error budget of 0.1 micro-g. Like gravity, the biases can not be measured directly, but must be inferred from other observations of the vehicle position, velocity, and attitude time-histories, applied to appropriate models. Alternatively, the accelerometers can be instrumented on a precision controlled motor table system which will generate centrifugal force to help

estimate the bias and the scale factor. This latter technique for accelerometer bias and scale factor calibration has been proven on an Air Force Low-G Accelerometer Calibration System (LOGACS, Pearson, Aerospace Corporation Report TR-0074, Vol. I, 1973) [4.4]. We should also mention here that this same technique is also proposed for use with NASA OARE experiment [4.5]. In this concept the accelerometer is mounted on a table so that the center of mass of the sensitive element is at known distance R from the center of rotation, and the table acts as a centrifuge with known angular velocity. The accelerometer output in different operating modes is recorded and used to estimate the accelerometer bias and the scale factor. A preliminary packaging diagram (taken from [4.5]) for the OARE experiment including motor table system is shown in Figure 4.12.
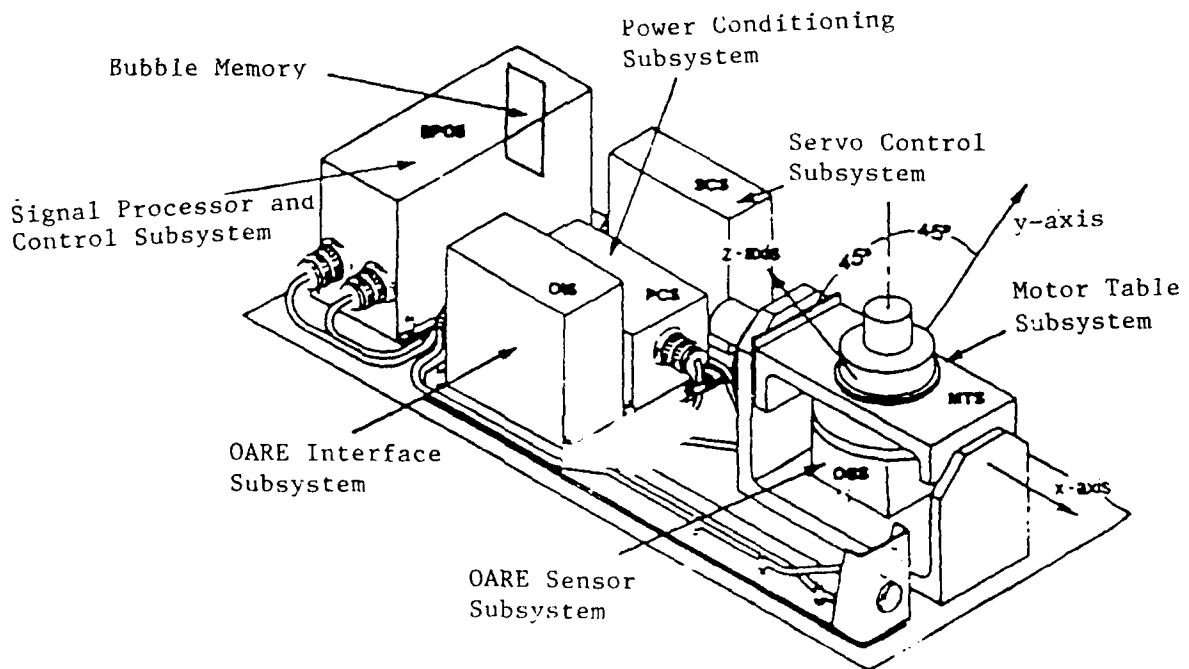

Figure 4.12 Packaging Concept of NASA OARE Experiment Including the Motor Table System

The four different modes and the resulting accelerometer outputs
are described below.

Mode	Accelerometer Output

1. No rotation, sensitive axis $A_1 = K (B + A_D)$
   forward

2. No rotation, sensitive axis $A_2 = K (B - A_D)$
   aft

3. Rotation at fixed angular $A_3 = K (B + A_D \cos wt + R w^2)$
   rate w

4. Rotation at fixed rotation $A_4 = K (B + A_D \cos 2wt +$
   rate 2w $4 R w^2)$

where A_1 is the accelerometer output, B is the accelerometer
bias, A_D is the drag, and K is the scale factor.

Solving the first two measurement equations will give the
bias in terms of the scale factor. Using the other two equations
we can solve for both the bias and the scale factor. Solution
accuracy of these measurement equations do of course depend on
how stable the drag is over the time period of the data
collection, and how small are other disturbance terms, like out-
gassing and the vernier thrust at the time of the instrument
calibration.

The LOGACS experiment data [4.4] h_s shown that the Bell MESA
accelerometer bias can be calibrated on orbit and is stable to

0.1 micro-g. One of the concerns related to the application of
LOGACS technique to the STAGE experiment is that this technique
assumes that no dynamic disturbances (maneuvers) are present
during the periods of calibration which is difficult to ensure
for a Shuttle type mission. As mentioned earlier, the NASA OARE
(Orbiter Accelerometer Research Experiment) is slated to this
same technique [4.5] and therefore carries this limitation.
Additional work is required in the areas of examining the
behavior of drag during the calibration period, out-gassing, and
effect of other non-gravitational forces if this technique is to
be finally recommended for STAGE. An alternate technique, which
does not require the rotating table, but will require Shuttle
rotation maneuvers, which can be measured by the experiment IMU
gyros, is attractive from cost considerations. The performance
of this technique is being analyzed under a separate effort
[4.3].

4.2.2.2   On-Orbit Transfer Alignment

The initial misalignment (due to instrument block mounting
and due to Shuttle body flexure) and the alignment error due to
the gyro drift rate over a Shuttle flight exceed the 1 mrad error
budget of the STAGE experiment. An on-orbit transfer alignment
technique was developed to transfer alignment data from the
Shuttle IMU to the experiment IMU. This alignment technique,
details of which are provided in Section 5, uses the Shuttle
rotation maneuvers along two principal axes to resolve alignment
in 3-axes. The Shuttle IMU is aligned, with respect to the
inertial space, using the onboard star tracker measurements which
are accurate to about 60 arcsec (about 0.3 mrad). Therefore, the
error introduced by the transfer alignment estimation technique
should be about 0.95 mrad ($\sqrt{1-0.3^2}$). The analysis and
covariance simulation results presented in the next section
readily support this accuracy goal.

REFERENCES

4.1 Paul S. Jorgensen, "Various Uses of the OCS Tracking Data," Paper Presented at the Eighteenth Annual PTTI Applications and Planning Meeting, Washington, D.C., December 1986.

4.2 Paul S. Jorgensen, "Obtaining the Short Term Stability of the GPS Satellite Clocks From Tracking Data," Proceedings of the Institute of Navigation, pp 235-239, 1984.

4.3 Upadhyay, Triveni, N. et al., Global Gravity Field Mapping, Final Report, SBIR Phase I Program, Mayflower Communications Company, Reading, MA, 1989.

4.4 J. A. Pearson, The Low-G Accelerometer Calibration System, Final Report, Volume I, The Aero Space Corporation, Report No. TR-0074(4260-10)-1, July 1973.

4.5 R. C. Blanchard, M.K. Hendrix, J. C. Fox and D. J. Thomas, "The Orbital Acceleration Research Experiment," Paper presented at the AIAA 3rd Space Systems Technology Conference, AIAA Paper No. 86-1195, San Diego, CA, June 1986.

4.6 Klein, D. and B. Parkinson, "The Use of Pseudo-Satellites for Improving GPS Performance", Journal of the Institute of Navigation, Vol. 31, No. 4, Winter 1984-85.

4.7 Profumo, V. (editor), "Experimenter's Planning Guide for Department of Defense Space Test Program", Aerospace Corporation, Report No. SD-TR-83-24, Reissue A, February 1987.

4.8 Martin, C. F. and J. McCarthy (1987), "Error Analysis of
Anomalous Gravitational Acceleration Estimation from GPS
Tracking by the STS", EG&G Final Report, WASC TR-W41-
001(87).=, Lanham, MD, August 1987

SECTION 5

PAYLOAD IMU TRANSFER ALIGNMENT

5.1. The Basis for Transfer Alignment

To support the objective of this experiment, the orientation of the accelerometer input axes must be known to high accuracy at all times during data collection. This information is to be derived from the strapdown IMU which is part of the experiment package. The strapdown gyros indicate increments of rotation which can be processed into a quaternion representing the change in experiment package orientation, relative to inertial coordinates, from its initial orientation. The initial orientation must be inferred from some source of information external to the experiment IMU.

The external reference which provides the initializing information in this case is the Shuttle IMU. This is a platform-mounted inertial system used to provide attitude and navigation information necessary for Shuttle operations. Star sights are processed at intervals to update the platform orientation and thus contain the error growth due to gyro drift. This platform orientation is the reference to which we wish to align the experiment IMU. The Shuttle navigation system outputs attitude data in the form of a quaternion representing the rotation from inertial coordinates to the Shuttle body at the location of the Shuttle IMU. The experiment attitude calculation can simply be initialized with this quaternion. This transfer of alignment data, however, suffers from errors due to a number of causes:

- Shuttle IMU gimbal readout errors

- Shuttle body bending between the locations of the
  two IMUs
- Misalignment in mounting the experiment IMU

It is therefore necessary to improve this alignment information
by some means.

The physical basis for estimating the misalignment between
two inertial systems, which then permits correction of the
misalignment, is measurement of some common inertial quantities
by both systems. If these inertial quantities are the same at
both IMU locations, they should be observed as the same by both
systems. Any discrepancy in the measurements produced provides
information about the difference in coordinate frames which are
indicated by the two systems. Any motion which both IMUs sense
can be used for this purpose. The choices are linear
acceleration (or an integrated linear acceleration - a Δv) or
angular rotation. The use of angular rotation is preferable
because it costs less fuel to produce a significant rotation of
the Shuttle than a significant Δv. Moreover, if Shuttle body
bending is a static offset rather than a continuing dynamic
process, the rotational motion is the same at all points whereas
linear acceleration is not in the presence of both linear and
rotational motion.

Estimation of the relative misalignment between two inertial
systems based on measurement of angular rotations can be
organized in two ways. One is to define distinct large-angle
rotations, process the orientation data from both IMUs at
beginning and end of these rotations, and compute the least-
squares estimate for the misalignment which causes the
differences in the two sets of measurements. This approach is
described in reference 5.1, among other places. At least two

rotations, preferably about nearly orthogonal axes, are required to permit three-axis misalignment estimation.

A disadvantage of the discrete-rotation approach is that one must have distinct rotations of reasonable size - which may or may not be a part of the normal operation of the Shuttle. Also, in the presence of the inevitable gyro drift, one cannot correctly process with this formulation two rotations which occur at significantly different times. An alternative formulation provides operational flexibility in that it uses any rotational motion which occurs, at any time, to its best advantage. This formulation is the recursive estimator. It is derived from optimal linear estimation theory and is applied to a linearized model of the error dynamics and measurement sensitivities. It utilizes the same physical principles as discrete-rotation processing and thus can be expected to produce good results only when significant rotations occur about two or more non-colinear axes. However, one need not decide when a rotation starts or stops; the estimator simply accepts the attitude data from both systems at all times and produces the best estimate of the misalignment that it can. To the extent that the error model used represents reality, this estimate is optimal in tne sense of minimum error variance. This is the approach to transfer alignment which has been analyzed in this work.

5.2 Error Modeling

The errors which are accounted for in the following are defined in the context of a number of coordinate frames. These frames are indicated schematically in Figure 5.1. The definitions of these frames are as follows:

I   =   True inertial reference frame

5-3

FIGURE 5.1 RELATIONSHIPS AMONG COORDINATE FRAMES
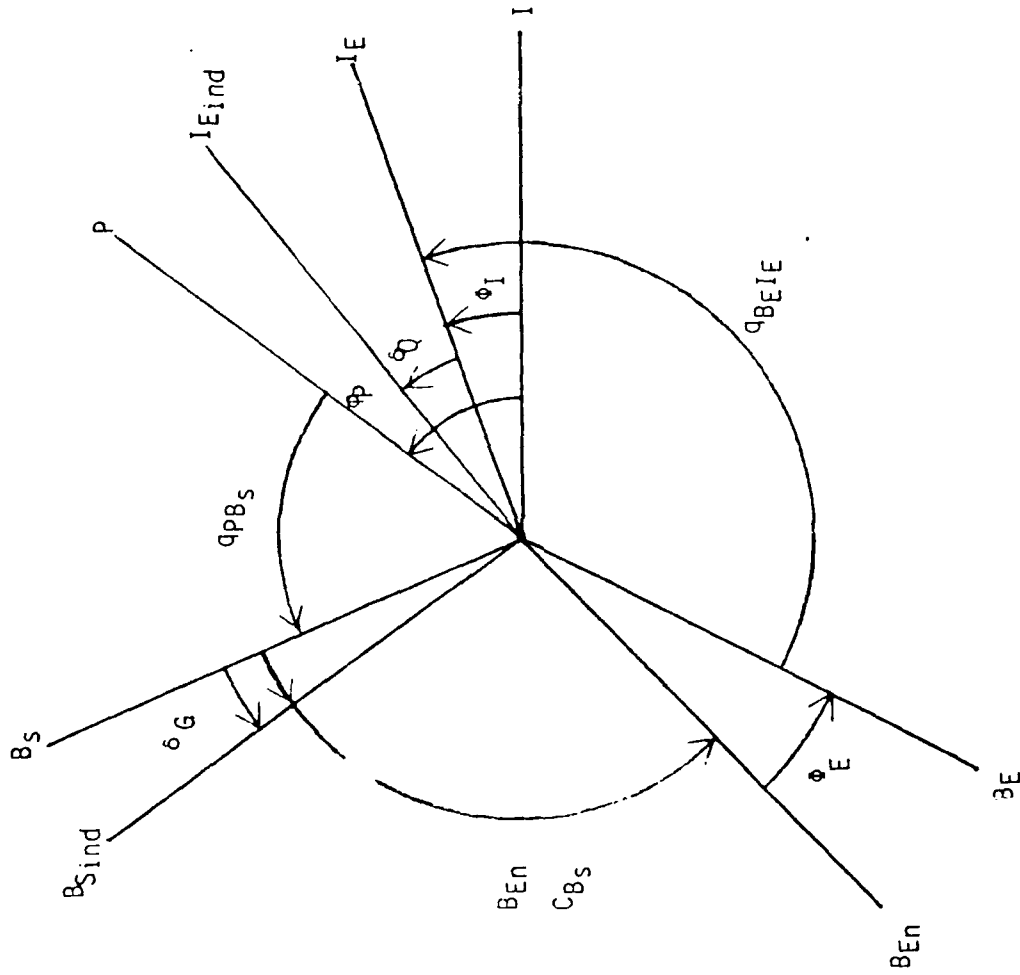
I_F = Inertial reference frame implied by the quaternion computed by the experiment attitude reference system

I_{Find} = Inertial reference frame indicated by the experiment attitude reference system; it differs from I_F by the system indication error - primarily gyro quantization

P = Coordinate frame fixed to the Shuttle IMU stable platform; it is intended to be aligned with I

B_s = Coordinate frame fixed to the Shuttle body at the base of the Shuttle IMU

B_{sind} = Shuttle body frame indicated by the Shuttle system attitude quaternion; it differs from B_s by the Shuttle IMU gimbal readout errors

B_{Fn} = Coordinate frame fixed to the nominal orientation of the experiment IMU instrument block; it differs from B_s only by a known transformation which reflects the intended alignment of the experiment IMU

B_F = Coordinate frame fixed to the actual experiment IMU instrument block; it differs from B_{Fn} by the mounting misalignment and Shuttle flexure

The dynamic models chosen for the important errors are described next.

Experiment IMU Alignment Error

$$\dot{\underline{\phi}}_I^{(I)} = - \underline{\delta W}_{IE}^{(I)}$$

$$= - C^I{}_{BF} \; \underline{\delta W}_{IE}^{(BF)}$$

The experiment IMU alignment error is treated as the error in indicating the inertial frame relative to the body frame at the experiment location. It is coordinatized in inertial coordinates

and is driven by the experiment IMU gyro drift rate which is defined in body coordinates.

Experiment IMU Gyro Drift Rate

$$\underline{\delta W}_{IF}{}^{(B)} = \underline{b}_F + \begin{bmatrix} K_x & 0 & 0 \\ 0 & K_y & 0 \\ 0 & 0 & K_z \end{bmatrix} \underline{W}_{JB}{}^{(BF)} + \underline{n}_R$$

$\underline{b}_F$ is the gyro bias drift rate

$\dot{\underline{b}}_F = 0$

$\underline{K}^T = [K_x \quad K_y \quad K_z]$ is the gyro scale factor error; it is modeled as a random constant.

$\dot{\underline{K}} = \underline{0}$

$\underline{n}_R$ is a white noise which drives the laser gyro random walk error

Shuttle Platform Alignment Error

$$\dot{\underline{\Phi}}_P{}^{(I)} = \underline{\delta W}_{IP}{}^{(I)}$$
$$= \underline{\delta W}_{IP}{}^{(P)} \text{ to first order}$$

The Shuttle platform gyro drift rate is defined in platform coordinates. This error quantity coordinatized in P or I is the same to first order in error quantities since P and I differ by an error quantity.

Shuttle IMU Gyro Drift Rate

$$\underline{\delta W}_{IP}{}^{(P)} = \underline{b}_P + \underline{r}_P$$

$\underline{b}_P$ is the platform gyro bias drift rate

$\dot{\underline{b}}_P = \underline{0}$

$\underline{r}_P$ is the platform gyro random drift rate; it
is modeled as a first order Markov process.

$$\dot{r}_{P\,i} = -\frac{1}{\tau_{P\,i}} r_{P\,i} + n_{P\,i} \qquad i = x,y,z$$

Experiment IMU Misalignment

$$\underline{\Phi}_E = \underline{\Phi}_{E\,B} + \underline{\Phi}_{F\,R}$$

$\underline{\Phi}_{E\,B}$ is a bias misalignment error due to instrument
block mounting error and a static offset due to Shuttle
body flexure.

$$\dot{\underline{\Phi}}_{E\,B} = 0$$

$\underline{\Phi}_{F\,R}$ is a random contribution to misalignment due to
variations in Shuttle body flexure; it is modeled as a
first order Markov process.

$$\dot{\Phi}_{F\,R\,i} = -\frac{1}{\tau_{E\,i}} \Phi_{F\,R\,i} + n_{F\,i} \qquad i = x,y,z$$

These error quantities are the elements of the state vector for
this problem. The state vector, $\underline{x}$, is defined as:

$$\underline{x}^T = [\underline{\Phi}_I{}^T \ \underline{b}_E{}^T \ \underline{k}^T \ \underline{\Phi}_P{}^T \ \underline{b}_P{}^T \ \underline{r}_P{}^T \ \underline{\Phi}_{F\,B}{}^T \ \underline{\Phi}_{F\,R}{}^T]$$

The dynamical models defined above are assembled into the
differential equation for this state vector; it has the form

$$\dot{\underline{x}} = F\underline{x} + \underline{n}$$

with

$$
F = \begin{bmatrix}
O_3 & -C_{BE}{}' & -C_{BE}{}'\,\text{Diag}(W_{IB}{}^{(BE)}) & O_3 & O_3 & O_3 & O_3 & O_3 \\
O_3 & O_3 & O_3 & O_3 & O_3 & O_3 & O_3 & O_3 \\
O_3 & O_3 & O_3 & O_3 & O_3 & O_3 & O_3 & O_3 \\
O_3 & O_3 & O_3 & O_3 & I_3 & I_3 & O_3 & O_3 \\
O_3 & O_3 & O_3 & O_3 & O_3 & O_3 & O_3 & O_3 \\
O_3 & O_3 & O_3 & O_3 & O_3 & -\text{Diag}\!\left(\dfrac{1}{\tau_{P\,I}}\right) & O_3 & O_3 \\
O_3 & O_3 & O_3 & O_3 & O_3 & O_3 & O_3 & O_3 \\
O_3 & O_3 & O_3 & O_3 & O_3 & O_3 & O_3 & -\text{Diag}\!\left(\dfrac{1}{\tau_{E\,I}}\right)
\end{bmatrix}
$$

and

$$
\underline{n}^{T} = [\,-(C_{BE}{}'\;\underline{n}_R)^{T}\;\;O_3\;\;O_3\;\;O_3\;\;O_3\;\;\underline{n}_D{}^{T}\;\;O_3\;\;\underline{n}_E{}^{T}\,]
$$

There are also indication errors associated with both inertial systems. They are:

$\underline{\delta}_Q$ = Experiment IMU indication error; it is primarily the laser gyro quantization error and is treated as a wideband measurement noise.

$\underline{\delta}_G$ = Shuttle IMU attitude indication error; it is primarily due to errors in gimbal readout and is treated as a wideband measurement noise.

5.3 Measurement Processing and Sensitivity

The measurements which are processed by this estimator are the attitude quaternions computed by both inertial systems and which must be telemetered to the ground for post mission processing. The Shuttle attitude reference system produces the quaternion $q_{PBs,ind}$ which represents the indicated transformation from the Shuttle IMU stable platform to B_S – the coordinate frame

fixed to the body of the Shuttle at the base of the Shuttle IMU. The experiment attitude reference system produces the quaternion $q_{BEIEInd}$, which represents the indicated transformation from the experiment instrument block coordinates to the inertial frame implied by this system. In addition, the quaternion q_{BABEn} representing the transformation from B_A to B_{En} coordinates is known; it depends only on the definition of the nominal instrument block coordinates.

Since the two inertial systems run on independent clocks, they do not compute their quaternions at synchronous times. So, the first step in measurement processing is to interpolate the data on either one of the two data streams to produce the quaternion at times in common with the other data stream. An algorithm for this purpose is given in Reference 5.2.

Having synchronized quaternions, the following composite quaternion is computed.

$$q_n = (q_{PBBInd} * q_{BBBEn}) * q_{BEIEInd}$$

The symbol "*" means quaternion multiplication. If coordinate frames A and B are related by a rotation through angle Θ about an axis aligned with the unit vector $\underline{u}$, then the quaternion representing the transformation from A to B has the form

$$q_{AB} = \begin{bmatrix} q_0 \\ q_1 \\ q_2 \\ q_3 \end{bmatrix} = \begin{bmatrix} a \\ \underline{b} \end{bmatrix} = \begin{bmatrix} \cos(\Theta/2) \\ u_x \sin(\Theta/2) \\ u_y \sin(\Theta/2) \\ u_z \sin(\Theta/2) \end{bmatrix}$$

The quaternion product is defined as

$$q_3 = q_1 * q_2$$

with $a_3 = a_1 a_2 - \underline{b}_1^T \underline{b}_2$

$$\underline{b}_3 \;=\; a_1\,\underline{b}_2 \;+\; a_2\,\underline{b}_1 \;+\; \underline{b}_1 \;\times\; \underline{b}_2$$

The definition of q_s is such that if there were no errors in the system, it would represent the transformation from P to I, and since with no error P would be coincident with I, this would be the identity transformation. For the transformation from I to I, $\Theta = 0$ and the quaternion is

$$q_{I\,I} \;=\; \begin{bmatrix} 1 \\ 0 \\ 0 \\ 0 \end{bmatrix}$$

In the presence of the system errors, q_s represents the transformation through the small angle induced by all the errors in the chain from P to $I_{E\,I\,n\,d}$. Call this vector rotation angle $\underline{\Phi}_n$. Then q_s has the form

$$q_s \;=\; \begin{bmatrix} \cos(\Phi_n/2) \\ \underline{\Phi}_n \;\dfrac{\sin(\Phi_n/2)}{\Phi_n} \end{bmatrix}$$

$$\approx\; \begin{bmatrix} 1 \\ 0.5\,\underline{\Phi}_n \end{bmatrix} \qquad \text{to first order}$$

So the error rotation is computed as

$$\underline{\Phi}_n \;=\; 2\,\underline{b}_s$$

where $\underline{b}_s$ is the last three elements of q_s. This is the measure of system errors used by the estimator.

The contribution of each error source to this total system error is found by writing the complete chain of transformations from I to I going through all the intermediate coordinate frames shown in Figure 5.1. This identity is linearized in the error quantities to produce the linearized error sensitivity relation. The details of this derivation will appear in a forthcoming Masters' thesis from the Department of Aeronautics and Astronautics at MIT. The result is

$$\underline{\Phi}_A = \underline{\Phi}_I - \underline{\Phi}_P - C^I{}_{BEn}\ \underline{\Phi}_{EB} - C^I{}_{BFn}\ \underline{\Phi}_{ER} + \underline{\delta}_O + C^I{}_{BS}\ \underline{\delta}_G$$

This linearized measurement sensitivity relation has the form

$$\underline{\Phi}_A = H\underline{x} + \underline{v}$$

with

$$H = [I_3\ \ O_3\ \ O_3\ \ -I_3\ \ O_3\ \ O_3\ \ -C^I{}_{BFn}\ \ -C^I{}_{BEn}]$$

and

$$\underline{v} = \underline{\delta}_O + C^I{}_{BS}\ \underline{\delta}_G$$

It is clear from this measurement sensitivity that the experiment IMU alignment error, $\underline{\Phi}_I$, is not strongly distinguishable from the Shuttle platform alignment error, $\underline{\Phi}_P$. They are distinguished only by the differences in their dynamic characteristics. This is as expected; the alignment scheme is sensitive to the alignment of the experiment IMU relative to the Shuttle IMU - not relative to the true inertial coordinates. The same is true of the separability of $\underline{\Phi}_{EB}$ and $\underline{\Phi}_{ER}$ - but the distinguishability of these sources of misalignment is not of central importance to the estimate of $\underline{\Phi}_I$.

5.4 The Recursive Filter

The optimal estimator for the state of a dynamic system, with the system dynamics and measurement linearized as we have done, is the Kalman filter. The measurements in this case are made available at discrete points in time, so the discrete form of the Kalman filter is required. The recursion is:

Between measurements:

$$\hat{\underline{X}}_{k+1}{}^- = \Phi_k \ \hat{\underline{X}}_k{}^+$$

$$P_{k+1}{}^- = \Phi_k \ P'_k \ \Phi_k{}^T + Q_k$$

At a measurement point:

$$K_k = P_k{}^- \ H_k{}^T \ (H_k \ P_k{}^- \ H_k{}^T + R_k)^{-1}$$

$$\hat{\underline{X}}_k{}^+ = \hat{\underline{X}}_k{}^- + K_k (\underline{Z}_k - H_k \hat{\underline{X}}_k{}^-)$$

$$P_k{}^+ = (I - K_k H_k) \ P_k{}^-$$

Here $\hat{\underline{X}}_k$ is the estimate of the state vector $\underline{x}$ at the time t_k and P_k is the covariance matrix for the error in that estimate. The superscripts $-$ and $+$ imply before and after incorporation of the measurement at that time. The matrix Φ_k is the transition matrix for the linearized system dynamics between the times t_k and t_{k+1}. The continuous system dynamics matrix, F, consists of constant terms with the exceptions of $\underline{W}_{IR}{}^{(BE)}$ and $C_{BE}{}'$. In the interest of simplifying computations, both of these quantities have been treated as constants. In fact, the Shuttle angular velocity is nearly constant most of the time. This implies a nearly linear behavior for the elements of $C_{RF}{}'$ so an average of the values of this transformation matrix at t_k and t_{k+1} should give a very good approximation to the integrated effect of these terms over the

interval. In the simulations performed under this program, the value of C_{BE}' at t_k was used and treated as constant.

With F approximated as constant, the transition matrix has the form

$$\Phi_k = e^{F_k \Delta t} = I + F_k \Delta t + 1/2\ F_k^2 \Delta t^2 \ \ldots$$

with $\qquad \Delta t = t_{k+1} - t_k$

Corresponding to the form of F for our system dynamics, the transition matrix is

$$
\Phi_k =
\begin{bmatrix}
I_3 & -C_{BE}'\Delta t & -C_{BE}'\text{Diag}(W_{IB}{}^{(BF)})\Delta t & O_3 & O_3 & O_3 & O_3 & O_3 \\
O_3 & I_3 & O_3 & O_3 & O_3 & O_3 & O_3 & O_3 \\
O_3 & O_3 & I_3 & O_3 & O_3 & O_3 & O_3 & O_3 \\
O_3 & O_3 & O_3 & I_3 & I_3\Delta t & \text{Diag(bi)} & O_3 & O_3 \\
O_3 & O_3 & O_3 & O_3 & I_3 & O_3 & O_3 & O_3 \\
O_3 & O_3 & O_3 & O_3 & O_3 & \text{Diag(ai)} & O_3 & O_3 \\
O_3 & O_3 & O_3 & O_3 & O_3 & O_3 & I_3 & O_3 \\
O_3 & O_3 & O_3 & O_3 & O_3 & O_3 & O_3 & \text{Diag(ci)}
\end{bmatrix}
$$

with $\quad a_i = \exp(-\Delta t / \tau_{Pi})$

$\quad\quad\quad b_i = \tau_{Pi}(1-a_i)$

$\quad\quad\quad c_i = \exp(\Delta t / \tau_{Fi})$

The matrix Q_k is the covariance matrix for the integrated effect of the white driving noise on the system state over the interval Δt. If the white noise, $\underline{n}(t)$, has the correlation (zero mean and constant intensity are assumed)

$$\underline{n}(t_1) \, \underline{n}(t_2)^T = N \, \delta(t_2 - t_1)$$

then Q_k has the form

$$Q_k = \int_0^{\Delta t} \Phi(t) \, N \, \Phi(t)^T dt$$

The only states in our error model which are driven by white noise are $\underline{\Phi}_i$ due to the laser gyro random walk drift, $\underline{r}_P$ which is the Markov process component of the Shuttle IMU gyro drift rate, and $\underline{\Phi}_{FR}$ which is the Markov process component of the experiment package misalignment due to Shuttle body flexing. So the noise intensity matrix has the form.

$$N = \begin{bmatrix} Diag(N_R) & 0 & 0 & 0 & 0 & 0 & 0 & 0 \\ 0 & 0 & 0 & 0 & 0 & 0 & 0 & 0 \\ 0 & 0 & 0 & 0 & 0 & 0 & 0 & 0 \\ 0 & 0 & 0 & 0 & 0 & 0 & 0 & 0 \\ 0 & 0 & 0 & 0 & 0 & 0 & 0 & 0 \\ 0 & 0 & 0 & 0 & 0 & Diag(N_P) & 0 & 0 \\ 0 & 0 & 0 & 0 & 0 & 0 & 0 & 0 \\ 0 & 0 & 0 & 0 & 0 & 0 & 0 & Diag(N_E) \end{bmatrix}$$

Evaluation of the integral which defines Q_k then gives

$$Q_k = \begin{bmatrix} Q_1 & 0 & 0 & 0 & 0 & 0 & 0 & 0 \\ 0 & 0 & 0 & 0 & 0 & 0 & 0 & 0 \\ 0 & 0 & 0 & 0 & 0 & 0 & 0 & 0 \\ 0 & 0 & 0 & Q_2 & 0 & Q_3 & 0 & 0 \\ 0 & 0 & 0 & 0 & 0 & 0 & 0 & 0 \\ 0 & 0 & 0 & Q_3^T & 0 & Q_4 & 0 & 0 \\ 0 & 0 & 0 & 0 & 0 & 0 & 0 & 0 \\ 0 & 0 & 0 & 0 & 0 & 0 & 0 & Q_5 \end{bmatrix}$$

Each of these Q_i is a 3 x 3 diagonal matrix. The diagonal elements are:

$$Q_1 \,(i,i) = N_R \Delta t$$

$$Q_2 \,(i,i) = \tau^3{}_{p\,i} \; N_p \; [\Delta t / \tau_{p\,i} - 2(1 - e^{-\Delta t / \tau_{p\,i}})$$
$$+ \; 1/2 (1 - e^{-2\Delta t / \tau_{p\,i}})]$$

$$Q_3 \,(i,i) = \tau^2{}_{p\,i} \; N_p \, [1 - e^{\Delta t / \tau_{p\,i}} - 1/2 (1 - e^{-2\Delta t / \tau_{p\,i}})]$$

$$Q_4 \,(i,i) = 1/2 \; \tau_{p\,i} \; N_p \; (1 - e^{-2\Delta t / \tau_{p\,i}})$$

$$Q_5 \,(i,i) = 1/2 \; \tau_{F\,i} \; N_F \; (1 - e^{-2\Delta t / \tau_{F\,i}})$$

Random walk drift is a basic characteristic of a laser gyro, so the intensity of the noise which is visualized as driving the random walk is a specified quantity. Actually, the square root of N_R is usually given, and normally in units of deg/ $\sqrt{hr}$. N_p and N_F are most usefully interpreted in terms of the steady state RMS value produced by the Markov process model. The steady state variance is

$$\sigma^2 = (1/2) \; \tau \; N$$

so with σ and τ given, N can be computed.

The other statistical parameter in the Kalman filter recursion is the measurement noise covariance matrix R_k. The

measurement noise in this case models the readout errors of both
inertial systems:

$$R_k = \overline{\underline{V}_k \ \underline{V}_k{}^T}$$

with $\qquad \underline{V}_k = \underline{\delta}_\varphi + C_{BS}{}^1 \ \underline{\delta}_G$

Zero mean errors are assumed. $\underline{\delta}_\varphi$ is the laser gyro quantization
error; its variance is

$$\sigma_\varphi = 1/12(\text{Experiment gyro quantization})^2$$

$\underline{\delta}_G$ represents the gimbal angle readout errors for the Shuttle
IMU. Data are given for noise and resolver figure errors in
Reference 5.3. The effect of these errors on the output data was
treated as statistically equivalent in all directions and
independent between coordinate axes. This is certainly an
approximation, but gives the correct magnitude for the effects.
The variance of this error is

$$\sigma_G{}^2 = \sigma_n{}^2 + 1/2 \sum_{i=1}^{16} \sigma_{0i}{}^2$$

The resulting matrix R_k is then diagonal with diagonal elements
$$R(i,i) = \sigma_\varphi{}^2 + \sigma_G{}^2$$

In the standard notation of the Kalman filter, the
measurement at time t_k is called $\underline{Z}_k$. In this problem the
measurement is the computed error rotation which reflects all the
errors in the chain of transformations relating the Shuttle IMU
platform coordinates, P, to the inertial coordinates as indicated
by the experiment IMU, I_r. This is the vector $\underline{\Phi}_s$ which was
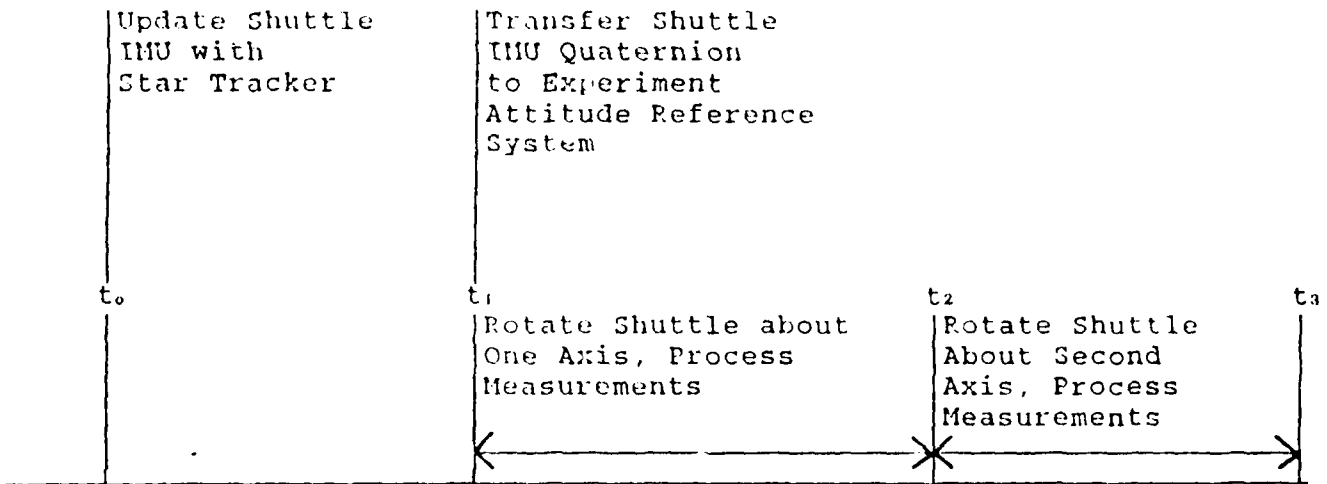discussed above.

It is very important that the covariance matrix for errors
in the estimate, P, be initialized in such a way as to represent

5-16

correctly the manner in which the physical system is initialized. The mission timeline which has been considered in the work is indicated in Figure 5.2. The statistics of the errors associated with the Shuttle IMU are defined at time t_0 when a star tracker update is performed. Each axis is treated as independent of the others. The error in stable platform alignment at that time is the residual error after star tracker update, for which data are given in Reference 5.3. The gyro bias error is a constant for which the variance is also specified. At that point the gyros have been operating for a long time so the random error, modeled by the first order Markov process, is in the statistical steady state. The steady state variance of this random drift is also given in Reference 5.3.

The experiment attitude reference system is initialized at time t_1. Rather than integrating Γ numerically between t_0 and t_1, the propagation of the error statistics over this interval was computed analytically. Only the P matrix elements associated with the Shuttle IMU are propagated in this way because they were defined at t_0. All the other P matrix elements are defined initially at t_1.

The errors in each of the coordinate axes propagate independently of each other. This, in effect, assumes that the gyro input axes are aligned with the reference inertial coordinates. The nominal inertial reference frame can, in fact, be chosen to satisfy this condition. Each 3 x 3 partition of $P(t_1)$ is then diagonal, and the diagonal elements of the partitions relating to $\underline{\Phi}_p$, $\underline{b}_p$, and $\underline{r}_p$, are as follows. Note that zero mean errors are considered throughout.

Figure 5.2   Simulated Mission Scenario Timeline

| Update Shuttle
IMU with
Star Tracker | Transfer Shuttle
IMU Quaternion
to Experiment
Attitude Reference
System | | |

t_0 .... t_1 .... t_2 .... t_3

| | Rotate Shuttle about
One Axis, Process
Measurements | Rotate Shuttle
About Second
Axis, Process
Measurements |

$$\overline{r_p(t_1)_i{}^2} = \overline{r_p(t_0)_i{}^2}$$

$$= (1/2)\tau_{p\,i}\,N_p$$

$$= \sigma_{r\,p}{}^2$$

This random drift rate was initialized in the statistical steady state, so the variance remains stationary.

$$\overline{b_p(t_1)^2} = \overline{b_p(t_0)^2}$$

$$= \sigma_{b\,p}{}^2$$

This is a random bias for which the statistics are constant.

$$\overline{\Phi_p(t_1)_i{}^2} = \overline{\Phi_p(t_0)^2} + \sigma_{b\,p}{}^2\Delta t_1{}^2$$

$$+ \tau_{p\,i}{}^2\ \sigma_{r\,p}{}^2\ (1-e^{-\Delta t_1/\tau_{p\,i}})^2$$

$$+ 2\tau_{p\,i}{}^2\ \sigma_{r\,p}{}^2\ [\,\Delta t_1/\tau_{p\,i} - 2(1-e^{-\Delta t_1/\tau_{p\,i}})$$

$$+ 1/2(1-e^{-2\Delta t_1/\tau_{p\,i}})\,]$$

with $\qquad \Delta t_1 = t_1 - t_0$

$$\overline{r_p(t_1)\ b_p(t_1)} = \emptyset$$

$$\overline{r_p(t_1)\ \Phi_p(t_1)_i} = \tau_{p\,i}\ \sigma^2{}_{r\,p}\ (1-e^{-\Delta t_1/\tau_{p\,i}})e^{-\Delta t_1/\tau_{p\,i}}$$

$$+ \tau_{p\,i}\,\sigma_{r\,p}{}^2\ (1-e^{-\Delta t_1/\tau_{p\,i}})^2$$

$$\overline{b_p(t_1)\Phi_p(t_1)} = \sigma_{b\,p}{}^2\,\Delta t_1$$

The remaining elements of the P matrix are initialized directly at t_1. All 3 x 3 partitions are diagonal. The variances of the elements of $\underline{b_f}$ and $\underline{k}$ are given by specifications for the laser gyros used in the experiment IMU. The variances of the elements of $\underline{\psi}$ are defined by the combined uncertainty in instrument block mounting and Shuttle static flexure. The

5-19

elements of $\underline{\Phi}_{ER}$ are initialized in the statistical steady state just like the elements of $\underline{r}_P$.

Initialization of the P matrix elements which involve $\underline{\Phi}_I$ is somewhat more complex. This initialization must reflect the operational procedure of initializing the experiment attitude reference system quaternion with the value derived from the Shuttle inertial system. The quaternion would be the same if the nominal body coordinates at the experiment package are taken to be the same as the body coordinates at the base of the Shuttle IMU. If there is a difference between the definitions of these coordinate frames, then the Shuttle-derived quaternion would be adjusted for the effect of the known transformation $C_{BS}{}^{BFN}$ before initializing the experiment attitude reference system.

This means that at time t_1, the experiment attitude reference system alignment error, $\underline{\Phi}_I$, has contributions from all the other errors in the system.

$$\underline{\Phi}_I(t_1) = \underline{\Phi}_P(t_1) + C^T{}_{BFn}\ \underline{\Phi}_{EB}(t_1) + C^T{}_{BFn}\ \underline{\Phi}_{ER}(t_1) - C^T{}_{BS}\ \underline{\delta}_G$$

These transformation matrices reflect the coordinatization used in the definitions of these variables. This expression makes it clear that $\underline{\Phi}_I(t_1)$ is correlated with $\underline{\Phi}_P$, $\underline{\Phi}_{EB}$, and $\underline{\Phi}_{ER}$ at that time. Moreover, since $\underline{\Phi}_P(t_1)$ is correlated with $\underline{b}_P$ and $\underline{r}_P$, $\underline{\Phi}_I$ has initial correlations with those state variables as well. The complete set of P matrix partitions is as follows:

$$\overline{\underline{\Phi}_I(t_1)\underline{\Phi}_I(t_1)^T} = \overline{\underline{\Phi}_P(t_1)\underline{\Phi}_P(t_1)^T}$$

$$+ C^T{}_{BFN}\ \overline{\underline{\Phi}_{EB}(t_1)\underline{\Phi}_{EB}(t_1)^T}\ C^T{}_{BFn}{}^T$$

$$+ C^T{}_{BFN}\ \overline{\underline{\Phi}_{ER}(t_1)\underline{\Phi}_{ER}(t_1)^T}\ C^T{}_{BFn}{}^T$$

$$+ C^T{}_{BS}\ \overline{\underline{\delta}_G\ \underline{\delta}_G{}^T}\ C^T{}_{BS}{}^T$$

$$\overline{\underline{\Phi}_I(t_1)\underline{\Phi}_P(t_1)^T} = \overline{\underline{\Phi}_P(t_1)\Phi_P(t_1)^T}$$

$$\overline{\underline{\Phi}_I(t_1)\underline{b}_P^T} = \overline{\underline{\Phi}_P(t_1)\underline{b}_P^T}$$

$$\overline{\underline{\Phi}_I(t_1)\underline{r}_P(t_1)^T} = \overline{\underline{\Phi}_P(t_1)\underline{r}_P(t_1)^T}$$

$$\overline{\underline{\Phi}_I(t_1)\underline{\Phi}_{FB}(t_1)^T} = C^T{}_{BEn}\overline{\underline{\Phi}_{FB}(t_1)\underline{\Phi}_{FB}(t_1)^T}$$

$$\overline{\underline{\Phi}_I(t_1)\underline{\Phi}_{FR}(t_1)^T} = C^T{}_{BEn}\overline{\underline{\Phi}_{ER}(t_1)\underline{\Phi}_{ER}(t_1)^T}$$

All elements of P not discussed explicitly are zero at
initialization (t_1).

5.5 Simulation Results

The values used for the statistical parameters, and the
sources of these values, are shown in Table 5.1. The Markov
component of misalignment due to Shuttle body flexure was set to
zero in these runs because the character of Shuttle flexing is
not clearly documented, and even if it were, the Markov process
would look very much like a bias over the brief interval in which
measurements are processed. The bias component of initial
misalignment, on the other hand, was taken to be quite large;
a one sigma value of 1 degree.

The time t_0 was set to zero; this defines the origin of the
time scale. t_1 was taken to be 10 seconds. This may be an
unrealistically short interval of time between star tracker
update of the Shuttle IMU and the beginning of measurement
processing requiring experiment IMU data as well. However, the
results would not change significantly with several minutes of
delay.

Table 5.1

Values of the Statistical Parameters

Experiment gyro bias drift rate	σ_{bE}	$= 0.004$ deg/hr	Ref. 5.4
Experiment gyro scale factor error	σ_k	$= 5$ ppm	Ref. 5.4
Experiment gyro random walk drift	$\sqrt{N_R}$	$= 0.001$ deg/$\sqrt{\text{hr}}$	Ref. 5.4
Shuttle platform alignment error	$\sigma_{\phi P}$	$= 70$ arc sec	Ref. 5.3
Platform gyro bias drift rate	σ_{bP}	$= 0.022$ deg/hr	Ref. 5.3
Platform gyro random drift rate	σ_{rP}	$= 0.004$ deg/hr	Ref. 5.3
Experiment IMU bias misalignment	σ_{EB}	$= 1$ deg	Assumed
Experiment IMU random misalignment	σ_{ER}	$= 0$	Assumed
Experiment gyro quantization error	σ_Q	$= 1/\sqrt{12}(1$ arc sec)	Ref. 5.4
Shuttle platform gimbal readout error	σ_u	$= 12$ arc sec	Ref. 5.3
	σ_{u1}	$= 7.6$ arc sec	Ref. 5.3
	σ_{u0}	$= 19.0$ arc sec	Ref. 5.3
	σ_{u9}	$= 4.2$ arc sec	Ref. 5.3
	σ_{u16}	$= 20.0$ arc sec	Ref. 5.3
	σ_{ui}	$= 0$ (Other i)	Ref. 5.3
Time constant of Markov Model for platform gyro random drift	τ_{Pi}	chosen from a uniform distribution in the interval (1200, 3600) sec.	Ref. 5.3

A series of runs was made with individual error statistics
set to unrealistically large values. The purpose of this was to
see if the resulting performance, which was then dominated by one
error source, had the expected behavior. After the program was
fully debugged, all of these check cases were consistent with our
intuition about the problem.

The following series of figures shows the results of a run
using the correct values of all statistical parameters. Each
figure shows the results pertaining to one of the components of
Φ_I which is the error of interest - the experiment IMU alignment
error. The plus and minus 1 sigma values for the estimation
error are plotted along with a randomly chosen actual error and
the estimate of that error. These are all presented in
milliradians. The standard Shuttle motion was a one revolution
rotation about the x (longitudinal) axis over the interval 10 to
70 seconds followed by a one revolution rotation about the y
(pitch) axis in the interval 70 to 130 sec.

Figure 5.3 shows the results for the x axis. The initial
error standard deviation is about 17 mrad due to the dominating
effect of the 1 degree (1σ) misalignment error - $\Phi_{E\beta}$. The random
sample of actual error is about -8 mrad It is seen that the
computed error standard deviation does not change noticeably
during the first rotation about the x axis, nor does the estimate
deviate significantly from its initial value of zero. This is as
expected because there is no information generated about the x
axis component of misalignment in a rotation about x. However,
once the rotation about y begins, the computed standard deviation
drops very rapidly to its small steady state value - about 0.4
mrad - and the estimate of the error converges rapidly to the
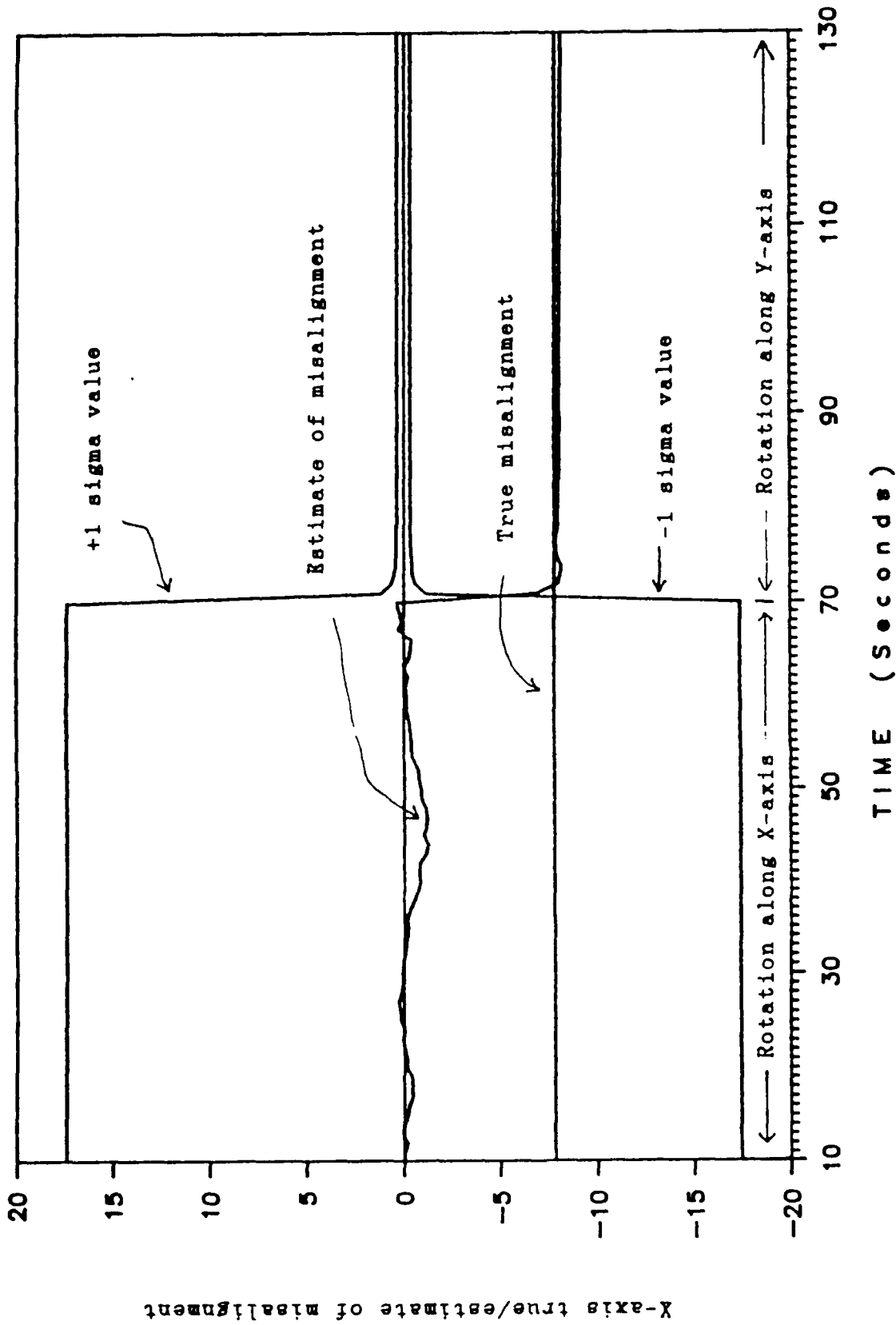actual value.

Figure 5.3: True and estimate of X-axis misalignment and its 1
sigma predicted value for Shuttle rotations of 1
rev/min along X-axis followed by rotation along Y-axis

In order to display more clearly the behavior of the filter
once the error has converged, the last half of the previous
figure is shown on an expanded scale in Figure 5.4. The plus and
minus 1 sigma values are shown together with the actual estimate
error for the sample case. The computed 1 sigma value is about
0.4 mrad as noted above and the actual estimate error happened to
be about a 1 σ value. Little noise is observed on the error
after its initial convergence. This is because the Kalman gain
shuts down very rapidly due to the relatively small measurement
noise variance. After the gain has been turned down, it is so
small that the measurement noise does not propagate significantly
through the individual measurements. The small gain also
explains why the error drifts slightly without correction. It is
often the case in practical applications of the Kalman filter
that additional state driving noise is inserted in the model for
the purpose of keeping the steady state gain somewhat higher.
This has the effect of controlling bias in the resulting error
history at the expense of somewhat greater noise.

The behavior of the estimator for the y axis component of
misalignment is shown in the next two figures. Figure 5.5 shows
the misalignment component and its estimate while Figure 5.6
shows the estimate error on an expanded scale. As one would
expect, the error and the computed 1 sigma value converge
immediately because the y component of misalignment is made
visible by the rotation about the x axis which begins at 10
seconds. The measurements are not sensitive to the y component
of misalignment during the rotation about the y axis in the
second half of the time interval, but the error behavior is not
significantly affected because the driving noises which cause
error growth - the gyro drift effects - are very small.

Corresponding information about the z axis is shown in
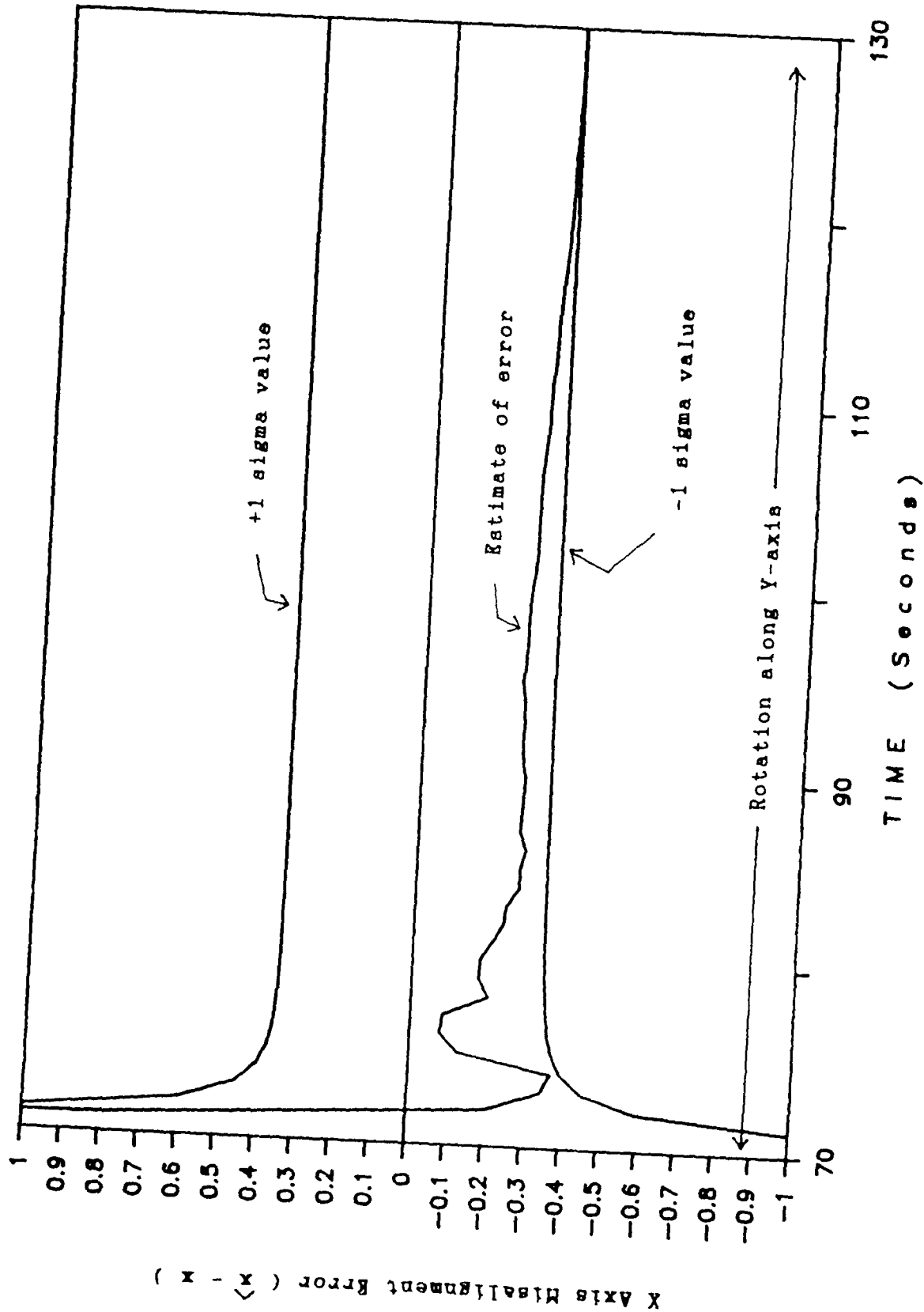Figures 5.7 and 5.8. The estimator has sensitivity to the z

5-25

Figure 5.4: Estimate of X-axis misalignment error and its 1 sigma preuicted value for Shuttle rotations of 1 rev/min along X-axis followed by rotation along Y-axis
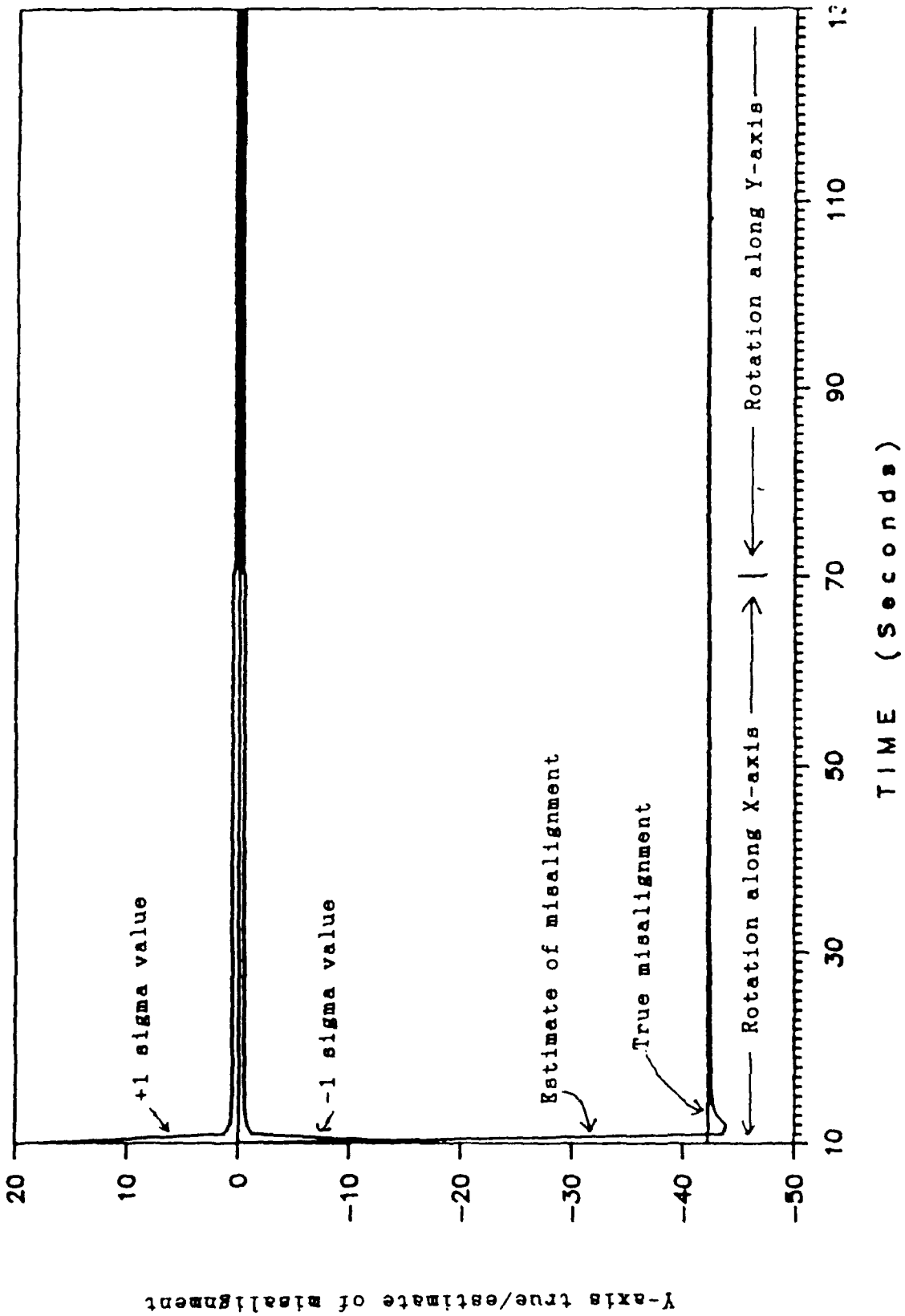
Figure 5.5: True and estimate of Y-axis misalignment and its 1 sigma predicted value for Shuttle rotations of 1 rev/min along X-axis followed by rotation along Y-axis
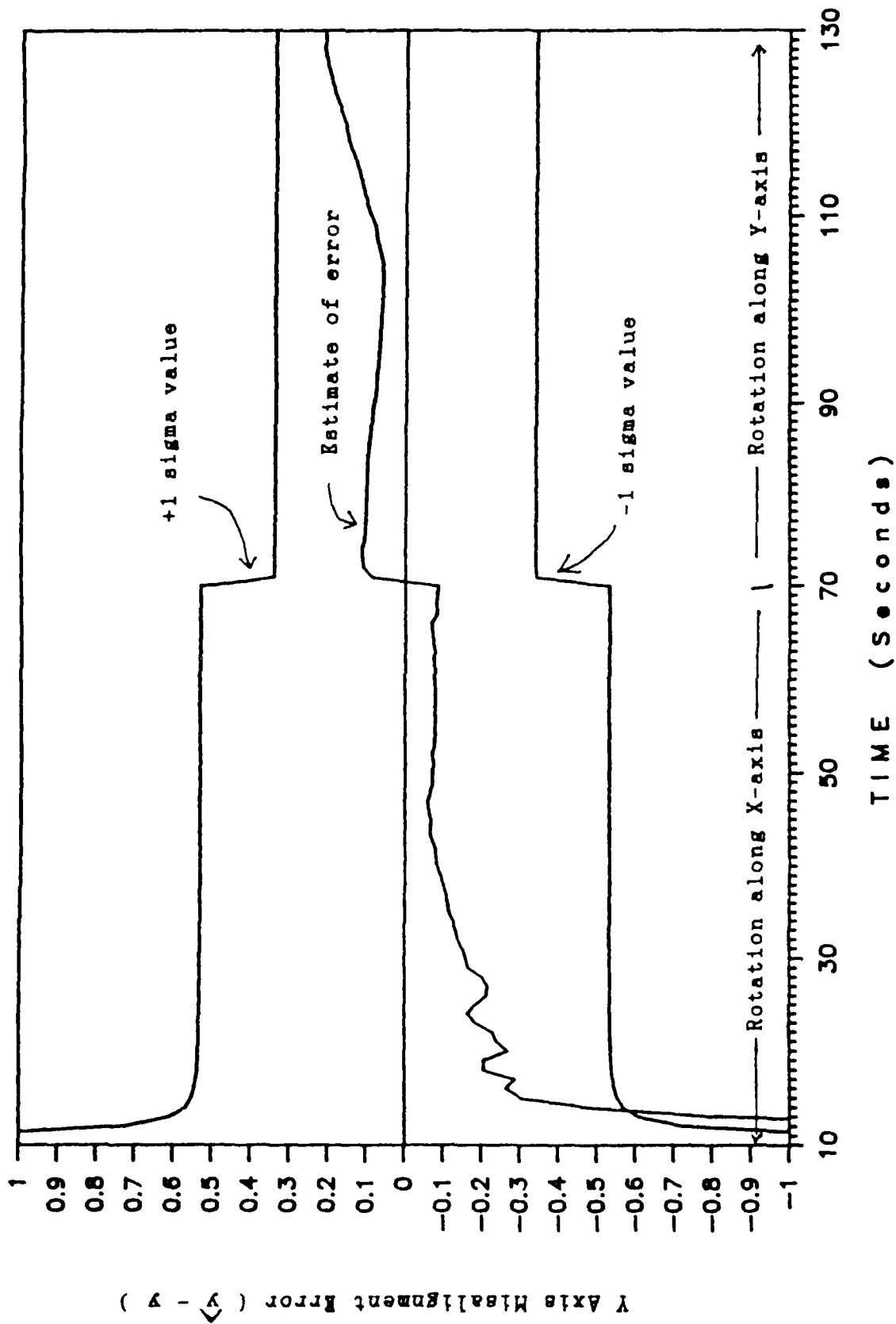
Figure 5.6: Estimate of Y-axis misalignment error and its 1 sigma predicted value for Shuttle rotations of 1 rev/min along X-axis followed by rotation along Y-axis

component of misalignment during both the x axis and y axis rotations. Again it is clear that the Kalman gain shuts down very quickly after each rotation is initiated. There is a small transient at the beginning of the y axis rotation at 70 seconds, but the error had already converged. Again the computed 1 sigma value settles down to something less than 0.4 mrad and the actual estimate error is less than the 1 sigma value.

5.6 Conclusions

The transfer of alignment information from one inertial system to another is dependent on the measurement of some common inertial quantities by both systems. For a Shuttle-based application, the most fuel-efficient inertial quantity to generate is an angular rotation. A misalignment estimator configured as an optimal recursive estimator has the advantage, relative to algorithms based on a sequence of discrete rotations, of operational flexibility. The recursive estimator can take advantage of whatever rotational motion occurs and at whatever time it happens.

The mission simulated involved full rotations of the Shuttle about two axes. This is not a severe operational burden - taking place in just 2 minutes of time. But the results make it clear that even this much motion is not necessary. Each component of misalignment error converges to a 1 sigma value of less than 1 mrad within 8 seconds of the time a rotation it is sensitive to begins. During that time, the Shuttle turns through only 48 degrees. For the rest of the rotation, the filter gain is shut down and the estimate hardly changes. At the end of the standard mission profile, all three components of experiment IMU misalignment are known to about 0.4 mrad, 1 sigma.
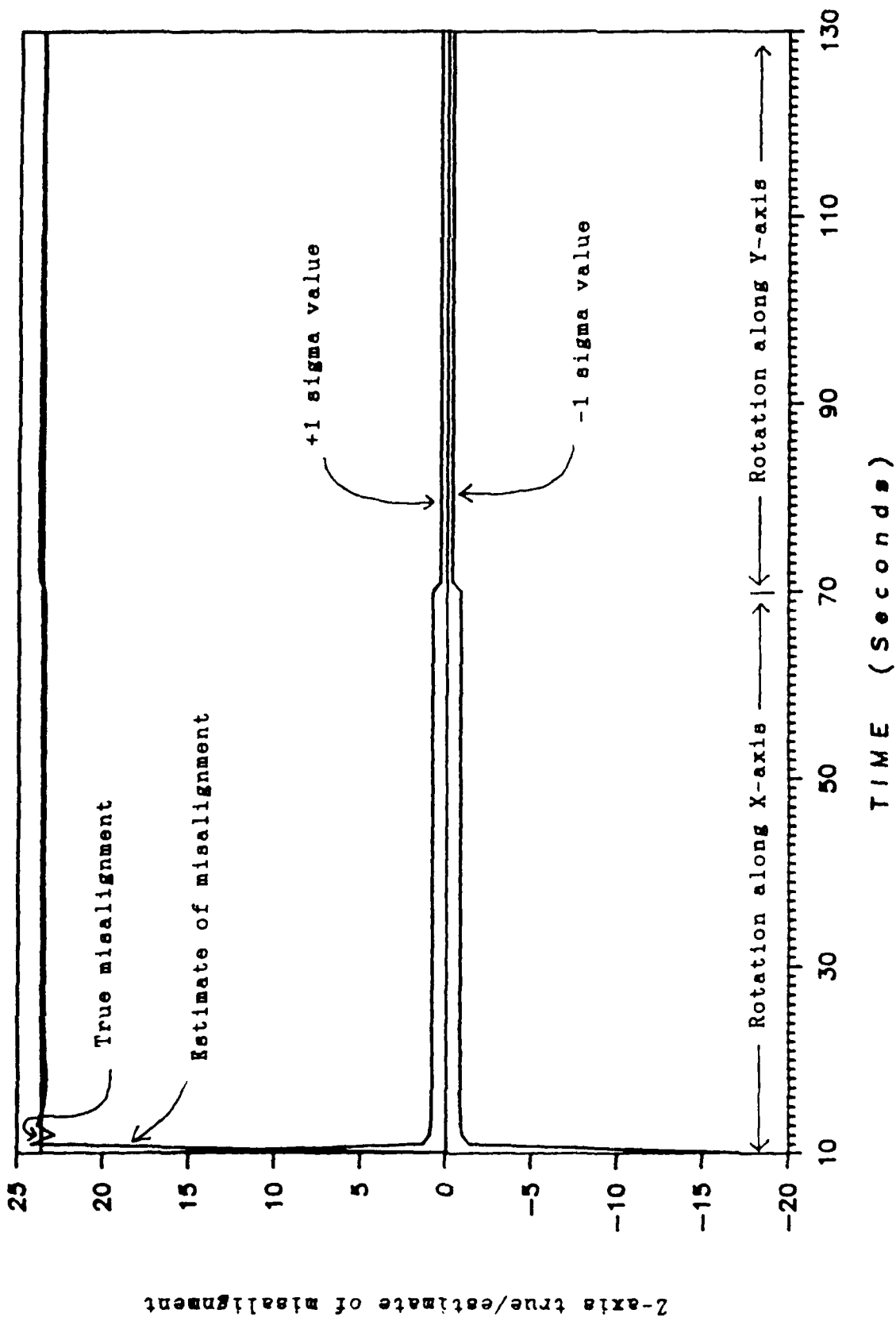
5-29

Figure 5.7: True and estimate of Z-axis misalignment and its 1 sigma predicted value for Shuttle rotations of 1 rev/min along X-axis followed by rotation along Y-axis
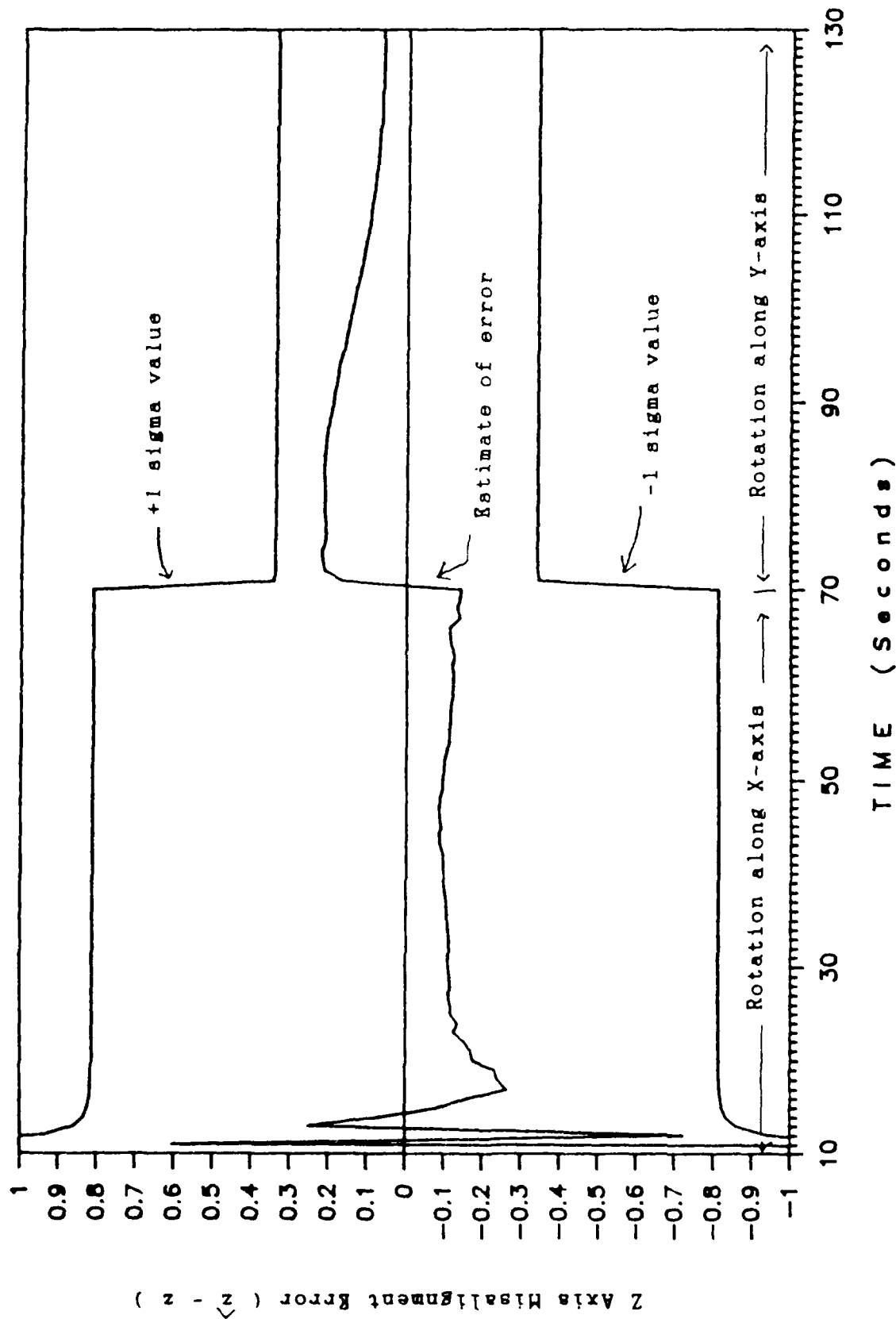
Figure 5.8: Estimate of Z-axis misalignment error and its 1 sigma predicted value for Shuttle rotations of 1 rev/min along X-axis followed by rotation along Y-axis

Further work should be done to assess the behavior of the estimator in the environment of rotations occurring naturally in the mission. Also, the long term behavior of the alignment error must be evaluated - both with and without continued processing of measurement data. But this initial evaluation suggests that the recursive estimation of alignment error in the presence of some Shuttle rotations holds a great deal of promise.

REFERENCES

5.1 - Treder, A., Norris, R. and Ruprecht, R.:
"Inflight Alignment of Payload Inertial Reference
from Shuttle Navigation System", Advances in
the Astronautical Sciences, Vol. 57, 1985.

5.2 - Meldahl, K., Norris, R. and Clark, J.: "Flight
Data Evaluation of a Technique for Payload
Inertial Reference Alignment Transfer from the
Shuttle Navigation System", Institute of Navigation,
Proceeding of Technical Meeting, Anaheim, CA,
January 1987.

5.3 - Onboard Navigation System Characteristics, JSC Report
No. JSC-14675, NASA Mission Planning and Analysis
Division; December 1981.

5.4 - Upadhyay, T.N., D.B. Cox and C. Jekeli, "STS-GPS
Tracking for Anomalous Gravitation Estimation -
STAGE", Presented at the Sixteenth Gravity Gradiometer
Conference, Sponsored by the Air Force Geophysics
Laboratory, Hanscom AFB, MA, February 1988.

5.5 Karsenti, Serge M., A Study of IMU Alignment Transfer,
M.S. Thesis, Department of Aeronautics and
Astronautics, MIT, Cambridge, February 1989, Mayflower
Communications Technical Report No.
MCCI-TR-89-861002-001

SECTION 6
SHUTTLE PAYLOAD INTEGRATION

This section describes the results of the experiment payload/Shuttle integration study. The objective of the integration study was to define a baseline experiment system configuration that is compatible with the Space Transportation System Orbiter (i.e., the Space Shuttle). The study was carried out with support from Rockwell International, Space Transportation Systems Division under a subcontract from Mayflower Communications Company, Inc. In this section we describe the trade-offs between different payload configurations that were analyzed and detail the selected configuration that is recommended to support the goals of the Air Force gravity estimation experiment.

6.1 Payload Configuration Options

The experiment payload integration analysis for the Shuttle required trade-offs of performance, cost, autonomy and required modifications to the Shuttle. In consultation with Rockwell, it was decided early on in the analysis that the selected configuration will have a higher probability of being manifested in future Shuttle flights if its operation does not interfere with normal Shuttle mission and that it requires minimum (or no) modification to the Shuttle hardware and/or software. This approach led to the following conclusions:

1. No real-time Shuttle telemetry interface to the experiment hardware should be established – the interface cost to store experiment data on the mission recorder will be excessive and cannot be supported. Therefore, the experiment payload should be autonomous and carry its own tape recorder to store experiment data during the Shuttle flight. The

Shuttle crew interface to the experiment payload should be kept to a minimum requiring them only to turn on power when the Shuttle is in its orbit, and possibly to load a new tape, if required during the flight.

2. The Shuttle INS navigation data cannot be made available for recording to the experiment computer/processor in real-time. Any discrepancy in aligning the time tags between the Shuttle and experiment data should be resolved during post-processing analysis. The reason for this decision is once again the excessive cost and risk of providing the interface between the Shuttle navigation mission computer (called GPC) and the experiment mission computer.

3. No optical alignment of the experiment payload IMU from the Shuttle star tracker (similar to the Shuttle IMU alignment) can be supported because NASA will not permit mounting of the experiment IMU on the Shuttle navigation base. For this reason, the feasibility of the experiment payload carrying its own attitude update sensor, i.e., a star tracker in the payload base, was analyzed for its cost and performance. This approach was traded-off against an alternate approach of transferring alignment from the Shuttle IMU to the experiment using Shuttle rotation maneuvers. Even though, the latter approach imposes some minimal constraints on the Shuttle mission, it was selected for this experiment since the complexity and cost savings over the first approach far outweigh the concerns on Shuttle mission. The performance of the proposed transfer alignment approach was analyzed and reported in Section 5. A comparison of the above two approaches for attitude estimation is described below.

In addition to the above issues affecting the experiment hardware configuration, other issues that were analyzed are:

size, power and weight of the hardware, the Shuttle environment and the space availability (with high probability of it being available over several Shuttle flights). These considerations led us to analyze the merits of the two selected configurations which were traded off. The two configuration options that were traded off are: (1) Aft flight deck/middeck location, (2) Payload bay location. In addition to the obvious differences in the location of the experiment hardware on the Shuttle, as identified by these two configurations, the two configurations differ in the composition of the actual hardware. The first configuration slated for the aft flight deck/middeck uses the existing GPS antennas and the star tracker on the Shuttle while the second configuration is completely autonomous and requires its own GPS antenna and star tracker. These two configurations are shown in Figure 6.1 and 6.2, respectively. A relative comparison of the two configurations is summarized in Table 6.1.

In Table 6.1 we observe that the advantages of the experiment hardware configuration option I are: (1) it requires no modification to the Shuttle, (2) the experiment hardware does not have to be space qualified, and (3) its low cost. Since this option does not require modifications to the Shuttle it has the maximum probability of being approved and manifested on the Shuttle. Its greatest disadvantage is that it will require Shuttle on-orbit rotation maneuver to align the experiment IMU. The transfer alignment problem has been investigated and the simulation results (Section 5) indicate that the requirements on Shuttle rotation maneuvers are benign - a fraction of a revolution (less than 60 degree rotation) is required to achieve the desired accuracy.

UPPER ANT*

PRE-
AMP

LOWER ANT*

IMU

NAV BASE

PWR

GPS
RECEIVER

EXP
PROCESSOR

FROM P/L
TIMING BUFFER

TAPE
RECORDER

EXPERIMENT PACKAGE

* Existing
NO Orbiter FLT SWR Deltas
ON Board recording, No TLM
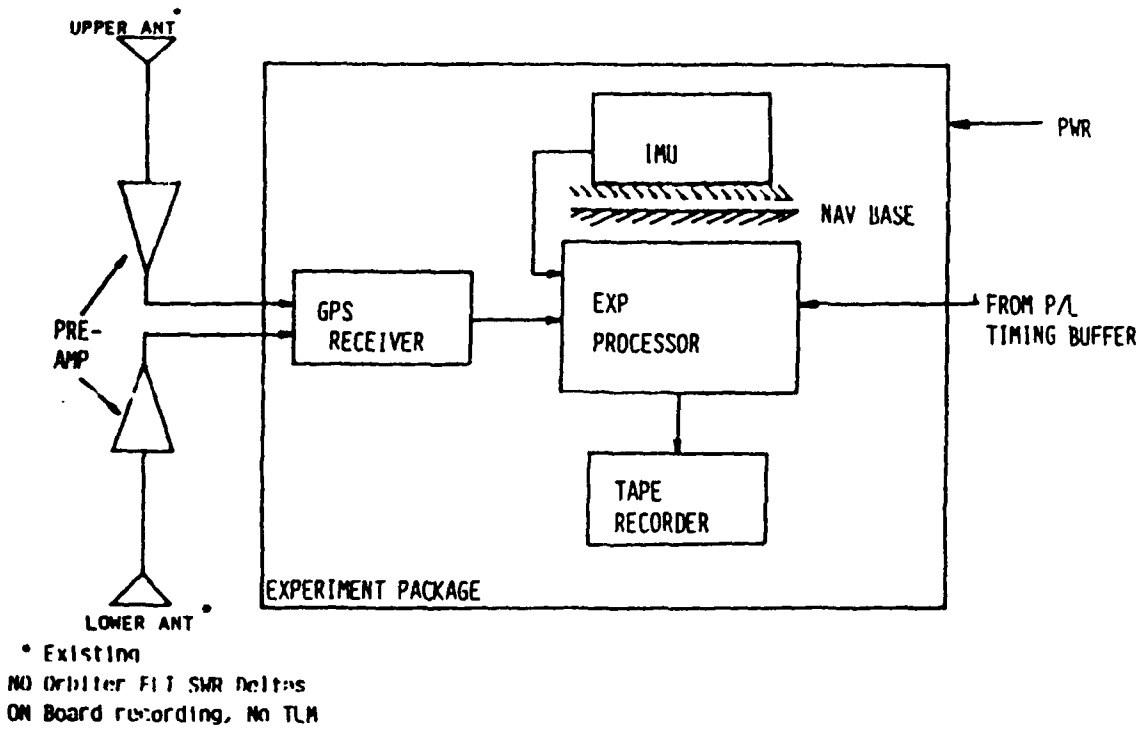
FIGURE 6.1
PAYLOAD OPTION 1:   AFT FLIGHT DECK/MIDDECK LOCATION

GPS ANTENNA (TBD)

PRE-
AMP

EXPERIMENT PACKAGE

IMU

STAR TRACKER

COMMON
NAV BASE

GPS
RECEIVER

EXP.
PROCESSOR

FROM P/L TIMING BUFFER

POWER.

TAPE
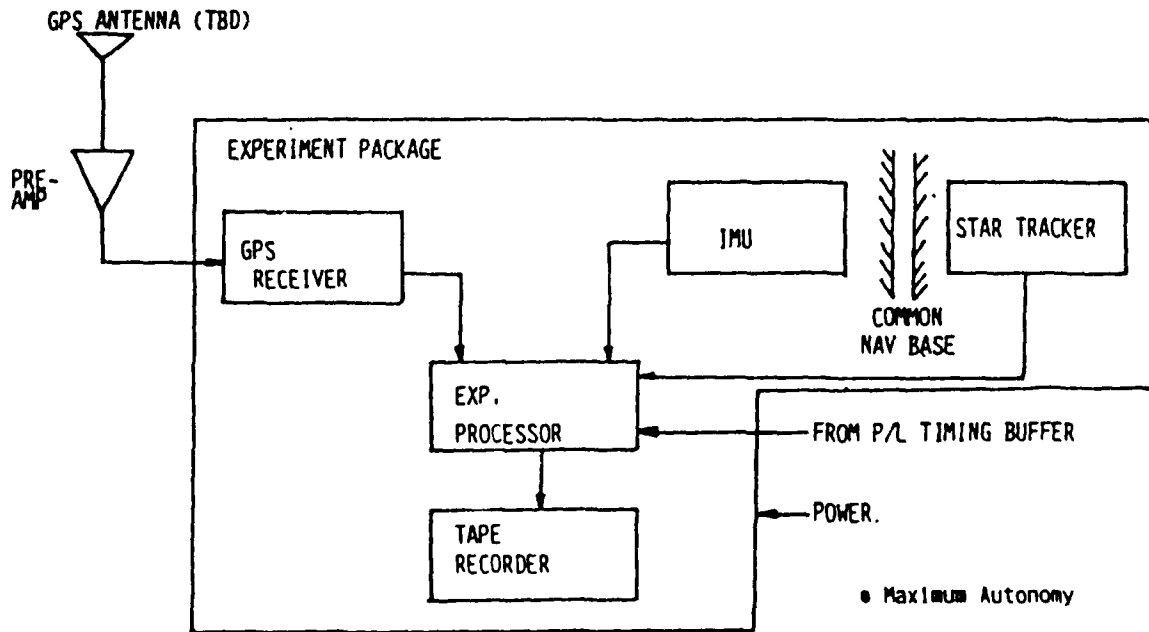RECORDER

• Maximum Autonomy

FIGURE 6.2
PAYLOAD OPTION 2:   PAYLOAD BAY LOCATION

Table 6.1 Comparison of Payload Hardware Configurations

	OPTION I Middeck/Aft Flight Deck	OPTION II Payload Bay
GPS Antenna*	Use Present Shuttle Antenna (Preamplifier to be supplied	New (Preamplifier to be supplied)
GPS Receiver	New	New
IMU	New	New Integrated
Star Tracker	Use Present Shuttle Tracker and OPS recorder data	New
Data Recorder	New	New

Advantages	1. Don't need to procure
	   Star Tracker (ST)
	
	2. GPS and IMU don't need
	   full space qual.
	3. Low cost
		1. Self-contained
		   (new ST, IMU,GPS
		   clustered)
		2 High alignment
		   acc.
		3. Don't need
		   transfer align-
		   ment maneuver

Disadvantages	1.Moderate alignment acc.
	
	2. Need Shuttle on-orbit
	   maneuver for alignment
	3. Need to process Shuttle
	   OPS recorder for ST
		1. Higher hardware
		   cost
		2. Higher integra-
		   tion cost

*Option I will benefit by a payload bay GPS Antenna.

The hardware configuration option II requires a star tracker
and new GPS antenna which along with the IMU will be located in
the payload bay. This option offers full autonomy and best
performance (alignment accuracy of the star tracker and minimum
lever-arm effect since the GPS antenna will be located near the
IMU). However, this option is less desirable because of its
excessive cost due to both the higher hardware procurement cost
(cost of the star tracker plus space qualifications) and the
higher Shuttle integration cost. For the above reasons, the
trade-off study resulted in the selection of option I as the

preferred choice.

A ROM cost estimate for the two configurations is presented in Table 6.2. We note the total cost of the experiment for option I is at about $6-7 million, while the cost for option II is about $10-12 million. As mentioned earlier, the higher cost of option II is due to the higher cost of the hardware due to space qualification requirements and due to the higher integration cost. The details of ROM orbiter integration cost for the selected configuration was developed by Rockwell. The cost estimates are summarized below in Table 6.2.

TABLE 6.2

STS-GPS TRACKING EXPERIMENT FOR GRAVITATION ESTIMATION
PAYLOAD COST ESTIMATE ROM

Item	Option I	Option II
1. Experiment Design and Lab Checkout	$1.5 M	$2 M
2. Experiment GPS	$1.0 M	$2-3 M
3. Experiment IMU	$1.0-1.5 M	$2 M
4. Experiment Star Tracker	----	$1 M
5. Recorder & Processor	$0.3 M	$0.3 M
6. Orbiter Integration*	$2.0 M	$3-5 M
7 Post-flight Data Processing	$0.5 M	$0.3M
Total	$6-7 M	$10-12 M

*Orbiter integration cost includes integration h/w, orbiter preparation (cabling, power), and assembly instructions.

The details of the selected configuration are presented next.

6.2 Selected Experiment Installation Configuration

The ground rules (assumptions) used in developing details of
the final installation configuration were:

1. The experiment will be installed as an orbiter mission kit
   with orbiter interfaces.

2. The experiment will utilize orbiter power and controls with
   crew module ECLSS cooling provisions.

3. The avionics and instrumentation will be compatible with the
   Shuttle electrical, thermal, structural and crew function
   interfaces.

Table 6.3 below presents a preliminary size, power and
weight estimates for the components of the experiment hardware
that were used in arriving at the recommended locations for each.

TABLE 6.3   EXPERIMENT HARDWARE SIZE, POWER, WEIGHT BREAKDOWN

Hardware Module	Size Cu inch	Power Watts	Weight lbs	Cooling
GPS Receiver	6"x6"x12"	35 W	14 lbs	Air Cooled
Inertial Measurement Unit (IMU)	17"x30"x12"	180 W	120 lbs	Heat Sink
Tape Recorder	23"x16"x7 1/2	115 W	57 lbs	Air Cooled
Processor	18"x12"x8"	50 W	30 lbs	Air Cooled

6.2.1   Physical Installation

Consistent with the above ground rules and incorporating the
general conclusions outlined in Section 6.1, the study

recommended the following installation configuration for the experiment hardware. The recommended installation complies with the size, power, and weight requirements for each hardware component (subsystem) of the experiment. The resulting recommended installation for the experiment is described below.

1. The GPS receiver will be located in the flight crew compartment in an area identified as L-10. The GPS receiver will utilize existing upper and lower fuselage installed antennas and coax provisions to the $X_o = 576$ bulkhead.

2. The inertial measurement unit (IMU) will be located on the centerline wing box structure adjacent to the vehicle center of mass (CG). This location provides a disturbance free environment and a solid structure to install the nav base on which the IMU will be mounted. The size, power and weight of the IMU can easily be accommodated on the recommended location.

3. The electronic processing assembly will be installed adjacent to the GPS receiver in area L-10 and will integrate the orbiter timing buffer.

4. The flight recorder will share the L-10 volume with ground support equipment access provisions. The recorder will be channelized for maximum experiment data acquisition. The ground support equipment interface hardware will be post flight carry-on to transfer recorded data via the orbiter T-0 umbilical.

The physical installation locations for each of the experiment subsystems is shown in Figure 6.3. The figure also shows the locations of the two GPS antennas and the location of
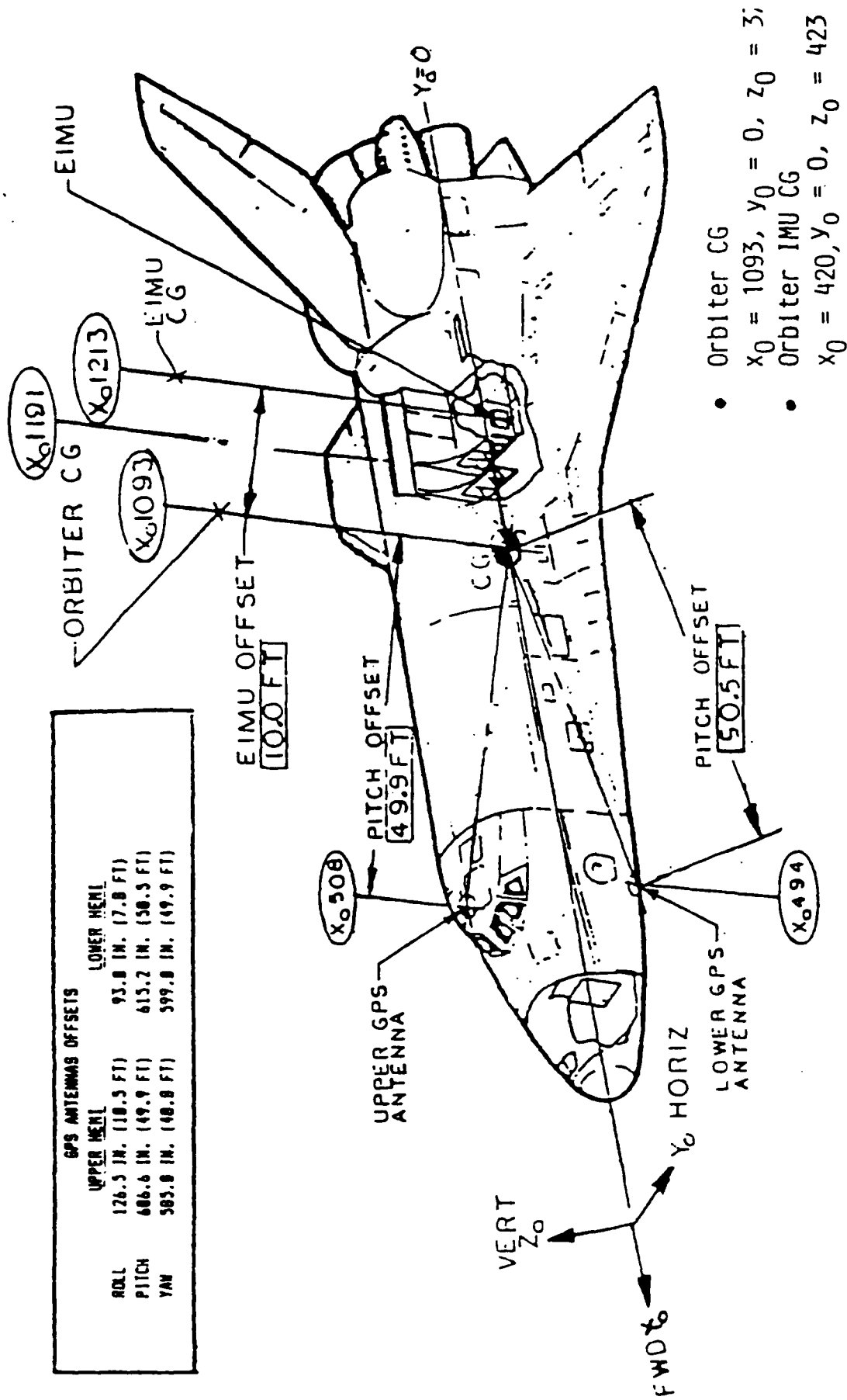
ORBITER EXPERIMENT C. G. MOMENTS

FIGURE 6.3 ORBITER INSTALLATION LOCATION FOR EXPERIMENT HARDWARE SUBSYSTEMS

the Shuttle IMU. From this installation figure, we note that the experiment IMU offset from the Shuttle CG is about 10 feet while its offset from the GPS antennas is about 50 feet. The location of the L-10 area which will house the GPS receiver, processor and recorder on the flight deck is shown in Figure 6.4. An expanded cross-selectional view of the L-10 volume is shown in Figure 6.5.

The installation of the experiment IMU on the centerline wing box including the alignment tooling is described next.

6.2.2 Experiment IMU Installation and Alignment

The experiment IMU will be installed on the centerline wing box Figure 6.6. The ground alignment tooling for the experiment IMU will come from another NASA experiment (OARE) and therefore will be made available to the Air Force experiment at no cost. This represents a substantial cost savings to the payload integration cost. Rockwell data shows that EIMU can be aligned using the existing alignment telescope to an accuracy of 3 arcmin (about 1 mrad) in each axis. EIMU alignment method and special tooling required for proper installation and alignment diagram is shown in Figure 6.7.

6.3 Electrical Installation and Data Transfer

A top level block diagram of the experiment system is shown in Figure 6.8. The output of the two GPS antennas is combined (after preamplification) and sent to the GPS receiver. The data interface between GPS receiver, experiment IMU, processor and recorder is shown in this diagram. The IRIG "B" time data from the orbiter timing buffer is sent to the experiment processor for recording on the tape recorder. The power and control connections to each of the instruments are shown in Figure 6.9 and the corresponding wiring interface is shown in Figure 6.10.

RECORDER

VOL L-10 (left side looking forward)

L-11

A7-A2 PANEL

switches

GPS RECEIVER

PROCESSOR
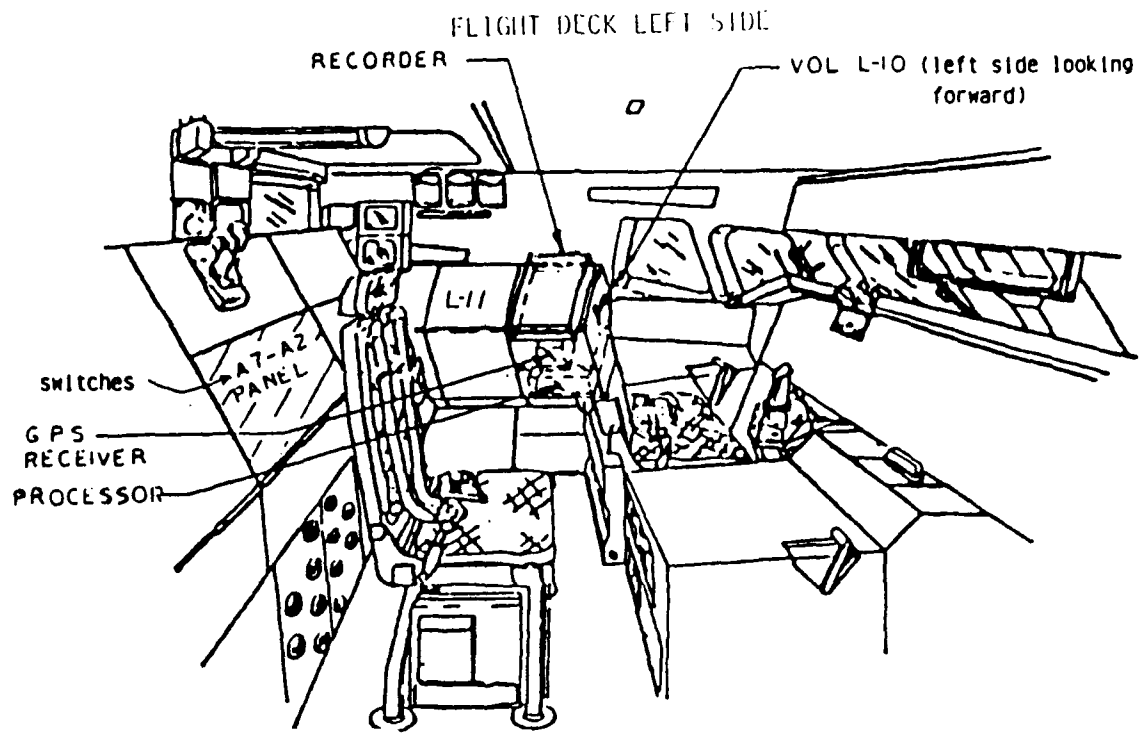
FIGURE 6.4   VIEW OF THE L-10 AREA ON THE FLIGHT DECK

VOLUME L-10 COMPONENT ARRANGEMENT

Zo 470.00

RECORDER

COOLING DUCT

GPS RECEIVER

Zo 440.00

PROCESSOR

UP

INBD
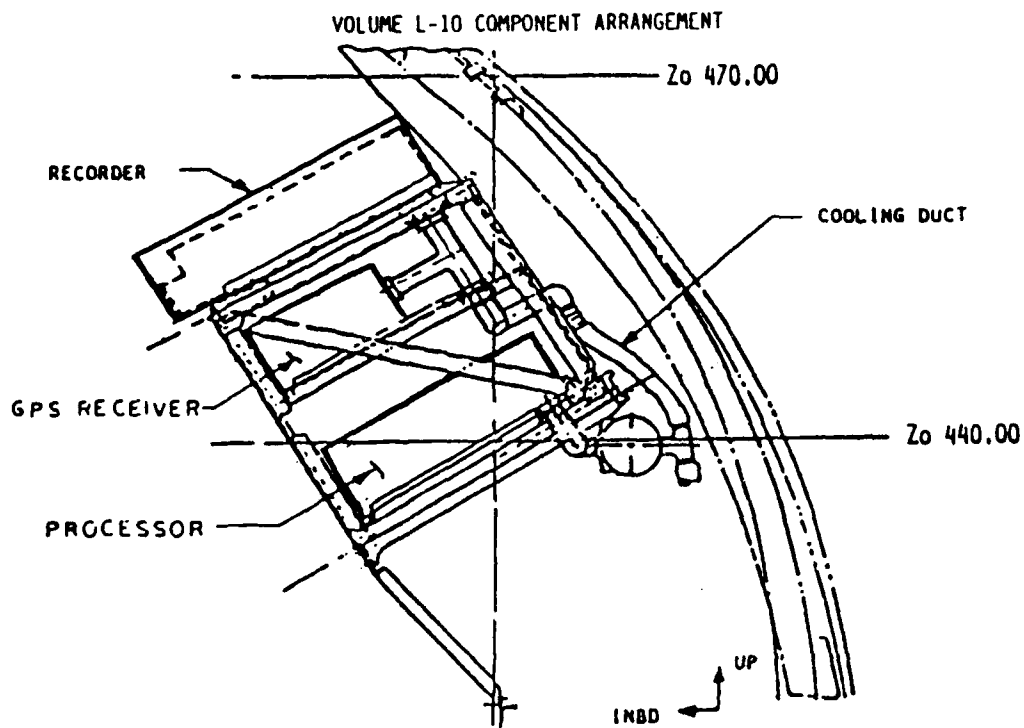
FIGURE 6.5   VOLUME L-10 COMPONENT ARRANGEMENT

ORBITER GPS TRACKING EXPERIMENT

EIMU INSTL ON CENTERLINE WING BOX

EIMU MOUNTING PANEL

FIBERGLASS ATTACH STRUCTURE

PAYLOAD BAY M_L

EIMU PKG

ALIGN DATUM

$X_o1199.26$

INSTRUMENT INDEX PINS

Z_o300

X_o1191

X_o1249

LOWER M_L

VIEW LOOKING INBOARD

Z_o

X_o
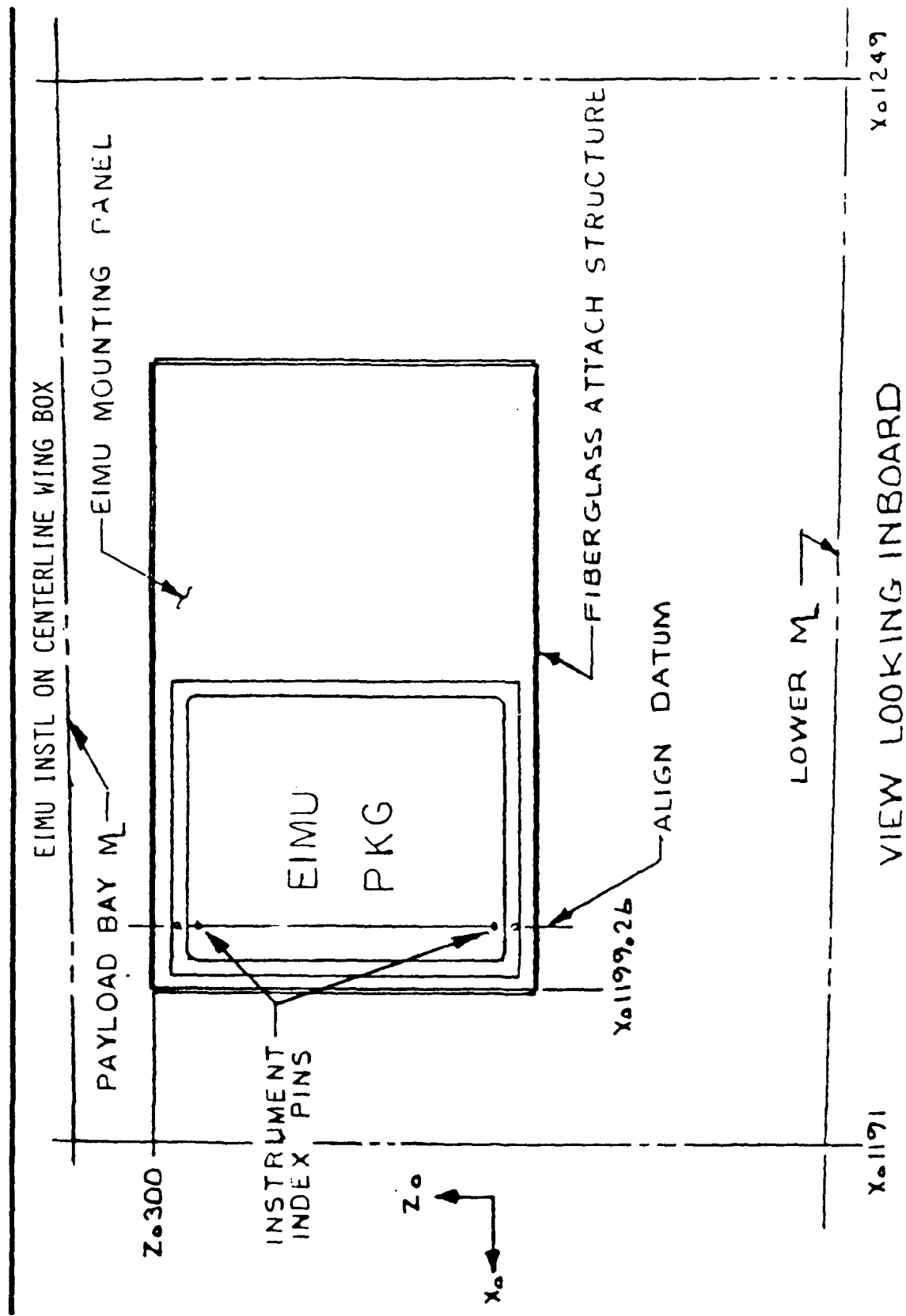
Figure 6.6

ORBITER GPS TRACKING EXPERIMENT

EIMU ALIGNMENT TOOLING

$X_o\ 0$
$Z_c\ .312\ REF$
LOS

LOS

LOS

BASE ALIGNMENT TOOL

$\mathbb{C}$ ALIGNMENT PINS

LOS = LINE OF SIGHT

$X_o\ 1249$ REF

$X_o\ 1191$ REF

ORBITER LOS ALIGNMENT ADAPTER

ALIGNMENT TELESCOPE

EIMU / ORBITER	
AXIS PARALLEL TO	TOLERANCE
X	WITH-IN 3 ARC MIN
Y	WITH-IN 5 ARC MIN
Z	WITH-IN 5 ARC MIN

VERT Z_o

X_c FWD

Y_c HORIZ
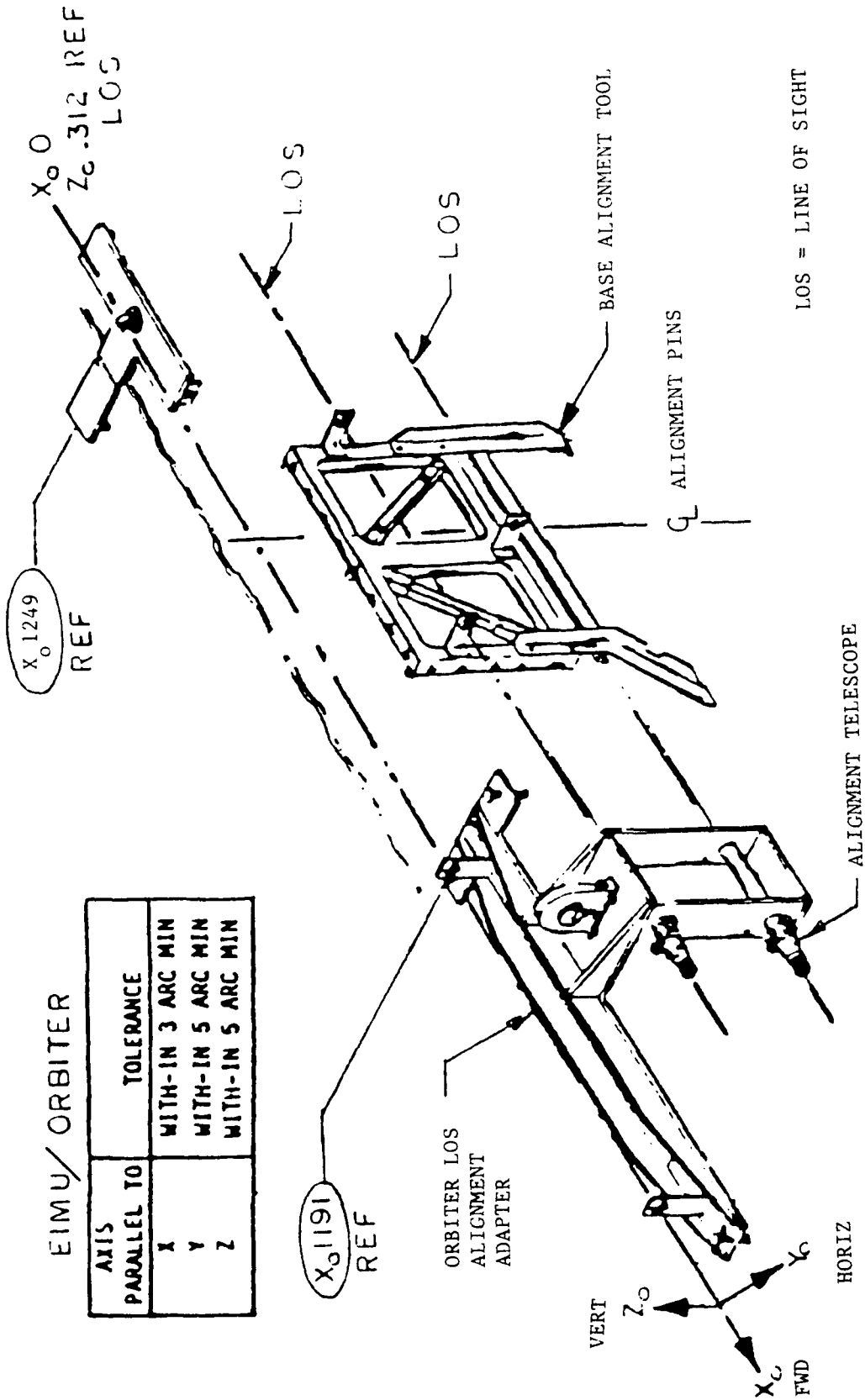
Figure 6.7

ORBITER GPS TRACKING EXPERIMENT BLOCK DIAGRAM
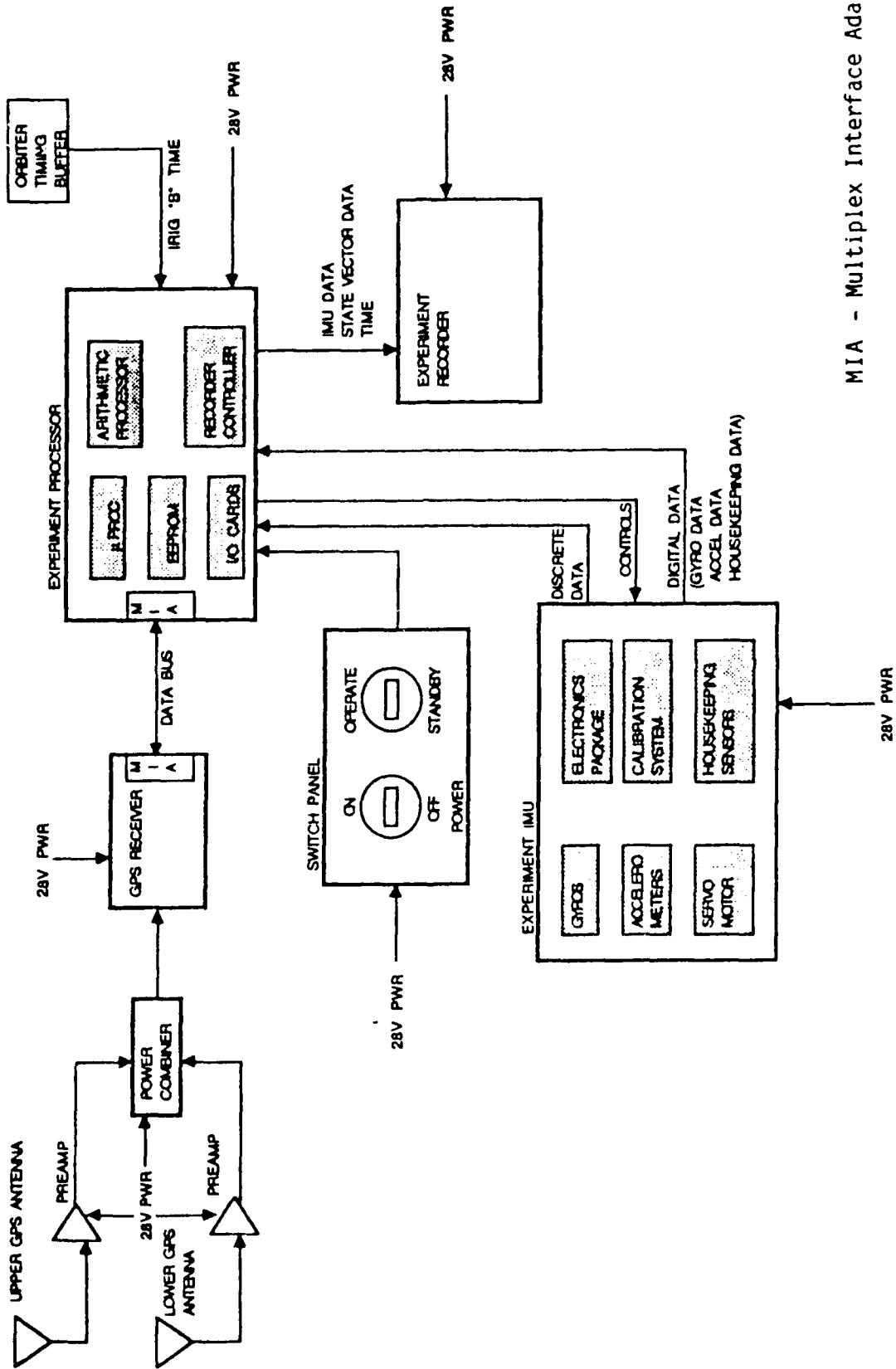
MIA - Multiplex Interface Adapter

Figure 6.8

ORBITER GPS TRACKING EXPERIMENT
POWER & CONTROL

Figure 6.9

ORBITER GPS TRACKING EXPERIMENT
WIRING INTERFACE

HO – High Voltage 28V
ML – Low Voltage 0-5V

Figure 6.10

6-16

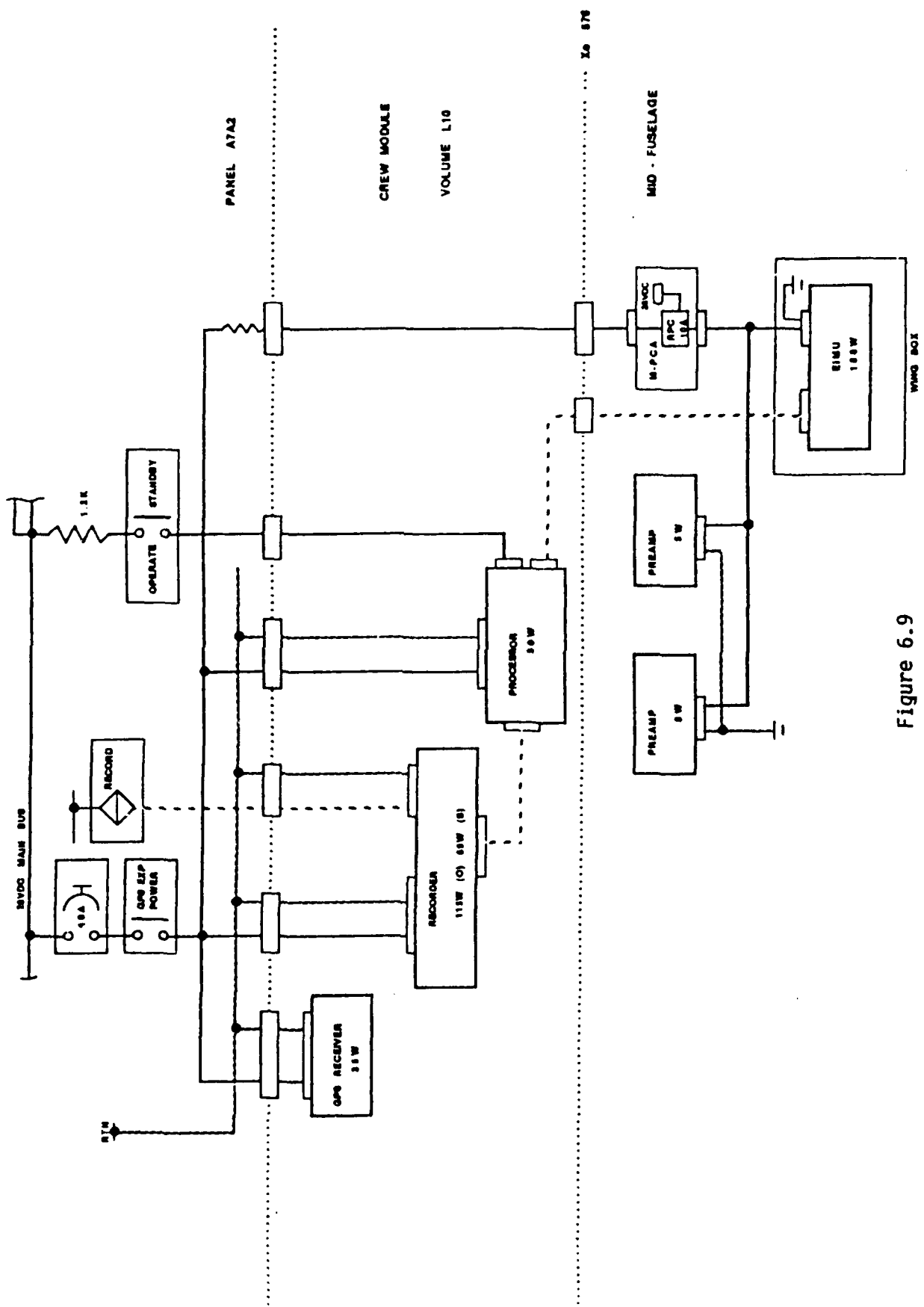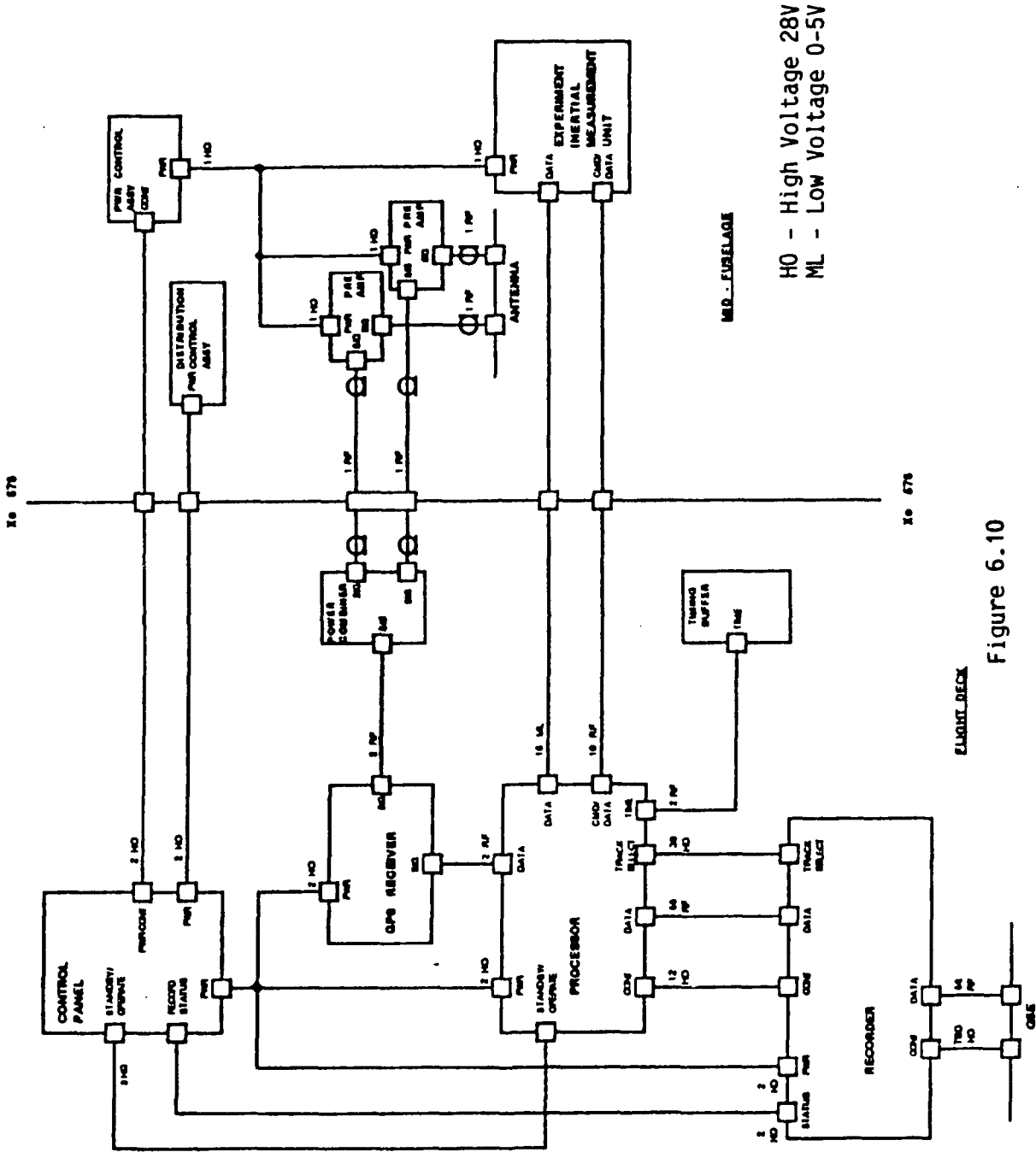These diagrams are included here to demonstrate the level of detail to which the payload integration analysis was carried out. Finally, in Figure 6.11 we show the access to the experiment recorder via the Driver Amplitude Module (DAM) which is the interface to the outside world. The data from the experiment recorder after flight can be easily transferred via the DAM.

6.4 Experiment Integration Cost Estimate

A preliminary cost estimate for orbiter integration was developed early on in the study (early 1987) based on the assumption of the experiment hardware configuration available at the time. This data was included in the hardware configuration trade-off study, Table 6.2. This cost estimate was detailed and further refined by Rockwell based on the experiment installation diagram presented earlier in Figures 6.8 - 6.10. The revised cost estimate of $1.47 million assumed the following program:

Authorization to proceed   January 1989

Engineering start/completion date   February - December 1989

Manufacturing   July 1989 - January 1990

Hardware on dock at
   Kennedy Space Center   March 1990

The revised orbiter integration cost estimate of $1.47 million included engineering, logistics support and manufacturing costs. The engineering tasks included subsystem layout, detailed drawings, schematics, ICD's, mission pits, failure modes and effects analysis, hazard analysis and support at KSC. The manufacturing cost included LRU installations, electrical interface power and control harnesses, structural provision and tooling for optical alignment, manufacturing aids and harness/templates. The above ROM cost estimate has sufficient detail backup available to provide high confidence in the

6-17

ORBITER GPS TRACKING EXPERIMENT
DATA TRANSFER
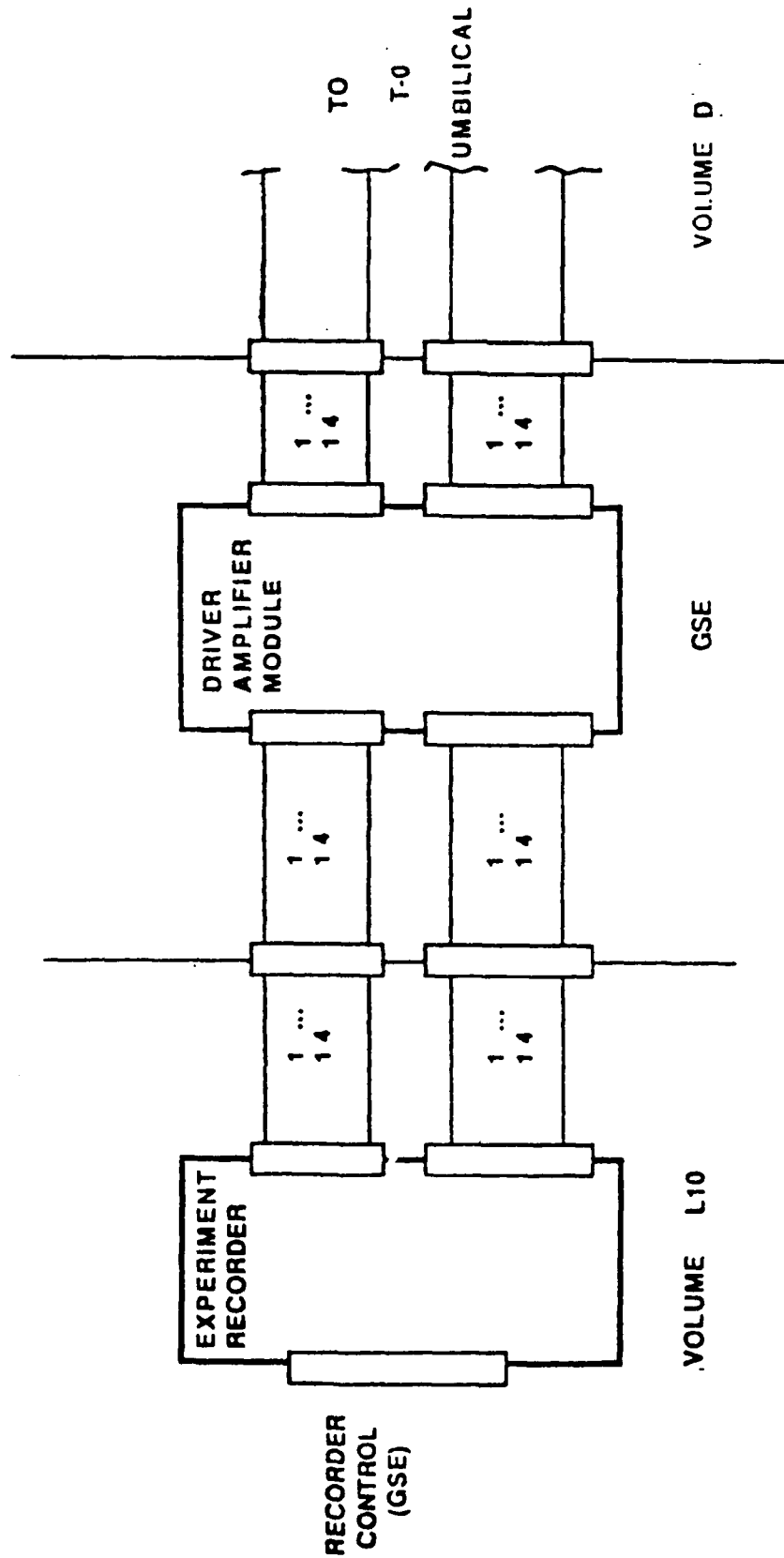
Figure 6.11

estimates. These cost estimates will be revised based on the new authorization date, when available

6.5 Summary

This section has discussed the underlying assumptions that were used in the orbiter payload integration analysis. Two hardware configurations were analyzed and traded-off for cost and performance. The selected configuration offers good performance at a reasonable cost. The selected configuration was detailed, electrical interconnect diagrams were developed and a realistic integration cost estimate was developed. The revised integration cost estimate of about $1.47 million compares favorably with our projection of $2-3 million developed in the early part of the study.

SECTION 7

NASA SPACE SHUTTLE GPS EXPERIMENT

In the previous sections of this report the feasibility of the Air Force STS-GPS Tracking Experiment for measuring the perturbations in the gravity vector at the STS Orbiter altitude was analyzed. A baseline experiment hardware configuration was developed and its integration into the Orbiter as a mission kit was investigated. The experiment hardware included: (1) a 5-channel L1/L2 P-Code GPS receiver; (2) a strapped-down IMU consisting of ring laser gyros and a precision 3-axis accelerometer assembly; (3) a micro-processor control assembly; and (4) a tape recorder. Preliminary specifications on the hardware subsystems were developed and candidate hardware for each subsystem was selected. Details of the hardware including their performance parameters were described in Section 3.

The primary objective of the Air Force STS-GPS Tracking Experiment (i.e., STAGE) is to collect the GPS and IMU data on the Orbiter and post-process it, along with the Orbiter navigation data and ground tracking GPS data, to estimate the gravitation parameters. During the course of the study it was recognized that the GPS tracking data collected on the Orbiter for gravitation estimation can also be used to support other DoD and NASA space missions. In particular, the STS-GPS tracking data can be used to validate precision navigation and attitude control concepts proposed for future NASA missions, such as the Space Station. NASA-JSC has also proposed a Shuttle flight experiment, the feasibility of which is documented in Reference [7.1], to gather GPS tracking data on the Shuttle and to process it for determining the Shuttle navigation solution. This section reviews the NASA-JSC GPS requirements to support future missions

and identifies commonality of requirements between the NASA-JSC
flight experiment and the present Air Force experiment.

7.1 NASA-JSC GPS Requirements

It is noteworthy to point out that the NASA Johnson Space
Center has been interested, for some time, in providing the GPS
capability on the Orbiter. Previous effort under NASA JSC
sponsorship [7.5] involved the formation of a Space Shuttle GPS
Panel to determine the feasibility and cost/performance benefit
of GPS onboard the Space Shuttle to provide improved navigation
capability. These efforts led to the development of GPS
requirements for the Shuttle [7.5] and resulted in the
development of GPS antennae which were implemented on the
Orbiters except for Columbia (OV-102). Furthermore, as a result
of these early efforts, space for GPS receivers was reserved in
the Shuttle avionics rack (Bay 3B) and provisions for cabling and
preamplifiers were made to support these NASA objectives. In
spite of these early successes the effort was terminated by NASA
in 1981 due to funding constraints. A brief review of these
early NASA efforts to implement GPS on the Shuttle was recently
presented by R. Fenner and J. Blucker at a NASA GPS Symposium
[7.6] held at the Jet Propulsion Laboratory.

Even though the Space Shuttle did not get the GPS capability
these early NASA studies were successful in proving the
feasibility of the concept and developing the ground work for GPS
acceptance on future NASA spacecraft. The NASA's OMV (Orbit
Maneuvering Vehicle) and the Space Station are examples where GPS
has been selected as part of the baseline navigation sensor suite
to provide the navigation and attitude update. Future Shuttle-
Derived Vehicles (sdvs), such as Shuttle-C and other spacecraft,
such as AOTV are candidates to have onboard GPS receivers. The

NASA GPS navigation requirements for the Space Station are summarized below [7.3,7.4,7.6]:

Table 7.1: NASA Space Station Navigation Requirements

Navigation Mode	Accuracy (rms 1-sigma)
Target Absolute Navigation [7.6]	10 meters (1 sigma)
Relative Navigation [7.6] at Docking/Berthing	3 meters (1 sigma)
Relative Navigation without Docking Maneuvers [7.4]	30 meters (1 sigma) or 1% of the range between the two spacecrafts, whichever is the greater
Attitude Update [7.4]	0.01 degree

Recent studies by Hughes [7.2], Axiomatix [7.3] and Texas Instruments [7.4] have concluded that these Space Station navigation and attitude control requirements can be met by GPS. In order to validate the proposed GPS processing concepts and demonstrate the accuracy, NASA-JSC has proposed a flight experiment which involves flying a GPS receiver on the Space Shuttle. The proposed flight experiment is based on a study [7.1] performed by the Applied Research Laboratories, University of Texas. The study analyzed the feasibility of a Shuttle experiment using a Texas Instruments Model 4100 GPS receiver (GEOSTAR) and associated recorder to gather GPS data during a Shuttle mission for post-mission analysis. The TI 4100 receiver was developed for ARL under contract to Naval Surface Weapons Center/Dahlgren Laboratory.

A review of the ARL study for the NASA-JSC Shuttle/GPS experiment is presented below.

7.2 NASA-JSC Flight Experiment

A feasibility study using TI 4100 GPS receiver to support a Shuttle flight experiment was carried out in 1983 by ARL, the results of the study are reported in [7.1]. The purpose of the study was to evaluate the effectiveness of the TI 4100 (GEOSTAR) GPS receiver as a space navigation unit for a Shuttle experiment. The goal of the NASA experiment is the acquisition and retrieval of Shuttle-GPS tracking data for the computation and evaluation of the accuracy of the solutions. Specific topics considered in the ARL study [7.1] were: GPS receiver location in the Shuttle; compatibility of TI 4100 receiver with the Shuttle environment; hardware modifications, if any, to the TI 4100 for compatibility with the Shuttle; and analysis of the receiver acquisition, tracking and navigation performance.

The ARL study was comprehensive in that it covered the major topics and its conclusions were supported by detailed analysis and simulations. The major finding of this study was that "there are no apparent obstacles to flying the TI 4100 GPS receiver in the Shuttle, as a low cost experiment". The study concluded that the TI receiver can be integrated in the Shuttle avionics bay 3B with only minor modifications to the GPS receiver. There were however, certain open questions regarding the compatibility of the TI 4100 receiver with the Shuttle environment, e.g., atmospheric pressures and humidities, radiation, external surface temperatures, and flammability and toxicity. The author of the report felt that these issues would be satisfactorily resolved since the equipment was designed by TI to be flown on helicopters and aircraft. But the degree of alteration to the equipment that would be required for compliance was not clearly identified. A

7-4

careful review of the ARL report permits us to concur with the study's general conclusions.

The report also presented baseline Shuttle navigation performance using ground Spacecraft Tracking and Data Networks (STDN) and TDRSS satellites, and compared it with the projected performance using TI 4100 GPS receiver parameters with a nominal navigation filter design. The comparative data is presented in Table 7.2.

One of the advantages of having GPS onboard will be that the Shuttle won't have to rely on the ground Spacecraft Tracking and Data Network (STDN) for tracking and to provide the state vector update. Furthermore, the Shuttle coverage from these STDNs is poor - only 15% of the time the Shuttle is visible from these stations. There are major tracking gaps over the South Pacific, the entire Asian continent, and the South Atlantic/Indian Ocean area [7.1]. The poor visibility problem is being addressed by NASA via TDRSS (Tracking and Data Relay Satellite System) satellites. It is estimated that the TDRSS satellites will provide about 85% visibility to the Space Shuttle.

Table 7.2: Shuttle On-Orbit Navigation
Accuracies (3σ) [7.1]

Tracking System	Position (Km)			Velocity M/S		
	Radial	Along Track	Cross Track	Radial	Along Track	Cross Track
STDN	1.5	10.5	1.5	11.7	1.8	3.0
TDRSS	1.1	5.6	1.2	6.7	1.0	1.2
GPS (18-SV Constellation)	0.03	0.03	0.03	0.1	0.1	0.1

From Table 7.2 we note the superior navigation performance projected by the GPS onboard the Shuttle. The improvement in navigation performance estimated to be achieved by TDRSS tracking of the Shuttle over the STDN tracking is about a factor of 2, however the major advantage of TDRSS tracking of the Shuttle is realized in the improved visibility.

While we concur with the general conclusions of the ARL study regarding the suitability of the TI 4100 to support a NASA-JSC flight experiment, we note certain limitations that are imposed by the above choice of the equipment and discuss its impact on the mission performance. We believe that these limitations can be easily removed, if warranted. The primary limitations of TI 4100 receiver and the associated recorder are discussed below.

7.2.1 Reduction in Received Signal-to-Noise Ratio

The ARL report correctly points out the 6 dB loss in received signal-to-noise power ratio due to the inherent multiplexed-channel receiver design of the TI 4100 GPS receiver. The link budget analysis presented on pages 66-67, accounts for it as a multiplex loss of 6 dB. Its effect is to reduce the link margin by 6 dB. As shown in Tables XII and XIII [7.1] and discussed on page 72, the link margin for carrier tracking at 80° half-cone angles (angles from zenith) is minimal for L_1 (C/A); and for L_1 (P) it is negative. At 75° half-cone angles, the margins increase by 3 dB, making each link positive. The report associates the weak link margin performance to two reasons:

"The first is the low gain of the Shuttle GPS antennas at very low elevations. The second factor is the 6 dB signal loss induced by four satellites multiplexing during receiver operation". [7.1]

7-6

We note here that the Shuttle GPS antenna characteristics (gain versus elevation angle) are fixed, and therefore the only remedy to improve the link margin performance is to select a GPS receiver that does not have a 6 dB signal-to-noise power penalty. A GPS receiver with parallel tracking channels (instead of multiplex channels) does not incur this penalty and therefore will offer a solution to this problem. An alternate solution, not necessarily recommended, will be to track only high elevation satellites (which will have good antenna gain) and possibly pay the penalty in terms of poor geometry (i.e., higher GDOP). Since there currently exist several GPS receivers with capability to simultaneously track four or more GPS satellites, we believe that there is no need to accept the degradation in performance. Most of these GPS receivers meet the NASA size and power budget and can be integrated in the Shuttle avionics rack 3B, similar to the TI 4100.

7.2.2 Cassette Data Recording

The TI 4100 GPS receiver (GEOSTAR) comes with its own data recording capability for geodetic applications. The data recorder unit connects to the receiver through the dedicated RS-232 interface. The ARL study estimated the amount of data that will be collected during the NASA experiment and calculated the number of tape cassettes that will be required to store this data. With the assumptions on the type of data that will be of interest and their frequency, the study concluded that the amount of data collected per day is approximately 4.6×10^7 bits. Assuming a data cassette can store 251×10^3 bytes (2×10^6 bits), the number of cassettes required per day is about 23. This means that the astronauts/mission specialists will have to change cassettes approximately every hour - this is very demanding and may be considered a serious constraint on the

mission. Furthermore, the experiment data for the nominal 7 day Shuttle flight will need about 160 casette tapes - a rather large number.

These limitations can be easily removed by carrying on-board a MARS (Modular Airborne Recorder System) tape recorder, the unit proposed for the Air Force flight experiment. The MARS tape recorder has been used by NASA on other missions. The preliminary calculations carried out for the Air Force STS-GPS Tracking Experiment indicates that one 14" 28-track reel magnetic tape at 1 7/8" per second will be adequate to collect the experiment data for the entire Shuttle on-orbit flight.

7.2.3 Experiment Calibration

The need for a reference system to calibrate the NASA-JSC flight experiment was recognized in the ARL study. Two potential independent sources were mentioned: (1) radiometric (interferometric) processing of the TDRSS and STDN tracking data; (2) laser tracking. It was estimated that in a post-processing environment, with three orbits of Shuttle/TDRSS data and post-fit ephemerides, an independent Shuttle orbit can be determined to the 200-300 meter level (1-sigma). Such accuracy is not adequate to calibrate GPS where accuracy of about 10 meter (1-sigma) is estimated. The tracking of the Shuttle with one of the standard NASA laser networks is estimated to provide, post-flight, accuracies similar to the post-flight GPS/Shuttle orbits. There are serious problems, however, in coordinating Shuttle flight so that good passes over laser sites can be obtained to calibrate the GPS experiment. Additionally, laser coverage can be impaired or completely eliminated by weather. For these technical reasons and for cost-considerations to install a retroflector on the Shuttle, the ARL study did not recommend the laser tracking of the Shuttle as a feasible approach to calibrate the experiment

GPS data.

For the above reasons the ARL study did not recommend a satisfactory solution to the calibration problem. This shortcoming can be removed by the Air Force STAGE experiment. The STAGE experiment data, if collected at the same Shuttle flight, will provide a very accurate reference system by virtue of it having a more capable GPS receiver and an independent IMU consisting of precision gyros and accelerometers. The specifications on the STAGE GPS receiver and the IMU were presented in Section 3.

7.3 Enhancement to NASA-JSC Flight Experiment

The baseline NASA-JSC flight experiment, described in the ARL study, emphasized the basic navigation capability (i.e., position and velocity) of the TI 4100 GPS receiver for the Shuttle application. The report did not analyze how the proposed flight experiment will support other navigation requirements, such as relative navigation and attitude update for rendezvous and docking. These NASA requirements for the Space Station are given in Table 7.1. In this section we discuss how these requirements can be met in an enhanced flight experiment.

7.3.1 Attitude Update

Recent studies by Texas Instruments [7.2] and Axiomatix [7.3] have investigated the relative navigation and attitude update capability of GPS tracking data. The Texas Instruments study [7.2] concluded that the Space Station attitude measurement accuracy of 0.01 degree can be met by using simultaneous GPS carrier phase measurements from 3 GPS antennas located at the apexes of an approximately equilateral triangle whose sides are 5 meters apart. The same three GPS satellites must be tracked at

each antenna and the effect of differential carrier multipath must be minimized to provide the required accuracy. One of the primary requirements for GPS attitude determination, from a receiver point of view, is that the receiver design must be able to produce the continuously counted carrier phase measurements from three or more GPS satellites and from three or more GPS antennas simultaneously.

The TI 4100 GPS receiver analyzed by ARL does not meet the requirements for attitude measurements. Also, the Shuttle has only two GPS antennas (top and bottom) which at best (subject to simultaneous satellite visibility at the two antennas) will limit the attitude determination capability to 2-axes only. The attitude in the third axis can only be resolved by either placing a third antenna or alternatively by inducing a rotation maneuver of the Shuttle. The latter approach has originally been suggested by Mayflower for the OMV spacecraft attitude update.

Returning to the receiver issue, several alternatives to TI 4100 exist which have been discussed in the Texas Instruments study [7.2]. TI recommends a more modern receiver, TI 420 to meet the attitude measurement requirement. The Air Force STAGE experiment GPS receiver - a modification of the TOPEX GPS receiver - will also meet this requirement, albeit not as efficiently as the TI 420.

7.3.2 Relative Navigation

The Texas Instruments and Axiomatix study results verified that the NASA's relative GPS navigation accuracy requirement of 30 meters or 1 percent of the distance between two spacecraft can be met by differencing the navigation state vector. The higher relative navigation accuracy of 3 meters (Table 7.1) required for docking can be met by pseudo-range difference techniques. Taking

pseudo-range differences ensures that all measurement bias errors and clock errors are eliminated and therefore provides the highest relative navigation performance.

An enhancement to the baseline NASA flight experiment, to demonstrate GPS relative navigation capability and the attitude determination capability, is proposed here. In this scheme (originally conceived at NASA-JSC) we may mount a third GPS antenna on the Shuttle RMA (Remote Manipulator Arm) and track this antenna signal with either the TI 4100 (or TI 420) while we use the existing Shuttle GPS antennas to track the same satellites. The latter can be achieved by either the TI 420 or any other GPS receiver onboard, e.g., the Air Force STAGE experiment receiver. The proposed enhancement to the NASA-JSC flight experiment will indeed increase the experiment cost, but the expected pay-off in terms of reducing the Space Station program risks for rendezvous and docking phases is also very high. The feasibility and cost of this enhancement should be analyzed.

In the next section we define the areas of commonality between the NASA-JSC flight experiment and the Air Force STAGE experiment and how this can be exploited to develop a unified Air Force/NASA Shuttle flight experiment.

7.4 Commonality Between the Air Force and NASA Shuttle Flight Experiment

The commonality between the two proposed Shuttle-based experiments is described here. This is done by presenting a comparison of their respective mission requirements and how these requirements are met by the proposed hardware.

At the very basic level, both the Air Force and NASA

experiments use the GPS satellite signals to track the Shuttle
during the on-orbit phase of the flight. Both experiments will
gather the same GPS data, i.e., the pseudo range (code phase) and
integrated carrier doppler phase during the Shuttle flight, and
will process these data to estimate the parameters of interest.
The onboard hardware, in both cases, is designed to produce real
time Shuttle GPS navigation solution. The navigation solution
(i.e., orbit determination) will be refined during the post-
mission data processing.

While the type of GPS data collected for both experiments
are similar, the data rates are not. The primary difference
being that the measurement data rate is 1 second in the Air Force
case while the NASA experiment will collect measurement every 6
second per SV. This difference is primarily due to the limited
recording capability of the TI 4100 GEOSTAR data recorder. We
believe that the TI 4100 receiver hardware/software is capable of
outputing measurements once per second. In addition, the Air
Force STAGE experiment will also collect IMU measurements of
delta-V and delta Θ. These IMU measurements describe the non-
gravitation disturbance environment of the Shuttle which will be
useful for post-mission processing of the data in both cases.
The similarities and differences between the two experiments are
summarized in Table 7.3.

From the comparative data in Table 7.3 one easily concludes
that the NASA-JSC flight experiment objectives, as described in
the ARL study report [7.1] can be met if merged with the Air
Force proposed flight experiment. In many cases, the Air Force
experiment measurements will be more accurate (because of 6 dB
higher signal-to-noise power ratio, Section 7.2) and a lot more
data will be available (a factor of 6 faster data collection rate
and more onboard recording capability) for post-mission
processing. The inclusion of the IMU data will provide an

Table 7.3: Functional Comparison Between the Air Force and NASA Experiments

Feature	Air Force STAGE Experiment	NASA-JSC Flight Experiment
I. Experiment Hardware		
GPS Receiver	5-Channel, L1/L2, simultaneous tracking; TOPEX GPS Receiver	1-Channel,L1/L2 multiplex tracking; TI 4100 GPS Receiver
IMU	Strapped-down IMU consisting of Honeywell 1342 RLGs and Bell MESA Acceleometers	None (will use the Shuttle INS data)
Data Recorder	Data Tape MARS recorder, 14" 28-track magnetic reel; 1 tape adequate for the mission	GEOSTAR recorder unit with two MFE 250-BF cassette drives in the recorder unit; 1 tape per hour of the mission
Processor Control	To be designed	Included in the GEOSTAR
II. Experiment Data Collection		
Pseudo-range	5 pseudo-range measurements per second	5 pseudo-ranges every 6 seconds
Carrier phase	5 carrier doppler phase measurements per second	5 carrier doppler phase every 6 seconds
Real-time navigation	Navigation solution once every second	Navigation solution every 6 seconds
Translational and rotation acceleration	Delta-V and delta-Φ measurements per second in the Shuttle body coordinates	N/A
III. Primary Application		
Post-mission	Estimate gravitation parameters	Shuttle orbit determination
IV. Processing Software	Process GPS code and carrier phase measurements to estimate Shuttle position, velocity and acceleration	Same

accurate evaluation of the dynamic disturbance environment of the
Shuttle which can be used to aid the post-mission processing.
Furthermore, the Air Force experiment IMU data can be used to
independently determine the Shuttle orbit which will serve the
need of providing an accurate independent reference system to
calibrate the GPS experiment accuracy. As pointed out earlier
the NASA-JSC experiment has the need of an independent, accurate
reference system. STDN or TDRSS tracking of the Shuttle data
will not meet this requirement. We should also note that the
Shuttle IMU instruments do not have the required precision to
meet this requirement.

In summary, we observe that the Air Force STAGE flight
experiment not only meets the NASA-JSC experiment objectives but
in many important areas it improves upon those objectives. The
Air Force experiment data will complement the NASA-JSC experiment
by providing a solution to the calibration problem. The post-
mission processing software developed for the Air Force
experiment can, with some minor modifications, be used to process
the NASA-JSC experiment data.

7.5 Enhanced NASA-JSC Flight Experiment

The previous sections have discussed the requirements of the
NASA-JSC basic flight experiment (using TI 4100 GPS receiver) and
how these requirements can be met by the Air Force STAGE
experiment. An enhanced NASA-JSC flight experiment concept which
emphasizes the Space Station requirements of relative navigation
and attitude determination for rendezvous and docking is briefly
discussed in this section. The enhanced NASA-JSC experiment
objectives of relative navigation and attitude determination can
be met by combining the elements of the basic NASA-JSC flight
experiment with the Air Force STAGE experiment.

The combined Air Force/NASA flight experiment will use all the elements of the Air Force STAGE experiment and NASA-JSC GEOSTAR experiment and in addition will require mounting a third GPS antenna on the Shuttle RMA. In the combined experiment, the GEOSTAR receiver will acquire and track GPS satellites using this antenna while the STAGE GPS receiver will acquire and track the GPS satellites using the existing top and bottom GPS antennas on the Shuttle. The non-docking relative navigation accuracy of 30 meters or better (1 sigma) for the Space Station can be demonstrated, post-flight, by the Air Force STAGE experiment tracking data along with the ground station GPS tracking data. The simultaneous GPS carrier phase tracking data collected at the Shuttle and at ground tracking stations can be used for differential GPS processing. The Air Force STAGE experiment processing concept involves double differenced GPS carrier phase processing to mitigate the effect of GPS satellite clock errors. This aspect of the Air Force experiment data processing is required to meet the NASA-JSC flight experiment objective of GPS relative navigation.

The GPS relative navigation performance requirement to support Space Station docking with other spacecraft (e.g., OMV) is established at 3 meters (1 sigma). This level of navigation performance can be demonstrated by the combined Air Force/NASA experiment. In this case, the Shuttle RMA can be commanded to move during data collection to simulate docking maneuver. The GEOSTAR (TI 4100) or a more modern model TI 420 can be used to support the NASA portion of the combined Air Force/NASA experiment.

The attitude determination requirement of 0.01 degree (1 sigma) for the Space Station can also be demonstrated with the above experiment set up. Furthermore, the Air Force STAGE experiment gyro data can be used to provide an independent

reference system for GPS attitude calibration. We note here that the candidate gyro sensors (Honeywell RLG 1342) for the Air Force experiment have about 2 orders of magnitude lower drift rate than the Shuttle IMU gyros.

The capabilities of the proposed combined Air Force/NASA experiment are summarized in Table 7.4. As seen in Table 7.4 the combined experiment uses the complementary features of both the experiments to demonstrate the GPS-related navigation mission performance of the NASA Space Station.

7.6 Conclusions

The NASA-JSC baseline flight experiment, based on the ARL study results with the TI 4100 GPS receiver, will demonstrate the GPS absolute navigation capability on the Shuttle. It was shown that the Air Force STAGE experiment will meet the above NASA-JSC flight experiment objectives and in many instances will improve upon it. The Air Force experiment data will also meet the much needed requirement of providing an independent reference system for calibration. It was also pointed out that the NASA-JSC baseline experiment was not designed to support other GPS-related objectives, such as relative navigation and attitude update. An enhanced flight experiment concept which combines the features of both the Air Force and NASA experiments was proposed. The preliminary study carried out here indicates that the combined Air Force/NASA experiment will demonstrate the Space Station GPS navigation performance in the critical areas of rendezvous and docking. All the elements (hardware and software) of the combined experiment can be developed from off-the-shelf components and can be ready to support a potential 1991 Shuttle flight. The data from this experiment will provide the STS-GPS tracking data for the Air Force global gravity field mapping and will validate the proposed GPS-based navigation concepts for the

TABLE 7.4: Combined Air Force/NASA Shuttle Flight
Experiment Capabilities

Features/Capabilities	Air Force STAGE Experiment	Modified NASA-JSC Experiment
I. Experiment Hardware	Same as in Table 7.3 baseline	TI 4100 or TI 420 with existing recorder
II. Antennas	Top and bottom GPS antennas used by the Air Force experiment	Third antenna mounted on RMA used by TI 4100
III. Relative Navigation - non-docking: 30 meters	STAGE experiment data alone is sufficient for this purpose	Not used
- docking: 3 meters	STAGE experiment flight data using existing antennas	GEOSTAR flight data using the new antenna
IV. Attitude Determination - both receivers track same satellites	STAGE data with one (top or bottom) antenna	GEOSTAR data with new antenna
- command movement of RMA will simulate attitude change		
V. Independent Reference - attitude reference for calibration	STAGE IMU gyros data	not applicable

NASA Space Station. Further investigation is recommended (e.g., to address the issues of mounting the third GPS antenna on the Shuttle RMA) to definitize the proposed combined Air Force 'NASA flight experiment. This study can be carried out rapidly because most of the elements of the proposed combined experiment are very well understood at this time.

REFERENCES

7.1 Peters, J.C., "Feasibility of GEOSTAR Experiment
Onboard the Space Shuttle", Technical Report
ARL-TR-83-18, Applied Research Laboratories, The
University of Texas at Austin, Austin, TX, June 1983

7.2 Hein, Doug, John Kelley, "Potential Applications of the
GPS as an Input Sensor for Spacecraft Systems", Final
Report No. H5517-023, Contract No. NAS9-17490, Hughes
Aircraft Company, 1986

7.3 Huth, Gaylord, et al., "Spacecraft Applications of
Advanced GPS Technology", Final Report No. P8805-5,
Contract No. NAS9-17681, Axiomatix, May 1988

7.4 Ward, Phil, et al., "Space Applications of Advanced
GPS Technology", Final Report No. U1-789130-F,
Contract No. NAS9-17781, Texas Instruments, Dallas, TX,
June 1988

7.5 STS-GPS Navigation System Design Data Base, Report No.
SD78-SH-0042B, Contract No. NAS9-14000, Rockwell
International, Shuttle Orbiter Division, Downey, CA,
August 1979

7.6 Slides from the NASA Symposium on GPS Space
Applications, hosted by the Jet Propulsion Laboratory,
Pasadena, CA, November 18-19, 1987